Gas/Particle Partitioning of Semi-Volatile Organic Compounds to Model Atmospheric Particulate Material

John Morse Elliot Storey
B.A., Harvard University, 1984
M.S., Duke University, 1986

A thesis submitted to the faculty of the
Oregon Graduate Institute of Science & Technology
in partial fulfillment of the requirements for the degree
Doctor of Philosophy
in
Environmental Science and Engineering

January 1993

The thesis " Gas/Particle Partitioning of Semi-Volatile Organic Compounds to Model Atmospheric Particulate Material" by John M. E. Storey has been examined and approved by the following Examination Committee:

JAMES F. PANKOW
Professor
Thesis Advisor

JAMES J. HUNTZICKER
Professor

RICHARD L. JOHNSON
Associate Professor

DAVID W. GRAINGER
Assistant Professor

ACKNOWLEDGEMENTS

This thesis was written in a timely fashion due in no small part to the superhuman editing efforts of my adviser, Jim Pankow. I want to thank him for taking me on four years ago, despite my referring to his work as a "mish-mash of stuff" at our first meeting. I also want to thank him for all of his support, financial, spiritual and emotional, as well as his understanding of the needs of small children.

My committee, Jim Huntzicker, Rick Johnson, and Dave Grainger have been extremely helpful at various different times. I appreciate all of the comments and editing as well as lively discussions with them concerning differing aspects of adsorption. I want to thank all of them for their time and efforts.

I wish to acknowledge EPA's Office of Exploratory Research and Daryn Pashayan for supporting this work for the last two years.

Lorne Isabelle has given me tremendous help with everything from the Finnigan to auto repair to swimming instruction. The successful design and construction of the experimental apparatus used here was the result of many consultations with Lorne. I hope we can continue to consult on other matters. Thanks for all the fun we've had.

Bruce Tiffany and Don Buchholz have been great friends as well as important resources for various lab mishaps and computer disasters. I want to thank them for that as well as many cheerful moments at the Helvetia Tavern and the Lunch Lab.

Judi Irvine has kept track of more stuff and pasted more figures together at the last minute than I could have ever imagined. Thanks to her and Pam Locke for being so helpful with everything.

The staff at O.G.I. including Gerry Boehme, Allan Ryall, Tim Bernard, Doug Davis, Dave Duncan, Jack McCarthy, Sandy Holt, Margaret Day, Donna Reed, and

Barbara Ryall have all contributed their extensive talents to this work. Thanks to all of them for their help and their patience with this graduate student.

I am fortunate to have worked for Jim Pankow because he always has great students in his group, and I have had a lot of fun with them. Ken Hart was a huge help early on and later as his stores of squirrelled-away equipment kept me in business for years. J. McPherson and Stewart Rounds were lots of fun to hang around with and an inspiration to finish quickly. Jim Tesoriero and I have had important discussions about politics, economics and science and has helped me finish up at the end.

Barb Turpin and Ge Su were great office mates putting up with considerable messiness on my part as well as sharing many insights into science and other more important topics.

All of the students I have encountered in my time have been terrific to be around. Tammy Wood and I managed to delay our degrees by a good six months with two Earth Day Symposia which were somewhat successful. Mark Nelson, Leah Matheson, Chee Choy, Paul Wittbrodt, Patty Toccalino, Tim Mayer, Bernie Bonn, Mike Elovitz, Kathy McCarthy, Liannha Sa, Claude Errera, Bill Bagby and Jane Allen have all made important contributions to my sanity over the years.

I wish to give special thanks to my grandmother, Janet Elliot, whose generosity and foresight made this long ordeal financially possible. I hope she knows that I finished finally. My parents have been great and very supportive the whole time, and they have been proud of my small accomplishments as well as big ones. I thank them warmly for everything they've given me and for having so much confidence in my abilities.

Finally, the most important acknowledgement is saved for Susan Coffey who was there from the first application I wrote to grad school. (little did she know...) She has put up with a lot over the last seven years and especially the last year. Her love and support have kept me going through rough times, and she seemed to always believe I would finish even when I didn't believe it. I thank you and Jeddy for your love and for putting it all into perspective.

DEDICATION

This thesis is dedicated to my wife Susan Coffey and our son Jedediah for bringing so much joy into my life.

Table of Contents

List of Figures

List of Tables

NOTATATION

A =measured gas phase concentration of the compound (ng m^{-3})

A_{QFF} = specific surface area of QFF (cm^2 µg^{-1})

A_{TSP}=APM specific surface area (cm^2 µg^{-1})

A_T =total in gas phase (%)

b_B =$e^{(Q1-Qv)/RT}$ = BET constant

b_L =Langmuir constant (atm^{-1})

b_p =y-intercept of log K_p vs. $1/T$ plot as determined by SLR

b_r =y-intercept of log K_p vs. log p_L^o plot as determined by SLR

B_A =BET constant for species A for multicomponent adsorption isotherm

B_B =BET constant for species B for multicomponent adsorption isotherm

c_g = gas phase concentration (ng m^{-3})

c_s = solid phase associated concentration (ng µg^{-1})

c_s/c_g = gas/solid partitioning coefficient (m^3 µg^{-1})

$(c_s/c_g)_s$ = surface-area-normalized gas/solid partitioning coefficient (m^3 m^{-2})

C_v = concentration in vial (ng µl^{-1})

CYIR = common y-intercept regression

dCH_2CL_2 = density of CH_2Cl_2 (g µl^{-1})

F = measured particulate associated concentration of the compound (ng m^{-3})

F_T = total particulate associated compound = $F + x$ (%)

H = Henry's Gas Law constant (atm m^3 mol^{-1})

K = a gas/particle partitioning coefficient (µg m^{-3})

K_p = the gas/particle partitioning coefficient (m^3 µg^{-1})

$K_{p,s}$ = the surface-area-normalized gas/particle partitioning coefficient (m^3 m^{-2})

m_p = slope of log K_p vs. $1/T$ plot as determined by SLR

m_r = slope of log K_p vs. log p_L^o plot as determined by SLR

M = molecular weight (g/mol)

MCH_2CL_2 = mass of CH_2CL_2 in vila (g)

M_F = Mass of filter (μg)

n = amount of adsorbed gas (mol)

n_m = amount of adsorbed gas for monolayer coverage (mol)

N_o = Avogadro's number (6.02×10^{23} molecule mol^{-1})

N_s = sorption sites on the surface of the APM (mol cm^{-2})

p_A = partial pressure (torr) of the sorbing species A

p_o = vapor pressure of the sorbing compound (torr)

p_L^o = sub-cooled liquid vapor pressure

p_S^o = vapor pressure of solid

p_{SOC} = partial pressure of generic SOC (atm)

p = partial pressure of a compound (torr)

P_{drop} = pressure drop across the filter (in. H_2O)

PE = photoelectric signal (%)

Q_v = enthalpy of vaporization from liquid phase (kJ/mol)

Q_l = heat of desorption from the surface (kJ/mol)

r = radius of micropores (m)

R = gas constant = 8.2×10^{-5} (m^3 atm mol^{-1} K^{-1}) or 0.008314 (kJ mol^{-1} K^{-1})

RH = relative humidity (%)

RF = response factor

s_o = surface area per sorption site (cm^2)

S = available sorption sites on a surface

S_l = filled sorption sites on a surface

ΔS_f = the entropy of fusion (kJ mol^{-1} K^{-1})

SLR = simple linear regression

$\{SOC\}$ = activity of a generic SOC in water (mol m^{-3})

t = temperature (°C)

t_0 = vibrational time of sorbed atom (typically 10^{-13}-10^{-12} sec)

T = temperature (K)

T_{amb}= ambient temperature (K)

T_i = initial temperature before cooling in Niessner and Wilbring (1989) (K)

T_m = melting point (K)

TSP = concentration of particulate in the atmosphere (µg/m^3)

TSP_i = initial concentration of aerosols in Niessner and Wilbring (1989) apparatus TSP (µg/m^3)

TSP_S = surface area concentration (m^2 m^{-3})

V = volume (cm^3)

V_{ATD} = volume sampled with ATD cartridge (m^3)

W_{H2O} = amount of water adsorbed to QFF (m^3 µg^{-1})

x = the amount bound in particulate phase (%)

Greek:

γ = surface tension (mJ m^{-2})

ρ = density of liquid (kg m^{-3})

ABSTRACT

Gas/Particle Partitioning of Semi-Volatile Organic Compounds to Model Atmospheric Particulate Material

John Morse Elliot Storey

Oregon Graduate Institute of Science & Technology, 1992
Supervising Professor: James F. Pankow

Partitioning between the gas phase and suspended particle phase plays an important role in determining the fate and transport of airborne semi-volatile organic compounds (SOCs). Current theoretical work suggests that varying environmental conditions, sampling procedures, and particulate characteristics can complicate the measurement of the corresponding gas/particle partitioning coefficients. These factors can also make it difficult to assess the relative importance of surface adsorption and phase absorption in determining the values of the partitioning coefficients. A series of experiments were designed to measure the gas/solid partitioning of SOCs to a model atmospheric particulate material (APM). An apparatus designed to control temperature, relative humidity, SOC concentration and particulate characteristics was constructed. The SOCs studied included six *n*-alkanes, namely heptadecane, nonadecane, eicosane, heneicosane, docosane and tricosane, along with five polycyclic aromatic hydrocarbons (PAHs), namely 2-methyl phenanthrene, fluoranthene, pyrene, benzo[*b*]fluorene, and benz[*a*]anthracene. The model APM was a pre-baked quartz fiber filter (QFF). The QFF was exposed to the gas phase SOCs until equilibrium was achieved as suggested by equivalent gas phase concentrations upstream and downstream of the filter. Gas phase concentrations were determined by

adsorption/thermal desorption (ATD) using Tenax as a sorbent, and sorbed concentrations were determined by extraction of the QFF in methylene chloride. If the quartz is assumed to be non-porous, the sorption that was measured represents simple physical adsorption.

The measured partitioning coefficients have been expressed in both a K_p (m^3 μg^{-1}) and $K_{p,s}$ (m^3 m^{-2}) format, and are compared to corresponding values for urban particulate material (UPM) at ambient relative humidity (*RH*). K_p is the ratio of the sorbed concentration (ng μg^{-1}) to the gaseous concentration (ng m^{-3}). $K_{p,s}$ is the ratio of the surface-area normalized concentration (ng m^{-2}) to the gaseous concentration (ng m^{-3}). The measured relationship between log $K_{p,s}$ and log p_L^o, the sub-cooled liquid vapor pressure, is highly-correlated and agrees well with the same relationship for the PAHs on UPM. The close agreement between the quartz surface and the UPM suggests that partitioning to APM can be modeled by non-specific, physical adsorption.

CHAPTER 1

INTRODUCTION

Much research has now demonstrated that the atmosphere is a major transport pathway for the movement of semivolatile organic compounds (SOCs) through the global environment. The broad designation of "SOCs" encompasses many environmentally-important classes of compounds including polycyclic aromatic hydrocarbons (PAHs), polychlorinated biphenyls (PCBs), and a variety of organochlorine pesticides. Fluxes from the atmosphere have contributed upwards of 50% of the PCB loadings to the Great Lakes basin (e.g. see Eisenreich and Looney, 1981) and many times more organic carbon to the Chesapeake Bay than river inputs (Velinsky, 1986). Pesticides such as DDT and hexachlorocyclohexane (HCH), although banned in the United States and Canada, are still used in certain tropical countries. Residues from prior use in countries such as the U.S. and Canada that are transported northward along with contributions from tropical countries (Pankow, 1992) result in measurable concentrations being found throughout North America (Bidleman, 1988). SOCs exist in the atmosphere as gases and/or associated with particulate matter and can reach the terrestrial environment by precipitation scavenging of gases and particles, or by dry deposition of both phases.

The partitioning between the gas phase of an SOC and the particulate phase in the atmosphere plays an important role in determining the fate and transport of SOCs. A fundamental understanding of this process will allow prediction of the gas/particle partitioning of other SOCs not yet specifically examined, but of environmental concern. In addition, an understanding of gas/particle partitioning behavior will aid local, regional, and global transport modeling efforts as well as the preparation of global budgets for SOCs. By examining the current understanding of gas/particle partitioning, this chapter will identify areas in need of further study and thus introduce the focus of the dissertation research.

1.1 Background

Pankow (1987) provides a detailed derivation of the thermodynamic relationships first used by Junge (1977) and Yamasaki *et al.* (1982) to describe gas/solid partitioning. This section will briefly summarize that derivation, beginning with the Langmuir and Brunauer-Emmett-Teller (BET) isotherms. It will also discuss recent theoretical work including: how non-exchangeable material can affect gas/particle partitioning (Pankow, 1988; Pankow and Bidleman, 1991); a new regression approach for examining the temperature dependence of measured partition coefficients (Pankow, 1991); a look at the kinetics of gas/particle partitioning (Rounds and Pankow, 1990; Rounds *et al.*, 1992); and the analysis of PAH sorption to laboratory-generated aerosols in terms of gas/particle partitioning theory (Storey and Pankow, 1992). This section will also review some of the many field and laboratory investigations of gas/particle partitioning on urban and rural particulate material (UPM and RPM). For example, Ligocki and Pankow (1989), Hart (1989), Foreman and Bidleman (1990), Cotham and Bidleman (1992), McVeety and Hites (1988), Eitzer and Hites (1989), and Baker and Eisenreich (1990) have all measured the gas/particle partitioning of SOCs, including alkanes, PAHs, organochlorine pesticides, polychlorinated dibenzofurans (PCDFs) and polychlorinated dibenzodioxins (PCDDs). In addition, Benner *et al.* (1989) measured gas and particle concentrations of PAHs in a roadway tunnel, and Masclet *et al.* (1989) carried out similar measurements over the Mediterranean Sea. In the laboratory, Foreman and Bidleman (1987) and Cotham and Bidleman (1992) have examined the gas/particle partitioning of organochlorines and PAHs to UPM under controlled laboratory conditions.

1.2 Theoretical Overview

For gas/solid partitioning, the familiar Langmuir isotherm is given by:

$$\frac{S_1}{S} = \frac{b_L p}{1 + b_L p} \tag{1.1}$$

where S_l/S is the fraction of sites occupied, p is the partial pressure of the compound and b_L is the Langmuir constant which can be derived from the kinetic theory of gases. The value of b_L depends mainly on the enthalpy of desorption (Q_l) for the compound and surface of interest (Pankow, 1987). When p is very small, as for an SOC in the atmosphere, the isotherm is linear and is described by:

$$\frac{S_1}{S} = b_L p \tag{1.2}$$

When p is much less than the saturation vapor pressure of a compound (i.e. when $p << p_o$), then the BET isotherm can also be linearized:

$$\frac{S_1}{S} = b_B \frac{p}{p_o} \tag{1.3}$$

where b_B is directly related to b_L and depends on (Q_l-Q_v), the difference in the enthalpy of desorption and the enthalpy of vaporization from the pure liquid (Pankow, 1987); and p_o = the saturation vapor pressure of the compound. Pankow (1987) explains in detail the equivalence of the BET-based treatment of Junge (1977) and the later, linear Langmuir-based treatment of Yamasaki *et al.* (1982) for describing gas/particle partitioning. Both Junge (1977) and Yamasaki *et al.* (1982) use simple, physical adsorption to model gas/particle partitioning without consideration of specific molecular interactions between the sorbates and the surface. Although on a molecular scale there are many types of attractive and repulsive forces between surface groups and sorbents, these interactions are not considered on an individual basis because of the tremendous complexity and heterogeneity of atmospheric particulate material

(APM) surfaces. The Q_l parameter provides an average measure of the effects of these interactions.

1.2.1 Derivation of K_p, the Partitioning Coefficient

Yamasaki *et al.* (1982) started with Equation 1.2 in the derivation of an expression for a gas/particle partitioning coefficient, K:

$$K = \frac{A}{F/TSP} \qquad K_p = \frac{F/TSP}{A} \tag{1.4}$$

where A (ng m^{-3}) is the air concentration, F (ng m^{-3}) is the particulate-associated concentration, and TSP is the total suspended particulate concentration (µg m^{-3}). Pankow (1991) uses $K_p = K^{-1}$ so that the partitioning coefficient corresponds more closely with other environmental partitioning coefficients. An increase in K_p, therefore, corresponds to an increase in the tendency for sorption.

1.2.2 Temperature Dependence of Log K_p

For urban particulate material (UPM) in Osaka, Yamasaki *et al.* (1982) found that for each of the compounds they studied, log K_p depended inversely on temperature (T) according to:

$$\log K_p = \frac{m_p}{T} + b_p \tag{1.5}$$

For gas/solid partitioning, thermodynamic expressions for the slope and the y-intercept can be derived (Pankow, 1987):

$$m_p = \frac{Q_1}{2.303R} - \frac{T_{amb}}{4.606} \tag{1.6}$$

and

$$b_p = \log \frac{A_{TSP}\, t_0}{2.75\times10^6 (M/T_{amb})^{1/2}} \tag{1.7}$$

where A_{TSP} is a specific surface area (cm^2 µg^{-1})of the particulate matter; T_{amb} is the average ambient temperature (K); R is the gas constant; t_0 is a characteristic molecular vibration time (s); and M is molecular weight (g mol^{-1}). Equations (1.6) and (1.7) show that the slope is dependent on Q_l and that the y-intercept is controlled mainly by A_{TSP}. Within a given compound class and for a given type of particulate matter, b_p should be largely independent of the compound. Equations 1.5, 1.6 and 1.7 are discussed further in Chapter 2.

1.2.3 SOC Vapor Pressure and K_p

At constant T, Pankow (1987) shows that if non-specific sorption is occurring, and if $(Q_l\text{-}Q_v)$ is constant within a given group of compounds of interest, then a plot of log K_p vs. log p^o_L, the sub-cooled liquid vapor pressure, will have a slope near -1 and an intercept C which, within a given class of compounds, depends primarily on A_{TSP}:

$$\log K_p = -\log p^o{}_L + \log C \tag{1.8}$$

The value of p^o_L at a given T is determined from the p^o_S, the vapor pressure of the solid compound by the following:

$$\ln \frac{p^o{}_L}{p^o{}_S} = \frac{\Delta S_F(T_m - T)}{RT} \tag{1.9}$$

where ΔS_f = the entropy of fusion; and T_m is the melting point. Bidleman *et al.* (1986) and Pankow (1987) point out that the sorption behavior of a compound is more appropriately parameterized in terms of p^o_L then in terms of p^o_S because the small amounts sorbed to the particulate may behave more like an amorphous liquid phase than a crystalline solid phase.

In cities all over the world, when K_p values are estimated from measured values of $(F/TSP)/A$, researchers have observed the type of linear relationship contained in Eq. 1.8, and slopes close to -1 have indeed been found. These observations have added to the evidence that non-specific sorption can describe the main mechanism governing gas/particle partitioning in the atmospheric environment.

1.3 Discussion of Current Theory and Recent Field and Laboratory Studies

1.3.1 Non-Exchangeable Material

If measured values of $(F/TSP)/A$ are to provide accurate estimates of K_p, then the measured values of A, F, and TSP must represent equilibrium values. Thus, all of the sorbed SOCs must be able to exchange freely with the gas phase. Pankow (1988) and Pankow and Bidleman (1991) have explored the effect of non-exchangeable (i.e., "bound") material on measured values of $(F/TSP)/A$ under constant temperature conditions, as well as under changing temperature and TSP levels. The constant T situation is summarized in Fig 1.1. $(F_T/TSP)/A_T$ represents the partitioning coefficient for the total amount of the *measured* compound where $F_T = F + x$, the percent of non-exchangeable material, and $A_T = A$. F and A can be expressed in units of percent because their units cancel in Eq. 1.4. Fig. 1.1 shows that even small amounts (e.g., $x < 1\%$) of bound material can lead to large differences between a measured $(F/TSP)/A$ value compared to the true underlying K_p value, particularly for compounds with higher p_L^o values. Such non-exchangeable material causes curvature in a plot of log $(F/TSP)/A$ vs. log p_L^o, causing difficulties in determining the true thermodynamic slope for the underlying plot of log K_p vs log p_L^o.

Just as non-exchangeable material complicates the study of relationships between K_p and p_L^o, it can complicate the estimation of Q_l values for individual compounds based on the measured values of log $(F/TSP)/A$ and Equation 1.7. Figs 1.2 a,b show the calculated plots of log $(F_T/TSP)/A_T$ vs. $1/T$ for phenanthrene at two different TSP levels. For this relatively volatile SOC, a small increase in the percent bound material can result in a large increase in the apparent K_p at higher ambient temperatures. The importance of this effect decreases as TSP increases. Figs 1.2 c,d show plots of log $(F_T/TSP)/A_T$ vs. $1/T$ for benzo[*a*]pyrene at the same TSP levels. For this relatively non-volatile, strongly sorbing SOC, we observe that non-exchangeable

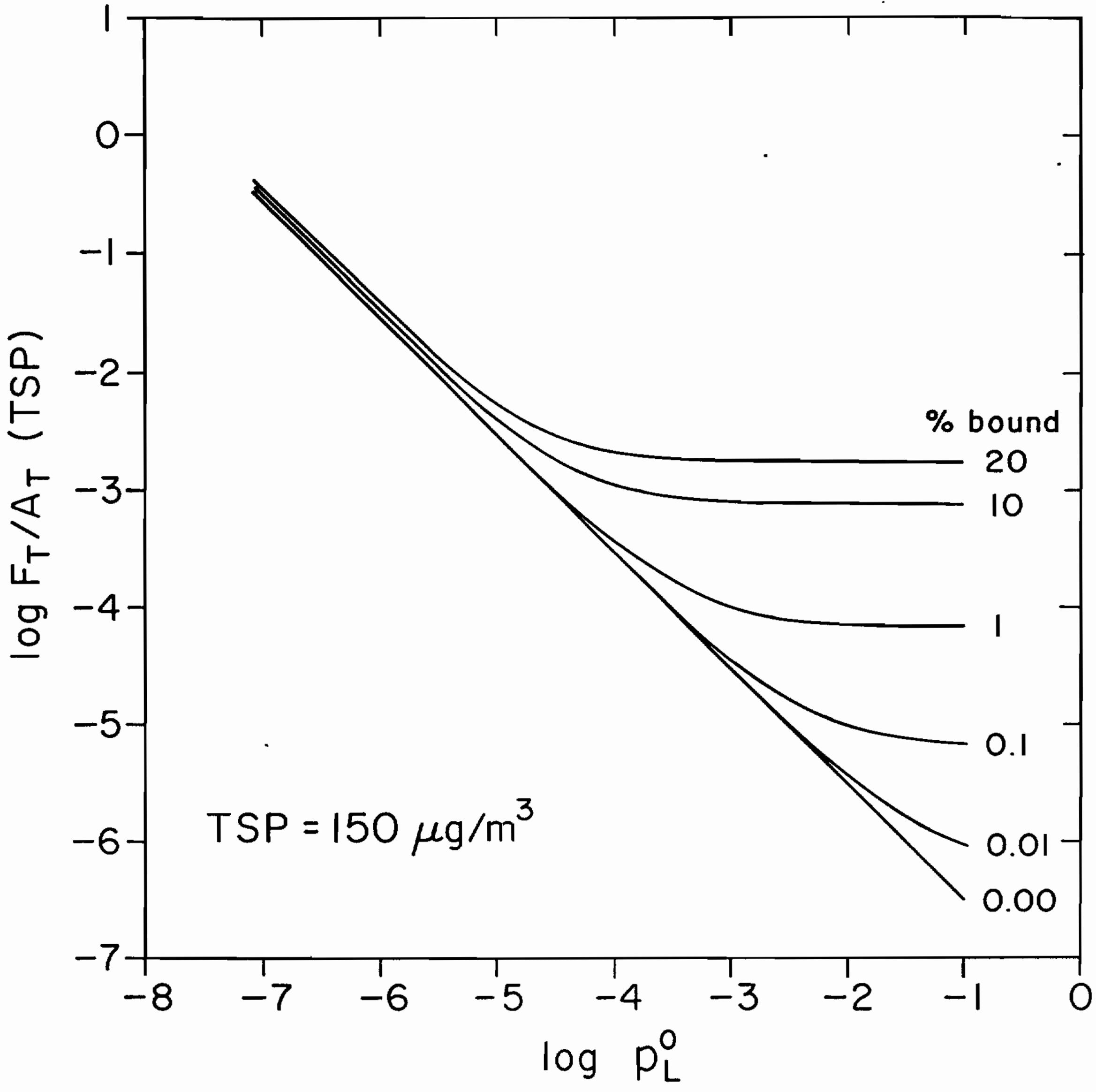

Fig. 1.1. Plots of log $(F_T/TSP)/A_T$ vs. log p_L^o at 293 K for TSP = 150 μg m^{-3} with various percentages (x) of bound compound. The value of x is assumed to be independent of p_L^o. The energetics of sorption are assumed to be similar to those for the PAHs. (Adapted from Pankow, 1988.)

material has little effect on the log *(F/TSP)/A* values, even at relatively high ambient temperatures.

1.3.2 Another Approach to the Estimation of Q_l Values

The Yamasaki *et al.* (1982) dataset was extensive enough to allow estimation of compound-dependent m_p and b_p values for Equation 1.5 using simple linear regression (SLR). However, the average degree of correlation for all compounds was low ($r^2 = 0.79$). Because the compounds studied by Yamasaki *et al.* (1982) were all members of the same compound class (i.e., all PAHs), Pankow (1991) has argued that another way to examine this important dataset is through a common y-intercept regression (CYIR) analysis. Therefore, assuming similar A_{TSP} values for the various sampling events, and similar characteristic molecular vibration times (t_0), Equation 1.7 shows that the b_p values for these compounds should all be very similar.

The details of the CYIR approach are given by Pankow (1991). Table 1.1 summarizes the Q_l values obtained by the CYIR analysis, as well as Q_v values obtained from the literature. One of the most significant results of that work is that the Q_l values determined by CYIR are much more highly correlated with the corresponding Q_v values ($r^2 = 0.991$) than are the Q_l values calculated by SLR ($r^2 = 0.590$). This provides strong support for the reliability of the m_p, b_p, and Q_l values obtained by CYIR.

1.3.3 Kinetics of Gas/Particle Partitioning

The study of gas/particle partitioning in the atmosphere requires accurate measures of *A* and *F* for given compounds. In addition to the non-exchangeable material effects discussed above, one must be concerned with artifacts due to sampling procedures. Another important problem is possible kinetic limitations on the approach to equilibrium between the gas phase and the particulate phase during a given sampling event. These effects can result in measured values of *(F/TSP)/A* being different from K_p. In an effort to describe the kinetics of sorption to APM, Rounds and Pankow (1990) adapted a radial diffusion model to describe the kinetics of the

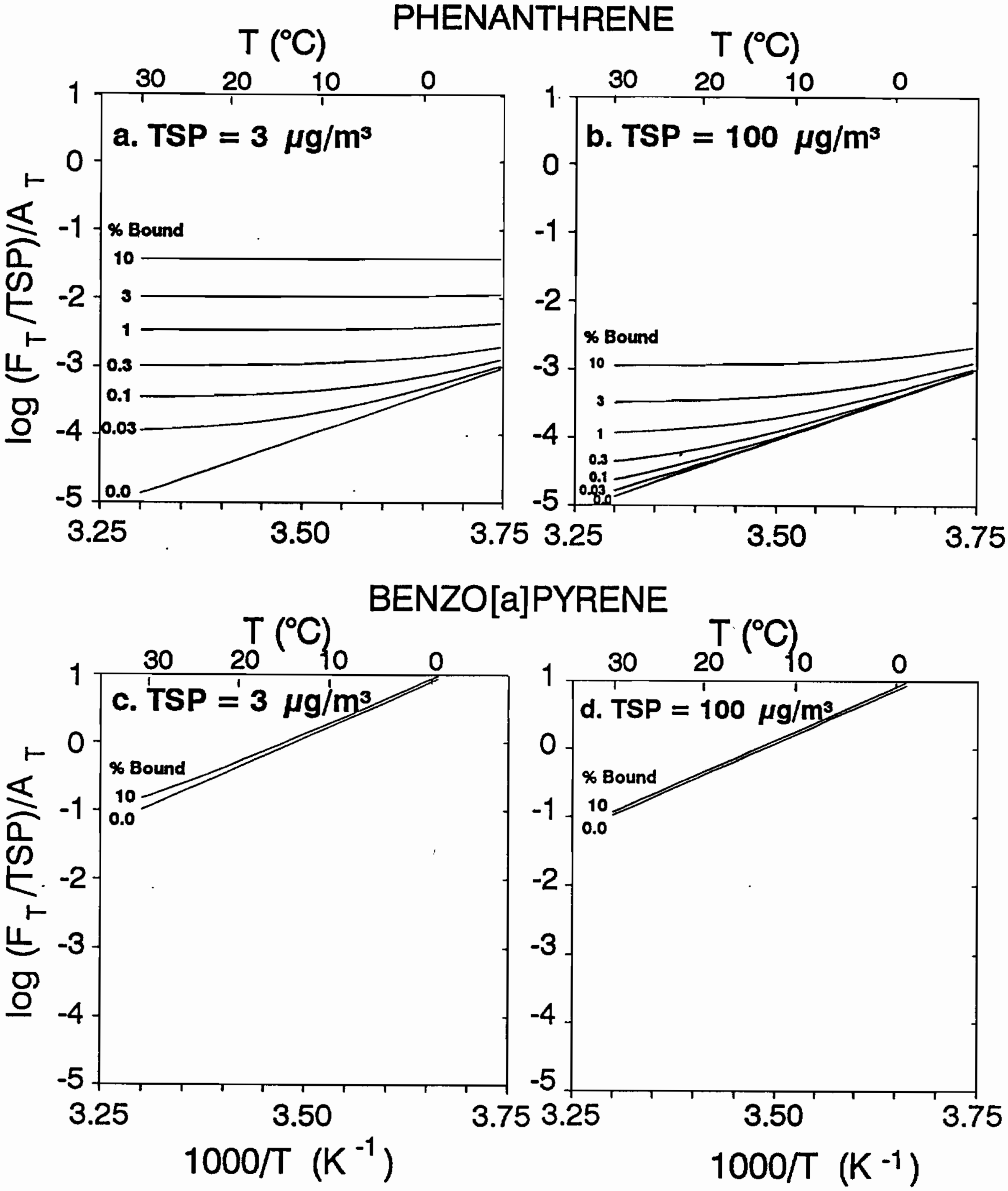

Fig. 1.2 Plots of log $(F_T/TSP)/A_T$ vs. $1/T$ for phenanthrene and benzo[*a*]pyrene for varying values of the non-exchangeable fraction (x), and varying values of *TSP*. The values of m_p and b_p are assumed to equal the CYIR values determined by Pankow (1991) for phenanthrene + anthracene for Osaka particulate matter, i.e., 4214 and -18.48, respectively. (Adapted from Pankow and Bidleman, 1991.)

Table 1.1. Q_l and Q_v Values at 298 °K for the Pure Sub-Cooled Liquids. Q_l Values Obtained by Fitting the PAH data of Yamasaki *et al.* (1982) Using a Common y-Intercept Regression (CYIR). Data from Pankow (1991).

Compound(s)	Q_l by CYIR (kJ mol^{-1})	Q_v^* (kJ mol^{-1})
Phenanthrene + Anthracene	80.2	71.3
Me-Phenanthrene + Me-Anthracene	82.4	-----
Fluoranthene	85.7	78.0
Pyrene	86.4	78.9
Benzo[*a*]fluorene + Benzo[*b*]fluorene	88.3	82.6
Chrysene + Triphenylene + Benz[*a*]anthracene	93.8	88.2
Benzo[*b*]fluoranthene + Benzo[*k*]fluoranthene	100.4	95.2
Benzo[*a*]pyrene + Benzo[*e*]pyrene	102.7	96.3

---

[*] Sub-cooled Q_v values according to Bidleman (1990). Where data are given for multiple compounds, the value given is the mean Q_v value. Values obtained by averaging the literature values cited in Yamasaki *et al.* (1984) with those of Hinckley *et al.* (1990), then regressing those values against the values of Yamasaki (1984). The final estimates were obtained by Bidleman (1990) by substituting the Yamasaki *et al.* (1984) values into the regression equation. Since the Yamasaki *et al.* (1984) data seems uniformly high, this method allows estimations of Q_v values for compounds studied only by Yamasaki *et al.* (1984), but as based on the non-Yamasaki database.

exchange of *n*-alkanes and PAHs between the gas and particulate phases in the atmosphere. The model, while not calibrated, does provide rough guidelines as to whether a compound is likely to display differences between measured values of $(F/TSP)/A$ and K_p that are kinetics-based. In a further study, Rounds *et al.* (1992) applied the model to the desorption of *n*-alkanes and PAHs from a highly particulate-loaded filter. They conclude that even for compounds with small values of K_p (i.e., $K_p < 10^{-5}$), adsorption to and desorption from particles is relatively slow, with a reaction time scale of hours to days depending on the conditions. For less volatile compounds, the time required to reach equilibrium is even longer. This work implies that ambient particles collected near a source may not have time to reach equilibrium with gas phase SOC prior to collection on a filter.

1.3.4 Summary of Field and Laboratory K_p Studies

While this section cannot possibly address all of the fine field and laboratory work that has been done since 1987, it will compile some of the results of these studies in the context of the previous discussion. From Eq. 1.8 above, one can see that when non-specific adsorption is the mechanism for gas/particle partitioning and when $(Q_l - Q_v)$ is roughly constant from compound to compound, then a plot of log K_p vs. log p_L^o should have a slope of -1 for similar compounds. Table 1.2 illustrates a compilation of the slopes and y-intercepts of various classes of SOCs from the last several years. While many of the values fall in the range -0.85 to -1.15, there are some slopes that are significantly lower and higher. Some reasons for the deviation from -1 might include sampling artifacts due to sorption of organics to the filter material (McDow and Huntzicker, 1990), volatilization of SOCs from the particulate matter on the filter (Zhang and McMurry, 1990) or possibly, variable thermodynamic effects due to variable relative humidity (Thibodeaux *et al.*, 1991). Furthermore, real differences in urban and rural particulate matter might be responsible for some of these variations. For instance, a marine aerosol, composed mainly of NaCl, might exhibit different sorption behavior than highly carbonaceous urban particulate matter.

Table 1.2. Values of m_r and b_r from Selected Studies. (Adapted from Pankow and Bidleman, 1992).

Compound Type	Air Type	Location	m_r	b_r	Reference
		Field Data			
PAHs	Urban	Denver	-0.76	-6.71	Foreman and Bidleman (1990)
PAHs	Urban	Portland	-0.88	-7.25	Ligocki and Pankow (1989)
PAHs	Urban	Osaka	-1.03	-8.11	Yamasaki *et al.* (1982)
PAHs	Rural	L. Superior	-0.59	-5.08	McVeety and Hites (1988)
PAHs	Rural	L. Superior	-0.61	-5.55	Baker and Eisenreich (1990)
PAHs	Rural	Oregon Coast	-0.98	-7.16	Ligocki and Pankow (1989)
Alkanes	Urban	Denver	-0.86	-7.29	Foreman and Bidleman (1990)
Alkanes	Urban	Portland	-0.87	-6.95	Hart (1990)
PCBs	Urban	Denver	-0.95	-7.87	Foreman and Bidleman (1990)
Pesticides	Urban	Denver	-0.93	-7.11	Foreman and Bidleman (1990)
Pesticides and PCBs	Urban	Columbia	-0.77	-7.31	Bidleman *et al.* (1986)
PCDDs and PCDFs	Urban	Bloomington	-1.15	-9.7	Eitzer and Hites (1989)
		Selected Laboratory Data Obtained with Urban Particulate Matter			
PAHs	Urban	Columbia	-1.18	-9.06	Foreman and Bidleman (1987)
Pesticides	Urban	Columbia	-0.98	-8.51	Foreman and Bidleman (1987)

1.4 Questions to Answer and Objective of This Research

This chapter has introduced the current understanding of gas/particle partitioning processes and has identified recent research into the partitioning behavior of SOCs on UPM. Evidence has accumulated that shows that a non-specific adsorptive process may be an important mechanism of gas/particle partitioning in the atmosphere. The question then becomes how can this knowledge be extrapolated to partitioning in non-urban/rural environments? Does the different makeup of continental particulate matter affect the manner in which SOCs partition to such material? If so, how does that affect the global fate and transport of these compounds? Answering these questions with field studies is very difficult. Field measurements of gas/particle partitioning to rural APM are subject to many variables including T, relative humidity (RH), the composition of APM, and the presence of absorbtive phases on the APM. Furthermore, the ambient concentrations of SOC in the rural environment are extremely low, and obtaining accurate A and F values can present tremendous analytical challenges (e.g. see Patton *et al.*, 1990).

A different approach to the above questions is to use laboratory studies to examine the gas/solid partitioning of SOCs. The objective of this research is to characterize the gas/solid partitioning of SOCs in the laboratory with control of the following variables: T and relative humidity (RH); the gas phase concentration of the SOCs. All of these factors carry the potential to greatly affect the value of K_p for a given compound. No previous study has systematically looked at K_p as a function of RH, even though RH varies widely in the field. Furthermore, by using model systems to examine gas/solid partitioning, the results can be compared to field studies to assess the ability of simple, physical adsorption to describe gas/particle partitioning in the atmosphere. This comparison represents an important contribution to the field, and can provide a feasible method of incorporating gas/particle partitioning into compartmental models which describe the global fate of SOCs.

CHAPTER 2

THE GAS/SOLID SORPTION OF SOCS TO FOUR MODEL ATMOSPHERIC PARTICULATE MATERIALS COMPARED TO THE GAS/PARTICLE PARTITIONING BEHAVIOR OF SOCS TO URBAN PARTICULATE MATERIAL

Yamasaki *et al.* (1982) obtain gas/particle partitioning data over a 30 °C range in their year-long study of UPM in Osaka. Their data can be used to compare measured K_p values for the same compounds for different samples *at different temperatures.* While comparison of the Yamasaki *et al.* (1982) K_p values with other field studies can indicate whether gas/particle partitioning of a PAH occurs to an extent that is similar to what was observed in Osaka, it cannot tell if the gas/particle partitioning process is absorptive or adsorptive in nature. However, a comparison of their data with data from a gas/solid sorption experiment using non-porous aerosols may reveal if the mechanism of gas/particle partitioning in the urban environment can be modeled by simple, physical adsorption. A model system, used to determine the temperature dependence of PAH sorption to aerosols of four well-defined materials, is discussed, and the results are compared with field measurements of the gas/particle partitioning of PAHs.

2.1 K_p vs. $1/T$ and Linear Langmuirian Adsorption

As mentioned previously, Yamasaki *et al.* (1982) found that log K_p values for PAHs depend inversely on T according to:

$$\log K_p = \frac{m_p}{T} + b_p \qquad (1.5)$$

According to Equation 1.6 and Equation 1.7, for simple, physical adsorption, the slope, m_p is dependent on Q_l, the enthalpy of desorption. The y-intercept, b_p, depends inversely on A_{TSP}, and will be similar for compounds of similar M and structure. Many researchers have found both in the field and in the laboratory that at a given T, the K_p for a given SOC is very similar for UPM, no matter where the UPM is collected. For example, Benner *et al.* (1989) measured values of (A/F) for PAHs on UPM in Baltimore, and then compared those values to (A/F) values predicted by the simple linear regression (SLR) equations of Yamasaki *et al.* (1982) for log $(F/TSP/A)$ vs $1/T$. Table 2.1 shows the remarkable agreement in this comparison for 12 samples and two compounds, phenanthrene and pyrene. There is often less than a twofold difference in the values. The close agreement between the observed and predicted values, however, does not indicate whether the gas/particle partitioning is absorptive or adsorptive in nature, only that the partitioning is similar. To distinguish between absorption and adsorption, one might compare gas/solid physical adsorption data with the gas/particle partitioning data of Yamasaki *et al.* (1982).

2.2 Sorption of PAHs to Aerosols Composed of Four Different Materials

2.2.1 Description of the Model System

In order to help determine whether gas/particle partitioning in urban air is governed by non-specific, physical adsorption, Storey and Pankow (1992) compared the Yamasaki *et al.* (1982) data to PAH gas/solid sorption data obtained by Niessner and Wilbring (1989). Niessner and Wilbring (1989) studied the sorption behavior of PAH to aerosols of graphitic carbon, $NaCl_{(s)}$, alumina ($Al_2O_{3\,(s)}$) and silica ($SiO_{2\,(s)}$) as "Aerosil 200". While those authors discussed their experiment in the context of developing methods for the *in-situ* monitoring of PAH sorption processes in higher temperature combustion processes, their results can be interpreted in the light of existing ambient temperature gas/particle partitioning theory. The authors graciously provided our research group with their experimental data. Their paper provides a complete description of their experimental methods, so only a brief summary is presented here.

Table 2.1 Observed and predicted* gas/particle ratios (*A/F*) for PAHs on UPM from Benner *et al.* (1989).

sample	TSP ($\mu g/m^3$)	phenanthrene obs *A/F*	phenanthrene pred *A/F*	pyrene obs *A/F*	pyrene pred *A/F*
A	1328	3.1	3.7	0.3	0.3
B	709	10.2	7.0	1.6	0.5
C	635	6.6	7.8	0.8	0.6
D	532	6.5	9.8	0.9	0.7
E	424	8.2	13.0	1.2	1.0
F	349	9.8	16.0	1.0	1.2
G	330	7.4	13.0	1.0	1.0
H	276	7.4	20.0	0.8	1.5
I	198	12.8	28.0	1.7	2.1
J	96	29.3	51.0	3.9	3.7

---

* predicted from the equation: $\log \frac{F/TSP}{A} = \frac{m_p}{T} + b_p$ by using the Yamasaki *et al.* (1982) m_p and b_p values with the values of *TSP* and *T* as measured by Benner *et al.* (1989).

A mono-disperse aerosol (19nm) of sorbent particles was generated and exposed to the vapors from a single PAH, then cooled to 13 °C in a flow tube. The cooling allowed the PAH in the gas phase to sorb onto the particles, or onto the walls of the tube. Niessner and Wilbring (1989) concluded the coverage on the particles was always less than a monolayer. In every case, the initial particle concentration was taken to be 55,000 cm^{-3}. The initial *TSP* (TSP_i, $\mu\mathrm{g\ m}^{-3}$) levels at the initial temperature (T_i, K) were 0.454 $\mu\mathrm{g\ m}^{-3}$, 0.429 $\mu\mathrm{g\ m}^{-3}$, 0.782 $\mu\mathrm{g\ m}^{-3}$, 0.523 $\mu\mathrm{g\ m}^{-3}$, for the graphitic carbon, $NaCl_{(s)}$, alumina and silica respectively. Densities of 2.30, 2.17, 3.96, and 2.65 g cm^{-3}, respectively for the four materials, have been assumed here.

The coated particles were then desorbed in a tubular heater at incrementally higher temperatures. The gas phase PAH was removed by a denuder system, and the PAH remaining on the particles was analyzed with a photoelectric (*PE*) aerosol sensor. If one assumes 100% efficiency for the denuders, and then no loss of PAHs on the particles to the denuder, then only the PAH molecules remaining on the particles after the thermal desorption step were measured with the *PE* aerosol sensor.

Niessner and Wilbring present their desorption data in terms of per cent *PE* signal vs. *T*. Fig. 2.1 shows what a typical desorption curve looks like. Niessner and Wilbring (1989) show that *PE* represents the percent of the PAH in the particulate phase. Therefore, a *measured* estimate of the partitioning coefficient, K_p, can be expressed by:

$$\frac{(F/TSP)}{A} = \frac{PE}{1-PE}\,\frac{1}{TSP_i(T_i/T)} \tag{2.1}$$

where the T_i/T term corrects the *TSP* values for the thermal expansion of the gas in the heated part of the desorber.

By using Equation 2.1, the Niessner and Wilbring data (1989) can be plotted in a log *(F/TSP)/A* vs. $1/T$ format just as the data in Yamasaki *et al.* (1982). Because Yamasaki *et al.* (1982) and Niessner and Wilbring (1989) examined some of the same compounds, the gas/particle partitioning behavior of these compounds can be compared in Fig. 2.2 - Fig. 2.5. Each sub-plot contains common y-intercept regression

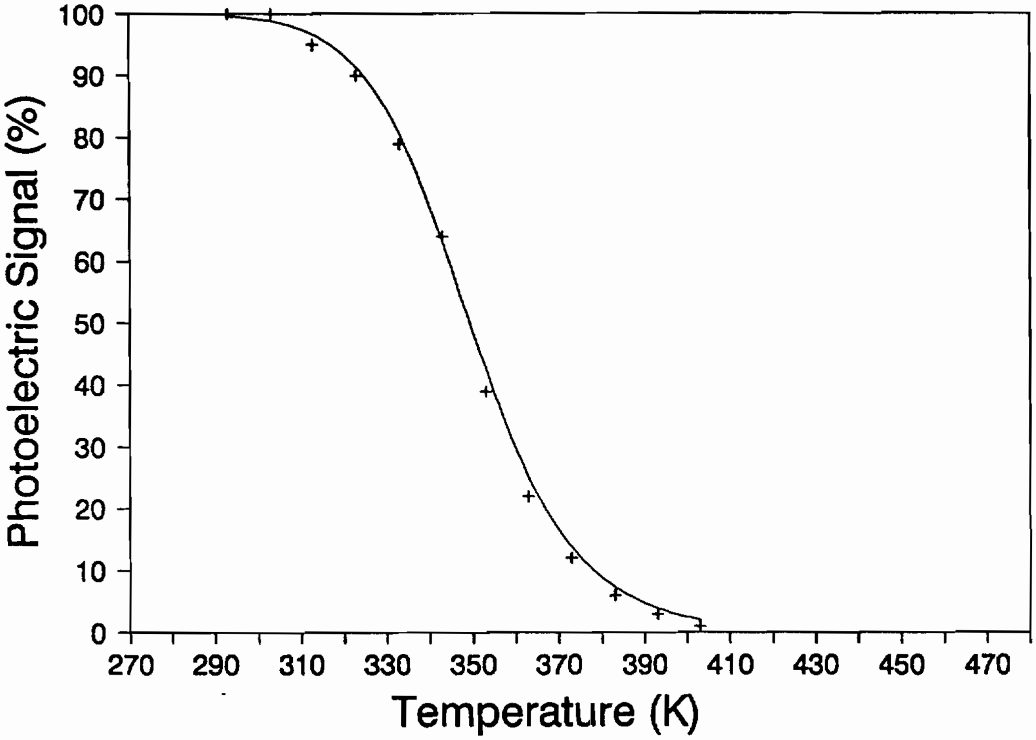

Fig. 2.1. Percent photoelectric signal vs. T for desorption of benzo[*a*]pyrene from graphitic carbon. Data courtesy of Niessner and Wilbring (1990). (Reproduced with permission from Storey and Pankow, 1992.)

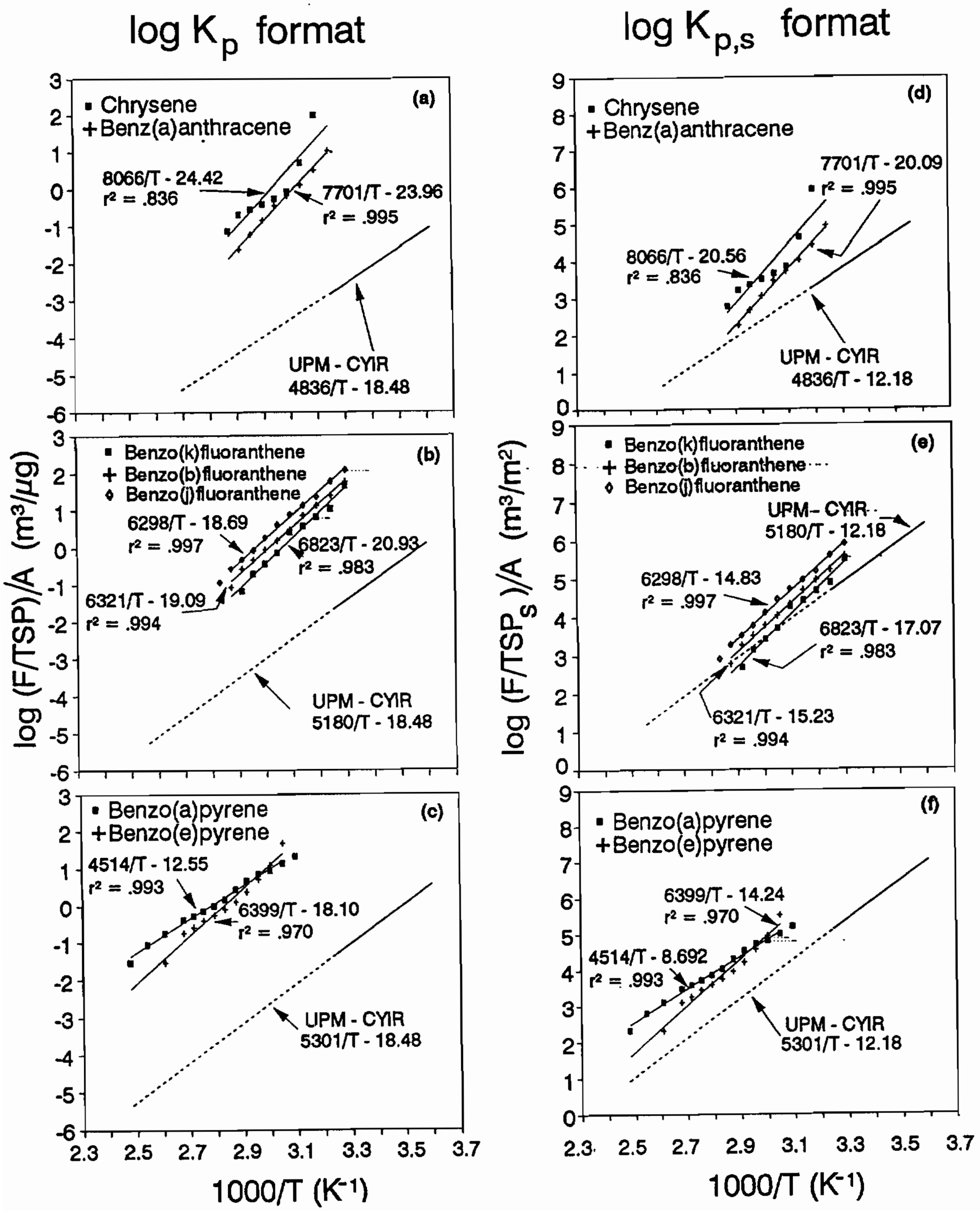

Fig. 2.2. Log *(F/TSP)/A* vs. *1/T* and log *(F/TSP$_s$)/A* vs. *1/T* for PAHs on graphitic carbon and on urban particulate material (UPM). The UPM lines are those obtained by Pankow (1991) using a common y-intercept regression (CYIR). The conversions from *(F/TSP)/A* to *(F/TSP$_s$)/A* assume A_{TSP} values of 1.37 and 0.025 cm^2 µg^{-1} for the graphitic carbon and UPM, respectively. (Reproduced with permission from Storey and Pankow, 1992.)

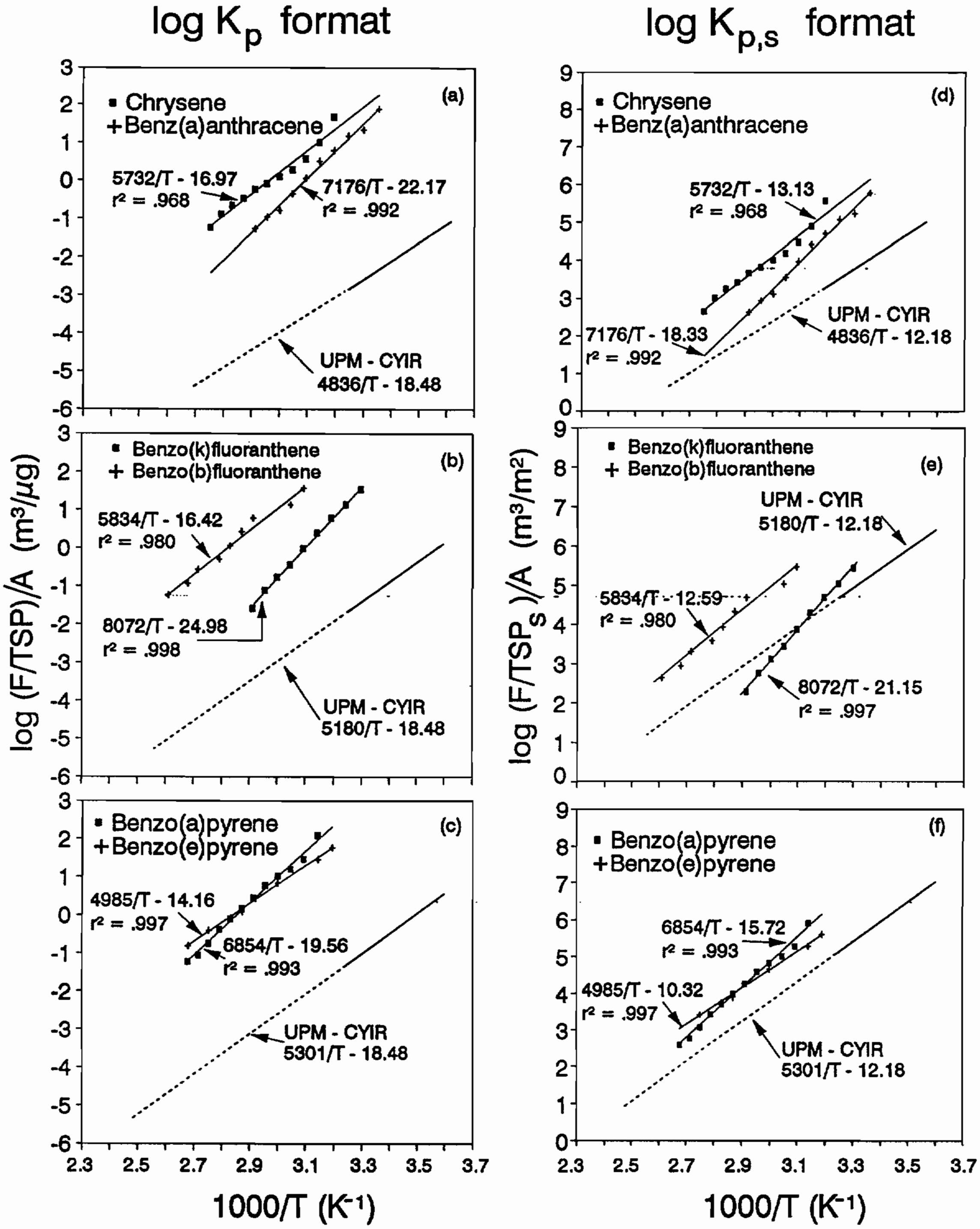

Fig. 2.3. Log *(F/TSP)/A* vs. 1/*T* and log *(F/TSP$_s$)/A* vs. 1/*T* for PAHs on $NaCl_{(s)}$ and on urban particulate material (UPM). The UPM lines are those obtained by Pankow (1991) using a common y-intercept regression (CYIR). The conversions from *(F/TSP)/A* to *(F/TSP$_s$)/A* assume A_{TSP} values of 1.46 and 0.025 cm^2 μg^{-1} for the $NaCl_{(s)}$ and UPM, respectively. (Reproduced with permission from Storey and Pankow, 1992.)

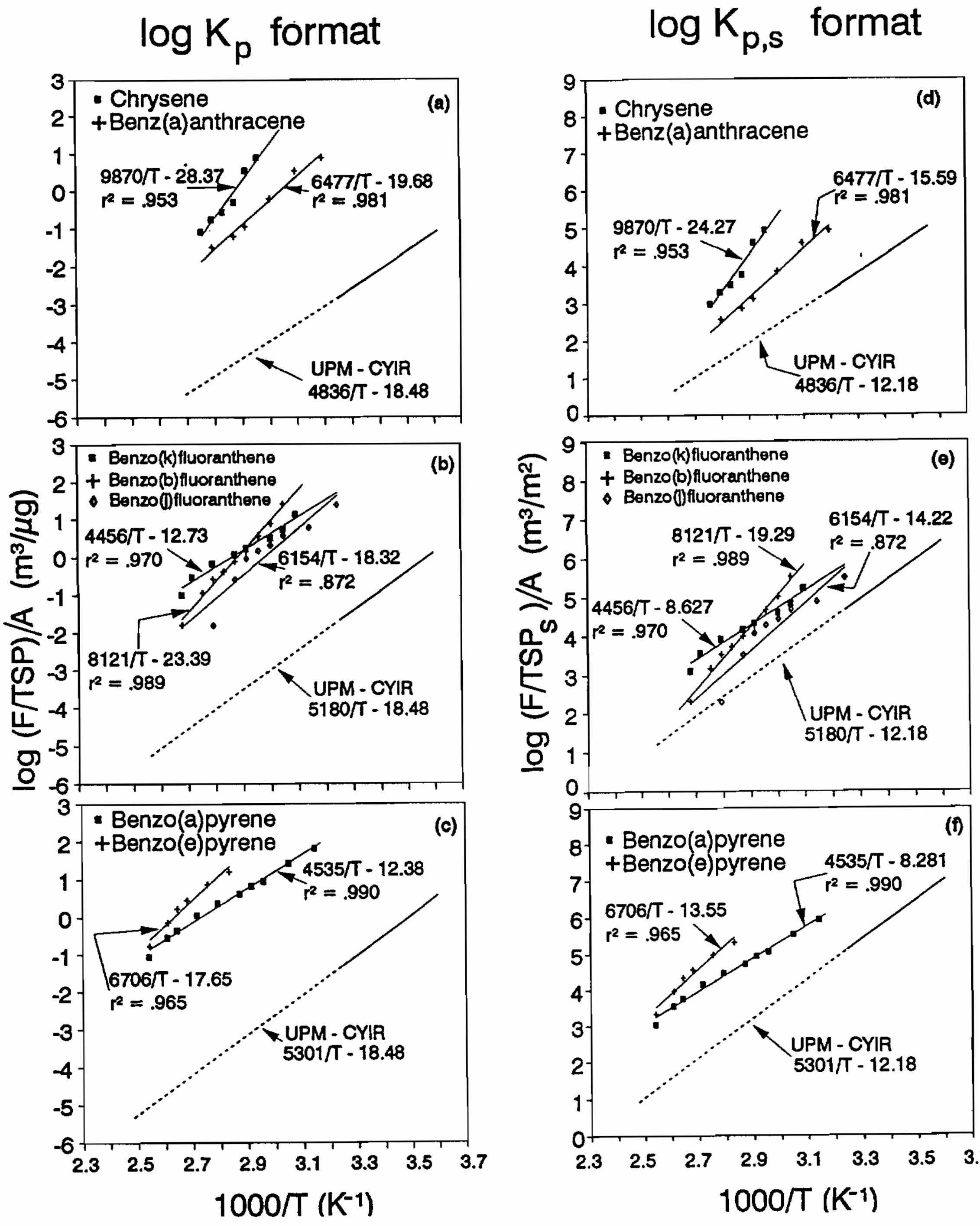

Fig. 2.4. Log *(F/TSP)/A* vs. 1/*T* and log *(F/TSP$_s$)/A* vs. 1/*T* for PAHs on alumina and on urban particulate material (UPM). The UPM lines are those obtained by Pankow (1991) using a common y-intercept regression (CYIR). The conversions from *(F/TSP)/A* to *(F/TSP$_s$)/A* assume A_{TSP} values of 0.796 and 0.025 cm² µg^{-1} for the alumina and UPM, respectively. (Reproduced with permission from Storey and Pankow, 1992.)

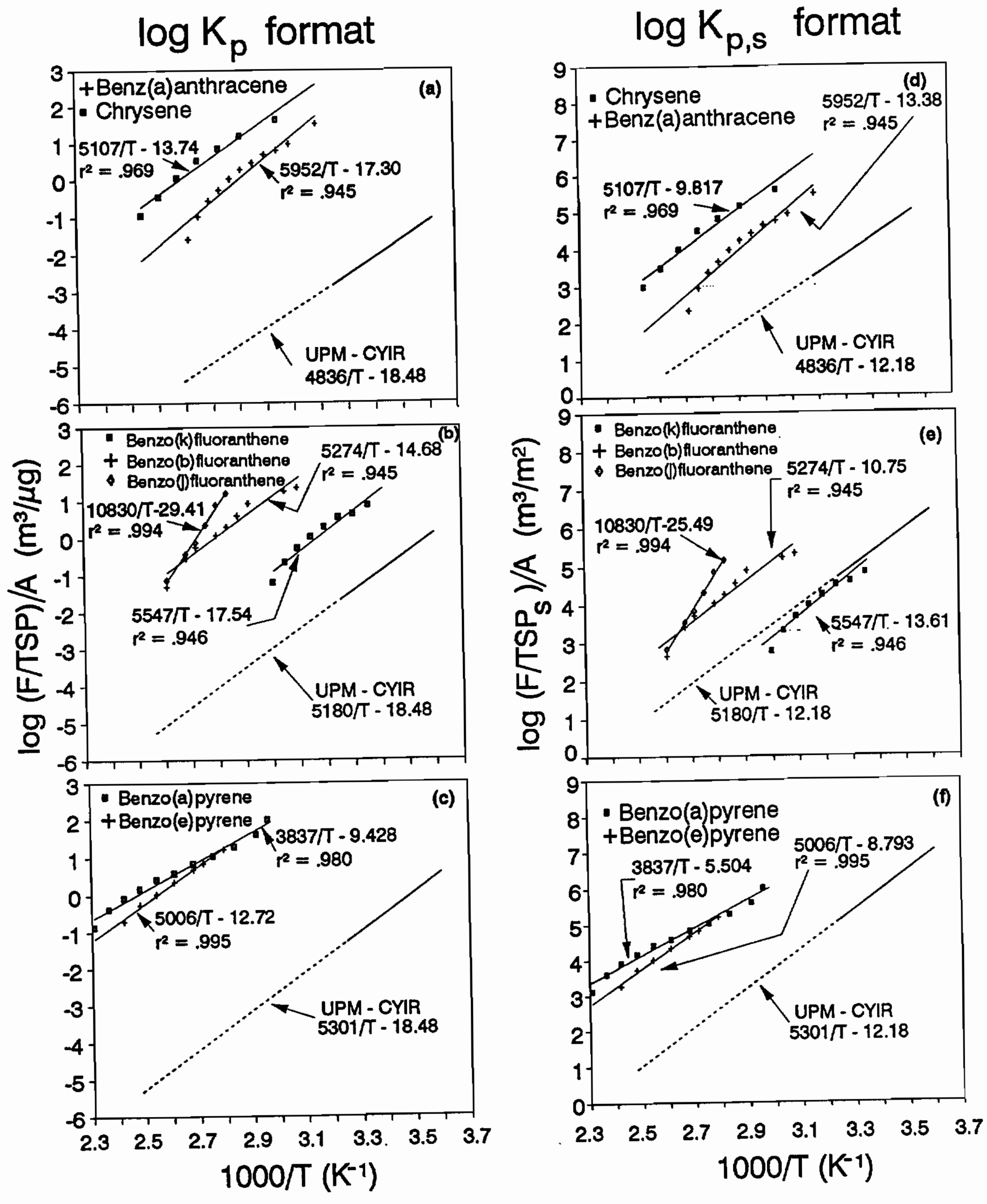

Fig. 2.5. Log *(F/TSP)/A* vs. 1/*T* and log *(F/TSP$_s$)/A* vs. 1/*T* for PAHs on silica and on urban particulate material (UPM). The UPM lines are those obtained by Pankow (1991) using a common y-intercept regression (CYIR). The conversions from *(F/TSP)/A* to *(F/TSP$_s$)/A* assume A_{TSP} values of 1.19 and 0.025 cm² µg⁻¹ for the silica and UPM, respectively. (Reproduced with permission from Storey and Pankow, 1992.)

(CYIR) lines for the Yamasaki dataset as determined by Pankow (1991) for one or more corresponding PAH isomers. Hereinafter, these lines will be referred to as the UPM-CYIR lines. In Fig. 2.2 - Fig. 2.5, the UPM-CYIR lines appear with both dashed and solid portions. The solid portion of the line refers to the range of $1/T$ values for the Yamasaki *et al.* (1982) data. The dashed portion is an extrapolation to the lower $1/T$ (higher T) values of the Niessner and Wilbring (1989) data.

2.2.2 $K_{p,s}$, a Surface-Area-Normalized Partition Coefficient

The offset of the lines in Fig. 2.2 - Fig. 2.5 is largely dependent upon the y-intercept, b_p, as given in Equation 1.7. The difference between A_{TSP} for two particulate materials can change the K_p value a like amount for a given SOC at a given T. Therefore, it is useful to define a surface-area-normalized partition coefficient, $K_{p,s}$, such that:

$$K_{p,s} = \frac{(F/TSP_s)}{A} \tag{2.5}$$

where TSP_s is simply a measure of the surface area concentration with units of m^2m^{-3}, so that $K_{p,s}$ has units of m^3m^{-2}. As noted by Storey and Pankow (1992), $TSP_s = TSP{\cdot}A_{TSP}/10^4$. A plot of log $K_{p,s}$ vs. $1/T$ is similar to a log K_p vs. $1/T$ plot, except that the dependence on A_{TSP} in the y-intercept has been removed.

2.2.3 Sorption to Graphitic Carbon and $NaCl_{(s)}$

Of the four aerosol types studied by Niessner and Wilbring (1989), carbon and $NaCl_{(s)}$ aerosols may be expected to sorb least specifically and are discussed first; the more active alumina and silica surfaces are expected to exhibit more specific type sorption processes and are discussed second. Fig. 2.2(a-c) and Fig. 2.3(a-c) contain the desorption data for PAHs from graphitic carbon and $NaCl_{(s)}$, respectively, and the UPM-CYIR line for the same PAH isomers, all in the log K_p (i.e. log $(F/TSP)/A$) vs $1/T$ format. The desorption lines have slopes that are very similar to the UPM-CYIR lines. The position of the lines in both Fig. 2.2 and Fig. 2.3, however, is shifted by

3-5 log units in the y-direction. From Equation 2.4, this shift can be attributed to the larger A_{TSP} of the Niessner and Wilbring (1989) aerosol compared to the UPM of Yamasaki *et al.* (1982).

To compare the two sets of data more directly, the right halves of Fig. 2.2 and Fig. 2.3 use the $K_{p,s}$ format and show the log $(F/TSP_s)/A$ values for the model system and the Yamasaki *et al.* (1982) UPM. In Fig. 2.2 and Fig. 2.3 (d-f), the A_{TSP} values were assumed to be 1.37 $cm^2 \mu g^{-1}$ and 1.46 $cm^2 \mu g^{-1}$ for the graphitic carbon and $NaCl_{(s)}$ aerosols respectively. These A_{TSP} values are based on assumed 19 nm spherical geometry and the densities of the two materials. For the UPM-CYIR lines, a rough estimate of 0.025 $cm^2 \mu g^{-1}$ was used for A_{TSP} (Pankow, 1987). For the benzofluoranthenes in Fig. 2.2 (e), there is great similarity between the log $(F/TSP_s)/A$ values for sorption on graphitic carbon and on $NaCl_{(s)}$. Also, the lines for chrysene, benz[*a*]anthracene and the benzopyrenes are much closer to the UPM-CYIR lines in Figs 2.2(d) and 2.2(f) than in 2.2(a) and 2.2(c). For partitioning to $NaCl_{(s)}$, the corresponding log $(F/TSP_s)/A$ values also bring the lines closer together although the agreement is not as good as that for the graphitic carbon. The most striking difference, however, between Fig. 2.2 and Fig. 2.3 is the dissimilar behavior of benzo[*k*]fluoranthene and benzo[*b*]fluoranthene. (Niessner and Wilbring did not look at the desorption of benzo[*j*]fluoranthene from NaCl.) In Fig. 2.2, these compounds exhibited very similar sorption to the graphitic carbon aerosol. However, the NaCl seems to bind the two isomers differently. Benzo[*b*]fluoranthene seems to have the slope and y-intercept values that are the closest to the Yamasaki *et al.* (1982) values, suggesting that the Yamasaki *et al.* (1982) benzofluoranthenes might have been predominately benzo[*b*]fluoranthene. In fact, many researchers have found an approximately 3:1 ratio of benzo[*b*]fluoranthene to benzo[*k*]fluoranthene in the field (e.g. Dennis *et al.*, 1983; Tan and Heit, 1981; Olufsen *et al.*, 1980).

2.2.4 Sorption to Alumina and Silica

Figures 2.4 and 2.5 show the sorption behavior of the PAHs on alumina and silica aerosols. These surfaces might be expected to bind more specifically than graphitic carbon and NaCl. The lower values of $1/T$, hence higher T, and higher values of log $(F/TSP)/A$ suggest a high enthalpy of sorption. The log $(F/TSP_s)/A$ lines plotted in Fig. 2.4(d-f) and Fig. 2.5(d-f) are obtained using values of A_{TSP} of 0.796 $cm^2 \mu g^{-1}$ (alumina) and 1.19 $cm^2 \mu g^{-1}$ (silica), again assuming 19 nm spheres for the particles. The correction for A_{TSP} does not bring the points much closer to the UPM-CYIR line. However, a specific sorption mechanism usually suggests a higher Q_l value than for non-specific sorption, and this is not consistent with the lower slope values as compared to those for graphitic carbon and $NaCl_{(s)}$. Becasue of the higher T values, extrapolation of the UPM-CYIR line may be unreliable. Another possible problem is incorrect values of A_{TSP} for both alumina and silica. If the aerosols had significant internal porosity, as suggested by Niessner and Wilbring (1989), then the log $(F/TSP_s)/A$ values would be smaller and hence closer to the UPM-CYIR values.

2.2.5 Enthalpies of Desorption

The slopes of the Niessner and Wilbring (1989) data obtained by SLR allow calculation of the enthalpies of desorption (Q_l) based on Equation 1.6. These estimates are contained in Table 2.2. In addition, Table 2.2 contains the values of slopes calculated by CYIR for the graphitic carbon, $NaCl_{(s)}$, alumina and silica, along with the corresponding Q_l values. The UPM-CYIR slopes and Q_l values from Pankow (1991) are also included for comparison. A brief look at Table 2.2 reveals some peculiar Q_l values and groups of values. In particular, the SLR derived Q_l values for benzo[*e*]pyrene and benzo[*a*]pyrene differ by 30-60% for all four of the sorbents, yet the similar structure of the two isomers would not suggest there would be that much difference for a given sorbent. Because Niessner and Wilbring (1989) studied each PAH individually, there may have been some difference in experimental conditions for the benzo[*a*]pyrene and benzo[*e*]pyrene that was not reported. A full discussion of Table 2.2 appears in Storey and Pankow (1992).

Table 2.2 Mean regression temperature, slope, intercept, and Q_l (kJ mol^{-1}) estimates for PAHs on four model sorbents and on urban particulate matter (from Storey and Pankow, 1992). Chr = chrysene; B*a*A = benz[*a*]anthracene; Tri = triphenylene; B*k*F = benzo[*k*]fluoranthene; B*b*F = benzo[*b*]fluoranthene; B*j*F = benzo[*j*]fluoranthene; B*a*P = benzo[*a*]pyrene; and B*e*P = benzo[*e*]pyrene.

		Carbon - SLR			Carbon - CYIR			UPM-CYIR†		
Compound	Mean *T*	m_p	b_p	Q_l	m_p	b_p	Q_l	m_p	b_p	Q_l
Chr	330.6	8066	-24.42	155.8	5720	-17.31	110.9	-	-	-
B*a*A	325.6	7701	-23.96	148.8	5540	-17.31	107.4	-	-	-
Chr+B*a*A+ Tri	290.2	-	-	-	-	-	-	4836	-18.48	93.8
B*k*F	320.6	6823	-20.93	132.0	5656	-17.31	109.6	-	-	-
B*b*F	325.6	6321	-19.09	122.4	5742	-17.31	111.3	-	-	-
B*j*F	328.1	6298	-18.69	122.0	5845	-17.31	113.3	-	-	-
B*k*F+B*b*F+ B*j*F	291.0	-	-	-	-	-	-	5180	-18.48	100.4
B*a*P	354.8	4514	-12.55	87.9	6199	-17.31	120.2	-	-	-
B*e*P	353.6	6399	-18.10	124.0	6118	-17.31	118.6	-	-	-
B*a*P+B*e*P	293.7	-	-	-	-	-	-	5301	-18.48	102.7

		$NaCl_{(s)}$ - SLR			$NaCl_{(s)}$ - CYIR			UPM-CYIR		
Compound	Mean *T*	m_p	b_p	Q_l	m_p	b_p	Q_l	m_p	b_p	Q_l
Chr	338.1	5732	-16.97	111.2	6232	-18.45	120.7	-	-	-
B*a*A	320.6	7176	-22.17	138.8	5989	-18.45	116.0	-	-	-
Chr+B*a*A+ Tri	290.2	-	-	-	-	-	-	4836	-18.48	93.8
B*k*F	353.0	8072	-24.98	156.0	5968	-18.45	115.8	-	-	-
B*b*F	323.1	5834	-16.42	113.1	6545	-18.45	126.7	-	-	-
B*k*F+B*b*F	291.0	-	-	-	-	-	-	5180	-18.48	100.4
B*a*P	345.6	6854	-19.56	132.7	6473	-18.45	125.4	-	-	-
B*e*P	343.1	4985	-14.16	96.9	6450	-18.45	124.9	-	-	-
B*a*P+B*e*P	293.7	-	-	-	-	-	-	5301	-18.48	102.7

---

† UPM-CYIR values from Pankow (1991).

Table 2.2 (cont.)

		Alumina - SLR			Alumina - CYIR			UPM-CYIR		
Compound	Mean *T*	m_p	b_p	Q_l	m_p	b_p	Q_l	m_p	b_p	Q_l
Chr	350.6	9870	-28.37	190.5	5605	-16.19	108.8	-	-	-
B*a*A	336.4	6477	-19.68	125.4	5306	-16.19	103.0	-	-	-
Chr+B*a*A+ Tri	290.2	-	-	-	-	-	-	4836	-18.48	93.8
B*k*F	346.9	4456	-12.73	86.8	5652	-16.19	109.7	-	-	-
B*b*F	348.7	8121	-23.39	157.0	5620	-16.19	109.1	-	-	-
B*j*F	334.4	6154	-18.32	119.2	5445	-16.19	105.7			
B*k*F+B*b*F+ B*j*F	291.0	-	-	-	-	-	-	5180	-18.48	100.4
B*a*P	355.6	4535	-12.38	88.3	5878	-16.19	114.0	-	-	-
B*e*P	373.9	6706	-17.65	130.0	6163	-16.19	119.6	-	-	-
B*a*P+B*e*P	293.7	-	-	-	-	-	-	5301	-18.48	102.7

		Silica - SLR			Silica - CYIR			UPM-CYIR		
Compound	Mean *T*	m_p	b_p	Q_l	m_p	b_p	Q_l	m_p	b_p	Q_l
Chr	362.4	5107	-13.74	99.3	4660	-12.50	90.7	-	-	-
B*a*A	346.9	5952	-17.30	115.4	4370	-12.50	85.1	-	-	-
Chr+B*a*A+ Tri	290.2	-	-	-	-	-	-	4836	-18.48	93.8
B*k*F	315.6	5547	-17.54	107.5	3961	-12.50	77.2	-	-	-
B*b*F	353.1	5274	-14.68	102.5	4509	-12.50	87.8	-	-	-
B*j*F	366.4	10830	-29.41	208.9	4640	-12.50	90.4			
B*k*F+B*b*F+ B*j*F	291.0	-	-	-	-	-	-	5180	-18.48	100.4
B*a*P	383.6	3837	-9.43	75.1	4999	-12.50	97.3	-	-	-
B*e*P	384.5	5006	-12.72	97.5	4923	-12.50	95.9	-	-	-
B*a*P+B*e*P	293.7	-	-	-	-	-	-	5301	-18.48	102.7

2.3 Summary

The close agreement between the Yamasaki *et al.* (1982) and the Benner *et al.* (1989) data is intriguing, but does not imply any particular mechanism. To resolve the question of mechanism, the Yamasaki *et al.* (1982) is compared to gas/solid sorption experiments with single PAHs and non-porous aerosols. In particular, surface-area-normalized partitioning (log $(F/TSP_s)/A$ values) of PAHs to aerosols of pure materials, graphitic carbon, $NaCl_{(s)}$, alumina and silica, is compared to the observed log $(F/TSP_s)/A$ values of PAHs to UPM as a function of T. Agreement is good between the graphitic carbon, a surface that might have been expected to sorb compounds in a non-specific manner, and the UPM. However, the agreement is less good for $NaCl_{(s)}$, and not good at all for alumina and silica. One possible explanation is incorrect A_{TSP} values for these materials. (The A_{TSP} values were calculated assuming smooth, uniform spherical geometry.) Furthermore, the extrapolation of the UPM-CYIR lines to the much higher temperatures of the Niessner and Wilbring (1989) study may also be a major source of error. In fact, it is known that Q_l values depend on T, and so we know that there will always be some error in such extrapolations.

The gas/solid partitioning experiments presented later in this thesis address the specific difficulties of the Niessner and Wilbring (1989) model system; the A_{TSP} of the model atmospheric particulate is known and the experiments were done under conditions of ambient T and RH.

CHAPTER 3

EFFECTS OF EXPERIMENTAL CONDITIONS AND SAMPLING ARTIFACTS ON THE DEPENDENCE OF MEASURED GAS/PARTICLE PARTITIONING ON VAPOR PRESSURE

A variety of field and laboratory experiments have been used to study the dependence of the gas/solid partitioning behavior for individual SOCs on temperature (e.g., see Yamasaki *et al.*, 1982; Niessner and Wilbring, 1989; Cotham and Bidleman, 1992). In contrast, a single sampling event or laboratory experiment can be used to investigate the dependence of K_p on the sub-cooled liquid vapor pressure (p_L^o) of the SOCs of interest. Knowing the dependence of K_p on p_L^o for some SOCs can helpin estimating the behavior of other SOCs in the atmospheric environment. For gas/solid partitioning, Pankow (1987, 1991) has derived that

$$K_p = \log \frac{N_s A_{TSP} T e^{(Q_1 - Q_v)/RT}}{16 p^o{}_L} \tag{3.1}$$

where N_s (mol cm^{-2}) is the surface concentration of sorption sites, and the other parameters have been defined above. This relationship can be used to look at individual gas/solid partitioning experiments, and then each experiment as a whole can be compared with other experiments.

For a given gas/solid partitioning experiment, the data are often presented as a plot of log *(F/TSP)/A* (log *measured* K_p) vs. log p_L^o. As expected from Eq. 3.1, these plots often exhibit a high degree of correlation (e.g., see Fig. 3.1). If the mechanism for gas/solid partitioning is simple, physical adsorption, and if N_s and $e^{(Q_1-Q_v)/RT}$ is

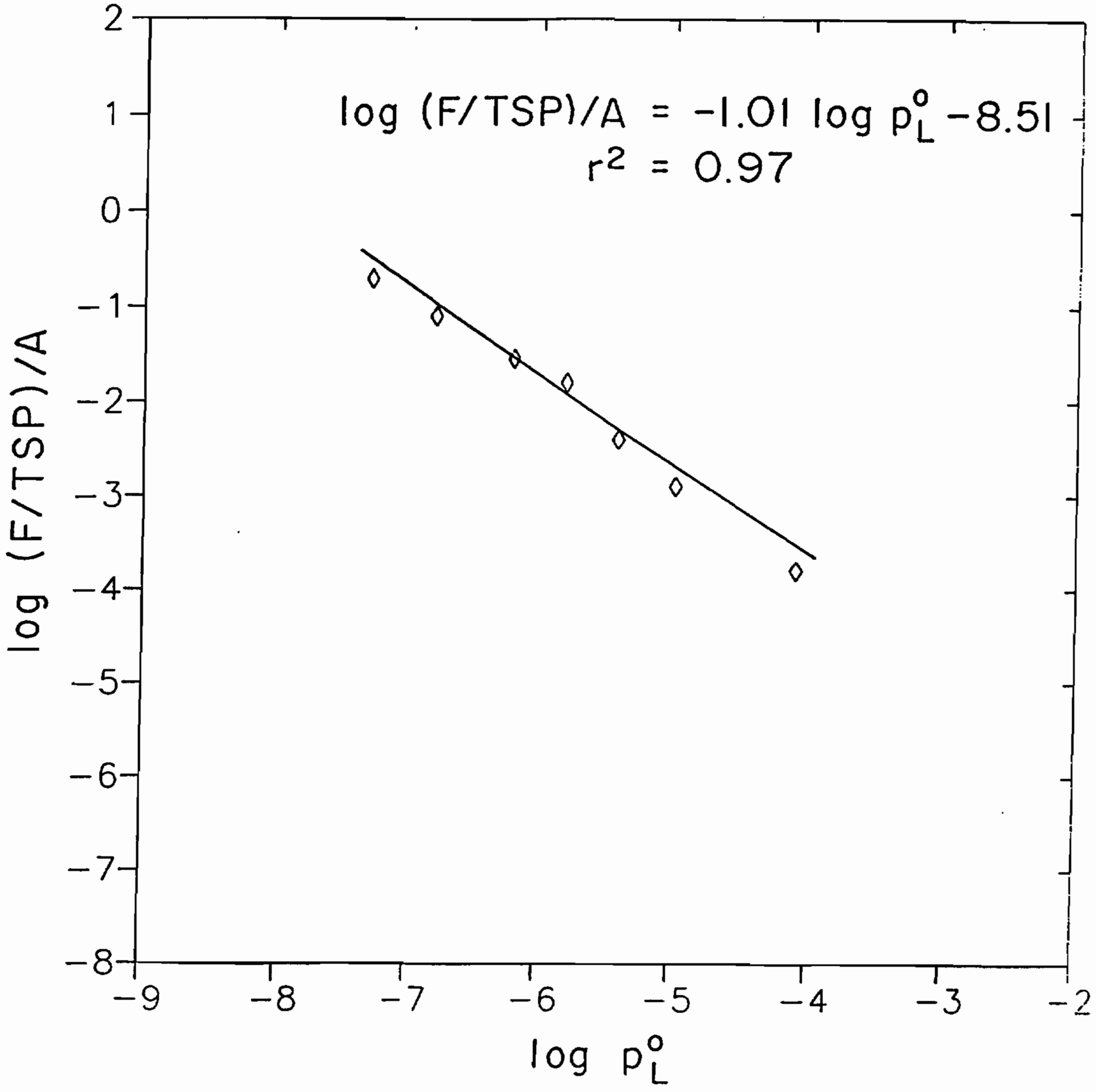

Fig. 3.1. Log *(F/TSP/A* vs. log p_L^o for C_{24} to C_{18} *n*-alkanes on Portland, Oregon on 27 February 1988. Data is from Hart (1989), and is corrected for adsorption to the filter by the "Teflon-corrected" method. (Reprinted with permission from Pankow and Bidleman, 1992.)

constant for the class of SOCs of interest, then for particulate matter with a specific A_{TSP}, we expect that

$$\log (F/TSP)/A = m_r \log p^{o}_{L} + b_r \tag{3.2}$$

where

$$m_r = -1 \tag{3.3}$$

and

$$b_r = \log \frac{N_s A_{TSP} T e^{(Q_1 - Q_v)/RT}}{16} \tag{3.4}$$

As shown in Table 1.2, there is considerable evidence that for air samples gathered around the world, and for laboratory gas/solid partitioning experiments with UPM, $m_r \approx -1$ for many types of SOCs. Pankow and Bidleman (1992) recently explored how different types of thermodynamic and non-thermodynamic effects can influence the results of a simple linear regression (SLR) of measured values of log $(F/TSP)/A$ vs. log p^o_L. In keeping with the goals of this research, this chapter summarizes that effort in the context of separating not only the different experimental conditions and parameters that affect the dependence of K_p on p^o_L, but also the actual sampling artifacts that affect measurement of values of $(F/TSP)/A$. The purpose is to be able to design model adsorption experiments that avoid any experimental conditions or artifacts that would prevent comparison of m_r and b_r between experiments, and thus can determine the true gas/solid partitioning of SOCs. Then, as in Chapter 2, the model system results can be compared to field data in order to ascertain whether simple, physical adsorption can describe the basic processes of gas/particle partitioning in the atmospheric environment.

3.1 Thermodynamic Sources of Variation in m_r and b_r

Because we are interested in comparing m_r and b_r values between gas/solid partitioning experiments, separating the sources of variability in these values is important. In particular, we note in Equation 3.3 that the thermodynamic expression for b_r depends on several different variables. For a given type of SOC, Pankow and

Bidleman (1992) point out that N_s will be fairly constant within a given class of compounds. Table 3.1 contains N_s values that have been calculated for some *n*-alkanes and PAHs. The molecular areas are calculated from the molar volumes using an equation given by Pankow (1987). In Table 3.1, the N_s values within each class of compound appear approximately constant. Therefore, while variability in N_s is not expected to cause much variability in b_r, variability in T, A_{TSP} and $(Q_l\text{-}Q_v)$ can be expected to cause noticeable variability in both b_r and m_r.

3.1.1 Effect of $(Q_l$ - $Q_v)$ Variability on b_r

The values for $(Q_l$ - $Q_v)$ for a range of SOCs will not necessarily be a constant for a given gas/solid partitioning experiment even if the composition of the particulate material is constant and conditions such as T and RH remain constant. Pankow (1991) has shown that the slope, m_q, of the linear regression of Q_l vs. Q_v is approximately equal to m_r. If $(Q_l$ - $Q_v)$ is constant, then this slope will be -1. If $(Q_l$ - $Q_v)$ is not constant, then $-m_q$ and hence m_r will not be -1. The effect this has on plots of log $(F/TSP)/A$ vs. log p^o_L from event to event is shown in Fig. 3.2(a).

$(Q_l$ - $Q_v)$ values for a range of SOCs can differ between gas/solid partitioning experiments in another way. Q_v for a class of SOCs should remain approximately constant over the narrow temperature range representing ambient conditions. Q_l is influenced by the composition of the particulate, both the surface content and morphology. For instance, we can consider two experiments; the first with a sampled air parcel containing soil dust and the second with a sampled air parcel that contains combustion-derived aerosol. The Q_l values for a given range of SOCs on these two different samples of APM cannot be expected to be similar for the two events. Thus, the $(Q_l$ - $Q_v)$ values for the range of compounds will be different for the two events, even when the T is the same.

3.1.2 Effects of Changes in A_{TSP} and T on b_r

Continuing to consider the soil and combustion-derived aerosols discussed above, we can expect that the value of A_{TSP} will likely be different for the two aerosols. Non-

Table 3.1. N_s values for several PAHs and alkanes calculated using equations given by Pankow (1987).

Compound Name	density (gm cm^{-3})	M (g mol^{-1})	area (Å^2)	N_s (mol cm^{-2})
PAHs				
phenanthrene	0.98	178	45.0	3.69×10^{-10}
anthracene	1.283	178	37.6	4.42×10^{-10}
2-methyl phenanthrene	1.05	192	45.2	3.68×10^{-10}
pyrene	1.271	202	41.1	4.04×10^{-10}
fluoranthene	1.252	202	41.6	4.00×10^{-10}
chrysene	1.274	228	44.5	3.73×10^{-10}
n-alkanes				
hexadecane	0.7733	226	61.7	2.69×10^{-10}
heptadecane	0.775	240	64.2	2.59×10^{-10}
octadecane	0.7768	254	66.5	2.49×10^{-10}
nonadecane	0.7855	268	68.5	2.43×10^{-10}
eicosane	0.7886	282	70.6	2.35×10^{-10}
heneicosane	0.7919	296	72.8	2.28×10^{-10}
docosane	0.7944	310	74.9	2.22×10^{-10}
tricosane	0.7969	324	77.0	2.16×10^{-10}
tetracosane	0.7991	338	79.0	2.10×10^{-10}

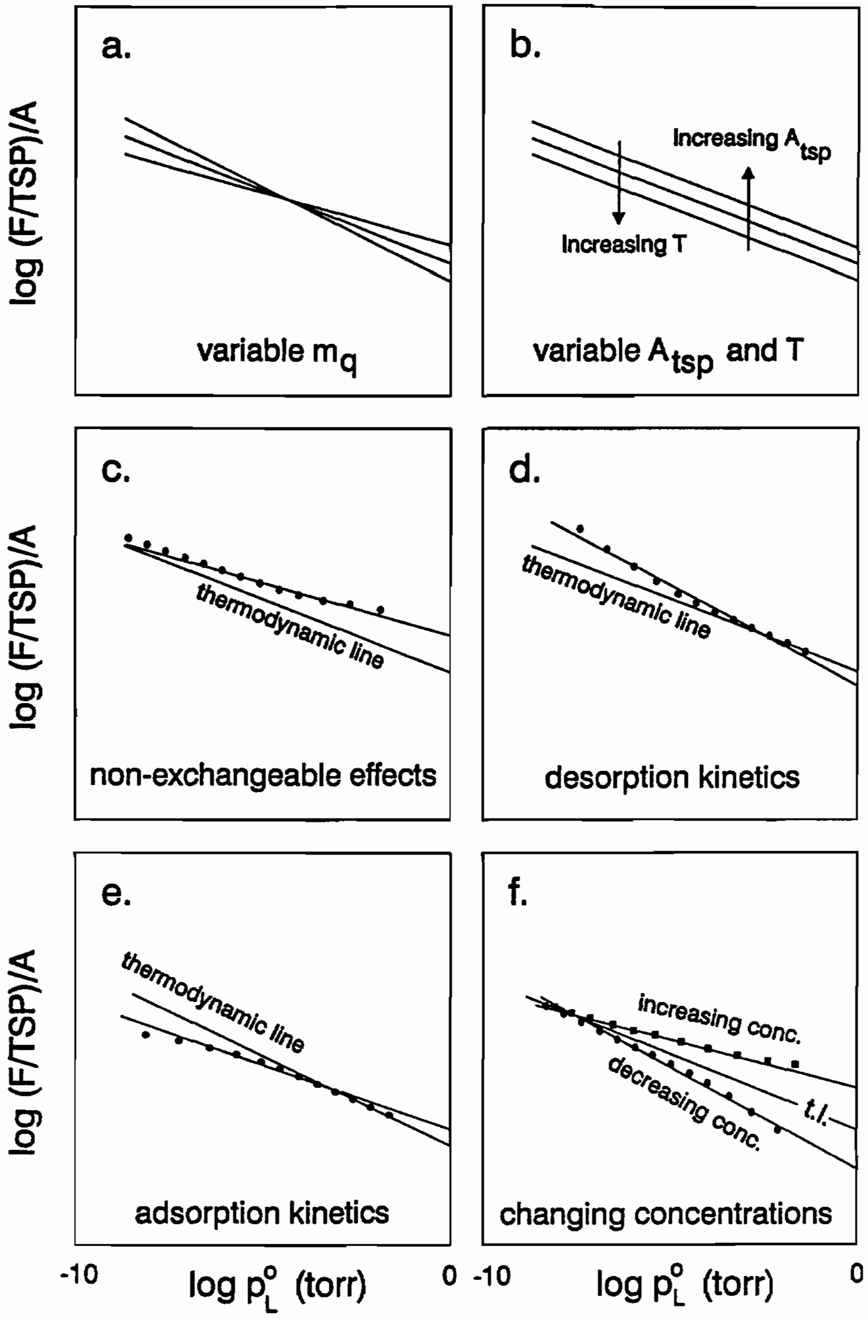

Fig. 3.2. Sources of event-to-event variability in m_r and b_r. t.l.= thermodynamic line. (a) variability in the value of $(Q_l\text{-}Q_v)$; (b) variability in A_{TSP} and T; (c) non-exchangeable effects; (d) desorption kinetics; (e) adsorption kinetics; (f) changing concentrations or changing T *within* a given event; since changes in concentrations or changing T within different events will occur differently, these changes will cause event-to-event variability in m_r and b_r. (Reprinted with permission from Pankow and Bidleman, 1992).

porous mineral materials of a size distribution consistent with the accumulation mode, can be calculated to have an A_{TSP} of 0.01 - 0.03 (cm^2 µg^{-1}) (Whitby *et al.*, 1972). In contrast, Ross *et al.* (1982) found that diesel particulate had specific surface areas ranging from 0.3 to 0.75 (cm^2 µg^{-1}). Pankow and Bidleman (1992) point out that for different samples of atmospheric particulate, b_r might vary by ± 0.5 due to a one order-of-magnitude variation in A_{TSP}. Similarly, if the ambient temperature range is 0-30 °C, then changes in T will cause at most a ± 0.15 change in b_r. Fig. 3.2(b) illustrates the effects of changes in A_{TSP} and T on b_r. Changes in A_{TSP} and T between two events will not change the m_r value for the two events, all other conditions remaining constant. However, if A_{TSP} or T changes during an individual event, there will be changes in *(F/TSP)/A* which will affect the constancy of both m_r and b_r values between events. This situation is covered in Section 3.2.5 below.

3.2 Non-Thermodynamic Sources of Variation in m_r and b_r

Just as thermodynamic effects can influence measured values of m_r and b_r from event to event, so too can other sampling-related problems affect these values. In addition to these event-to-event effects, changes in *T*, concentration, and *RH* can occur during a single gas/solid partitioning experiment. These effects, designated "within-event variabilities" by Pankow and Bidleman (1992), cause changes in the *(F/TSP)/A* for a single experiment from its true value based on K_p. This results in difficulty comparing m_r and b_r values between two different experiments.

3.2.1 Sampling-Related Artifacts - Sorption to Filters

Adsorption of SOCs to the filter media is an important source of error in measured *(F/TSP)/A* values. Many researchers have pointed out the ability of filters to adsorb a significant amount of organic carbon (Ligocki and Pankow, 1989; Hart, 1989; McDow and Huntzicker, 1990.) If corrections are not made for the additional amount adsorbed to the filter, the measured value of *F* is too high for each SOC, resulting in artificially high *(F/TSP)/A* values. In the context of effects on m_r and b_r, filter adsorption artifacts can occur in at least two ways. First, the filter medium can reach equilibrium with respect to the gas concentrations of all of the compounds. In this case, the slope, with respect to the gas concentrations of all of the compounds. In this case, the slope, m_r, will not change as long as the m_q value for the filter medium is equal to that for the particulate matter being sampled. The increase in F, under these conditions, can be thought of as an apparent increase in A_{TSP} (the extra surface area being the surface area of the filter). In Fig. 3.2(b), this results in an increase in the value of b_r. In contrast, a second case occurs when the gas phase compounds do not reach equilibrium with the filter because the filter is not exposed to a large enough mass of the compounds. In this situation, those compounds with a lower p_L^o are furthest from equilibrium, so the result is a change in both m_r and b_r.

One way to look at the second type of error of is to look at a "mass delivery" volume required for the filter to reach equilibrium with the gas concentration of an SOC. A compound that partitions strongly such as benz[*a*]anthracene ($K_p \approx 10^{-3}$ on a quartz fiber filter) would require at least 4000 m^3 of air (*independent* of the air concentration) to reach equilibrium with the hi-volume size quartz fiber filter (20 cm × 25 cm, weight 4 g). The calculation is:

$$V = K_p \cdot M_f = \frac{10^{-3} m^3}{\mu g} \cdot 4 \times 10^6 \mu g = 4000 \ m^3 \qquad (3.5)$$

where M_f = the mass of the filter and V = the minimum volume required to reach equilibrium.

For strongly sorbing compounds, the minimum required volume for equilibrium is often larger than the volume sampled. Indeed, a typical urban air sample volume is 800 m^3. Because the mass delivery volume is independent of concentration for a linear sorption isotherm, the extent to which a sample is out of equilibrium should remain constant from experiment to experiment when the sample volumes are similar. Thus m_r values for all the experiments would reflect a more gradual slope: the log *(F/TSP)/A* values for compounds with low p_L^o would be closer to the equilibrium log K_p values for the APM; the log *(F/TSP)/A* values for compounds with high p_L^o would be higher than the log K_p values for those compounds on APM reflecting equilibrium with the filter as well. The end result is a less negative value of m_r.

filter sorption is less important because of an increase in surface area of particulate relative to that of the filter. As stated earlier, many of these problems can be avoided by correcting for the sorption to the filter by placing a second filter behind the primary filter and subtracting the resulting quantity adsorbed to the back filter from the amount found on the front filter. This correction method assumes that the front and the back filter adsorb SOCs at the same rate during the experiment which is possible if the filters are inefficient at adsorbing SOCs. Another approach is to use Teflon membrane filters which have a very low surface area resulting in much less sorption. Hart (1989) and Hart *et al.* (1992) extensively discuss experimental methods for the correction of filter adsorption of gases during hi-volume air sampling.

In summary, during gas/particle partitioning experiments under field conditions, filter adsorption of SOCs can affect both the determination of K_p values from $(F/TSP)/A$ values and the m_r and b_r values for the sampling events. When designing laboratory experiments to investigate fundamental gas/solid partitioning processes, it will be necessary to ensure equilibrium of the solid phase with the gas phase.

3.2.2 Other Effects on m_r and b_r During a Single Experiment

As discussed in the introduction, Pankow and Bidleman (1991) recently described effects that can be expected when less than 100% of the sorbed compounds freely exchange with the atmosphere. Fig. 1.1 summarizes how the effect changes the measured log $(F/TSP)/A$ values for a high p_L^o compound, phenanthrene. If a simple linear regression (SLR) is performed on data that follows the curves in Fig. 1.1, the result would be a decrease in m_r and a resulting increase in b_r as shown in Fig. 3.2(c).

Another example of within-event variability occurs when the sample is collected near the source of the particulate material. In that case, it is possible for the kinetics of desorption to affect the measured particulate-bound concentration, F. For instance, either diffusion of the sorbed SOC to the surrounding clean atmosphere may be kinetically limited. The result is the collection of a particulate that is not at equilibrium with the atmospheric concentration of that SOC. Rounds *et al.* (1992) have shown that even high p_L^o compounds reach equilibrium slowly with a slightly porous particle of typical size. Fig. 3.2(d) shows the case where desorption kinetics increase m_r and thus decrease b_r, and Fig. 3.2(e) shows a case where adsorption kinetics decrease m_r and increase b_r.

During the often long sampling periods for ambient samples, the total concentration of airborne SOCs ($A + F$) may change due to a change in weather patterns. The resulting increase or decrease in ($A + F$) results in the particles already on the filter experiencing adsorption or desorption, respectively. Given enough time, though, the sampling process will yield a $(F/TSP)/A$ value that equals the value of K_p. In a forthcoming paper, Buchholz *et al.* (1993) model the behavior of a hi-vol filter collecting particle and gas phase SOCs when exposed to step changes in concentration. Their results indicate that a large change in log $(F/TSP)/A$ can occur initially, but by a time = 0.5 t, where t = the initial sampling time, the measured values of log $(F/TSP)/A$ value begin to return to the true K_p value. Therefore, changes in concentration late in the overall sampling event will affect the measured log $(F/TSP)/A$ values the most. Fig 3.2(f) illustrates these effects, the increase in concentration resulting in a shallower slope and thus a higher b_r. When the concentration decreases, the opposite effect is observed. Pankow and Bidleman (1992) illustrate how a change in T during a sampling event is similar to the change in concentration during an event. An increase in T results in a decrease in log $(F/TSP)/A$ and is reflected in an increase in m_r and a decrease in b_r. A decrease in T results in an increase in log $(F/TSP)/A$ in Fig. 3.2(f).

3.3 Summary Discussion

To summarize, the causes of event-to-event variabilities in m_r and b_r values include: changes in m_q, T and A_{TSP} between events; sorption to the filter material; non-exchangeable material effects; compound dependent adsorption and desorption kinetics in the atmosphere; changes in contaminant level of the atmosphere during a sampling event; and changes in T and during a sampling event. When investigating fundamental gas/solid partitioning, these types of variability need to either be controlled, or eliminated. In the field, this is difficult since there can be no control over many environmental parameters.

Foreman and Bidleman (1987) and Cotham and Bidleman (1992) collected UPM in Columbia and Chicago and measured the gas/solid partitioning of SOCs to the UPM under controlled environmental conditions in the laboratory. They found little variability observed in the log $(F/TSP)/A$ vs. log p_L^o relationship. The m_r values are very close to -1, and the b_r values are very similar (Table 1.2) for SOCs as different as organochlorine pesticides and PAHs. In these studies, both Foreman and Bidleman (1987) and Cotham and Bidleman (1992) were able to control T, RH, and SOC concentration, but not the characteristics of the particulate material, since they used UPM. Therefore, in order to investigate gas/solid partitioning at a more basic level, the particulate characteristics as well as the environmental parameters need to be controlled. Once the variabilities are controlled successfully, then laboratory gas/solid partitioning results can be compared to field studies to establish whether simple, physical adsorption can describe gas/particle partitioning in the atmospheric environment.

CHAPTER 4

THE EFFECT OF RELATIVE HUMIDITY ON GAS/PARTICLE PARTITIONING

Changing environmental conditions can be expected to affect the relationship between log K_p and log p_L^o among different sampling events. Chapters 2 and 3 have already discussed the role of temperature in this regard. Another potentially important environmental variable is relative humidity. Relative humidity (*RH*) has certainly been found to play a large role in controlling the gas/particle distributions of inorganic air pollutants such as sulfate and nitrate (e.g., see Witz *et al.*, 1982). Few researchers, however, have investigated *RH* effects on the measured gas/particle partitioning of SOCs. There is, nevertheless, strong evidence from the soil literature that the sorption of gas phase hydrocarbons can be enhanced at very low *RH* values.

Chiou and Shoup (1985) discuss the effect of *RH* on the sorption of gas phase benzene, chlorobenzene, dichlorobenzenes, and 2,4,6 trichlorobenzene to the mineral surfaces of certain soils with low organic matter contents (<1.5% organic carbon by weight). The sorption was enhanced at low *RH* (0%-20%), and they suggested that the removal of H_2O molecules from the mineral surface freed up adsorption sites for the organic compounds. Pennell *et al.* (1992) also reported increased gas phase xylene sorption to soils at low *RH*. Valsaraj and Thibodeaux (1988) examined the adsorption of volatile organic compounds (VOCs) to a wide range of soil materials and also found a similar increase in adsorption at low values of *RH*.

In the atmospheric literature, McDow and Huntzicker (1990) used the multicomponent adsorption theories of Hill (1946) and Gu (1981) to consider the effects of different *RH* values (20%, 50% and 70%) on the adsorption of gas phase organic carbon to quartz filters. Their analysis showed no uniform effect of *RH* on sorption of organic carbon. Thibodeaux *et al.* (1991) recently extended the theory of Hill (1946) for multicomponent adsorption of gas mixtures to the subject of gas/particle partitioning of SOCs, and explicitly considered the effects of *RH*. The following discussion will focus on two theories of multicomponent adsorption (Hill, 1946; Gu, 1981) using a single SOC and H_2O as the adsorptive components. An analysis of Thibodeaux *et al.*'s (1991) approach as well as a discussion the *RH* dependence of some field gas/particle partitioning results will be presented.

4.1 Multicomponent BET Adsorption

Many multicomponent adsorption theories begin with the Brunauer-Emmett-Teller (BET) isotherm for single components, given by:

$$\frac{n_A}{n_{A,m}} = \frac{B_A X_A}{(1 - X_A)[1 + X_A(B_A - 1)]} \tag{4.1}$$

where n_A = amount adsorbed, $n_{A,m}$ = amount in a monolayer, B_A = the BET constant related to the enthalpies of vaporization (Q_v) and desorption (Q_l), and $X_A = p_A/p^o$ the relative partial pressure of compound A. Equation 4.1 assumes that gas molecules adsorb in multiple layers, where the molecules in the first layer have an enthalpy of desorption Q_l, and the molecules in the subsequent layers have an enthalpy of desorption of Q_v. A further assumption is that vaporization can only occur from exposed layers (Brunauer *et al.*, 1938). BET theory works well with stable gases, and has been successful in describing adsorption of benzene and other volatile organics to surfaces (e.g., see Gregg and Sing, 1967). Because interactions between surface functionalities and sorbate molecules are all lumped into the Q_l term, BET theory also provides a tractable method of examining adsorption to complex surfaces such as those on atmospheric particulate material.

4.1.1 Hill and Gu Theories of Multicomponent Adsorption

Hill (1946) extended the BET theory to a mixture of multiple gases. In order to simplify the resulting expressions, one can assume for a binary system (e.g. A and

B) that each layer of adsorbed molecules above the first is made up of the same fraction of A molecules and B molecules as the first layer, and that the A molecules and B molecules are miscible in the liquid-phase layers. See Fig. 4.1(a). In addition, one can assume Raoult's law for ideal solutions is obeyed, so that the fractional partial pressure of A, i.e., X_A, is proportional to the mole fraction of A in the condensed layers. The adsorption isotherm for A in the two component system is given by Hill (1946, Equation 17a):

$$\frac{n_A}{n_{A,m}} = \frac{X_A B_A (X_A B_A + X_B B_B)}{(X_A B_A + X_B B_B)(1 - X_A - X_B)[1 + X_A(B_A - 1) + X_B(B_B - 1)]} \tag{4.2}$$

where $X_B = p_B/p^o$, the relative partial pressure of B, and B_B = the BET constant for B on the surface. When discussing SOC-H_2O adsorption, A will represent an SOC and B will represent H_2O. Although Equation 4.2 is a convenient approximation, it should be noted here that Raoult's Law will not apply well to non-polar organics in water.

Gu (1981) extends the BET approach to look at adsorption of binary mixtures of gas phase molecules which are immiscible when condensed. In this case, the simplifying assumption is that the A molecules only adsorb to A molecules and B molecules to B molecules and that there is no energetic interaction between A molecules and B molecules on the same layer or between layers. See Fig. 4.1(b). The equation for the Gu (1981) isotherm is then

$$\frac{n_A}{n_{A,m}} = \frac{X_A B_A (1 - X_B)}{(1 - X_A)[(1 - X_A)(1 - X_B) + X_A B_A (1 - X_B) + X_B B_B (1 - X_A)]} \tag{4.3}$$

This isotherm is similar in its behavior to the Hill isotherm. Gu (1982) later applied this immiscible equation to data from multicomponent adsorption experiments with miscible compounds. Even though the model assumes immiscibility in the sorbed phase, it was able to fit the adsorption of gas phase ethanol-benzene mixtures to silica well. However, the model did less well fitting the adsorption of benzene-cyclohexane to silica. Gu (1982) explains this difference by arguing that the first adsorbed layer is

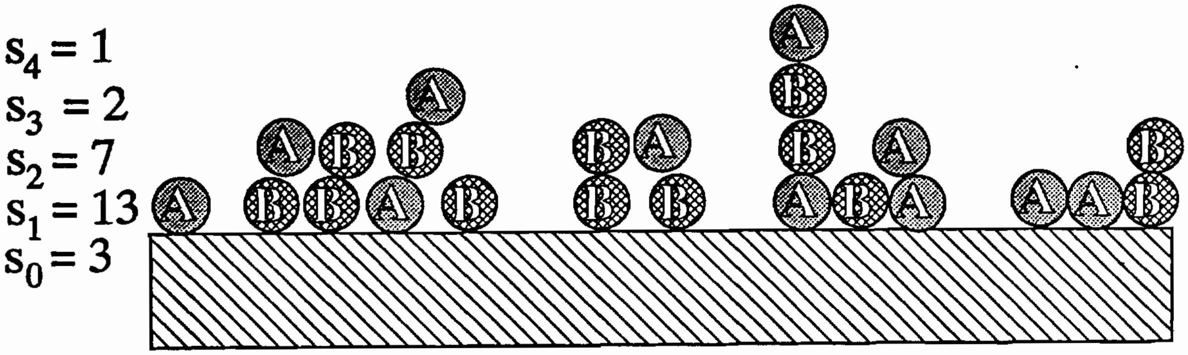

Fig. 4.1(a) Hill (1946) approach to gas/solid adsorption from a binary mixture of gases (Eq. 4.2) as derived from BET theory for single gases. The s_n value is the number of sites occupied with n molecules. X_A and X_B determine the mole fraction of A and B molecules in each layer.

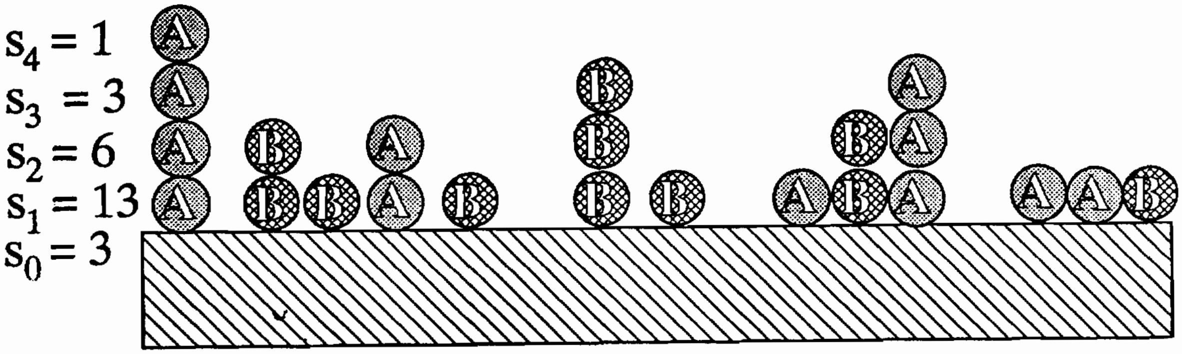

Fig. 4.1(b) Gu (1981) approach to gas/solid adsorption from a binary mixture of gases (Eq. 4.3) as derived from BET theory for single gases. The s_n value is the number of sites occupied with n molecules. Gu (1981) assumes that only A molecules can adsorb to A molecules, and B molecules to B molecules.

by far the most important when the p/p^o of the compounds is low, and the BET constant is high. If A molecules can only adsorb to A molecules, and B molecules to B molecules, as in Fig. 4.1(b), then the "stack" of molecules is low when the molecules stick to the surface (i.e. have high BET constants), and when X_A and X_B are low. Therefore, the compounds with higher BET constants will tend to follow the model behavior better at low relative partial pressures. The lack of molecules in higher layers means that there will be few interactions between A molecules and B molecules, and so the fact that the model assumes immiscibility in the higher layers is not a problem. Since ethanol and benzene on silica have relatively high BET constants compared to cyclohexane, so they tend to follow Equation 4.3 more closely, at least at low coverages.

Equation 4.2 and Equation 4.3 are plotted in Fig. 4.2, giving n/n_m, the fractional monolayer coverage of A adsorbed as a function of *RH* ($RH = X_B$ in Equation 4.2 and 4.3). The value of X_A is held constant at 0.01, approximately representing an ambient type of air concentration for an SOC; two values of B_A and B_B are used (10 and 100). Fig. 4.2 shows that both the Hill (1946) isotherm (Equation 4.2) and the Gu (1981) isotherm show that at low *RH* values, the adsorption of A molecules increases as *RH* decreases. Furthermore, when $B_B > B_A$, the competition from the B component (water) is very strong, so both isotherms show very little adsorption at *RH* values higher than 10%. In contrast to the Gu (1981) isotherms, the Hill (1946) isotherms show an increase in adsorption as the *RH* increases past 80%. This increase is due to the A molecules being " in solution " in the multiple layers of water. The Gu (1981) isotherm (Equation 4.3) does not predict an eventual increase in sorption with high *RH* like the Hill (1946) model because it assumes that the SOC and the water are immiscible, and therefore SOCs would not dissolve into the multiple layers of water.

4.1.2 Discussion of the Approach of Thibodeaux *et al.* (1991)

Thibodeaux *et al.* (1991) presented the first study that explicitly examined the effect of *RH* on gas/particle partitioning of SOCs in terms of multicomponent adsorption. They suggest that the observed variations in the measurement of

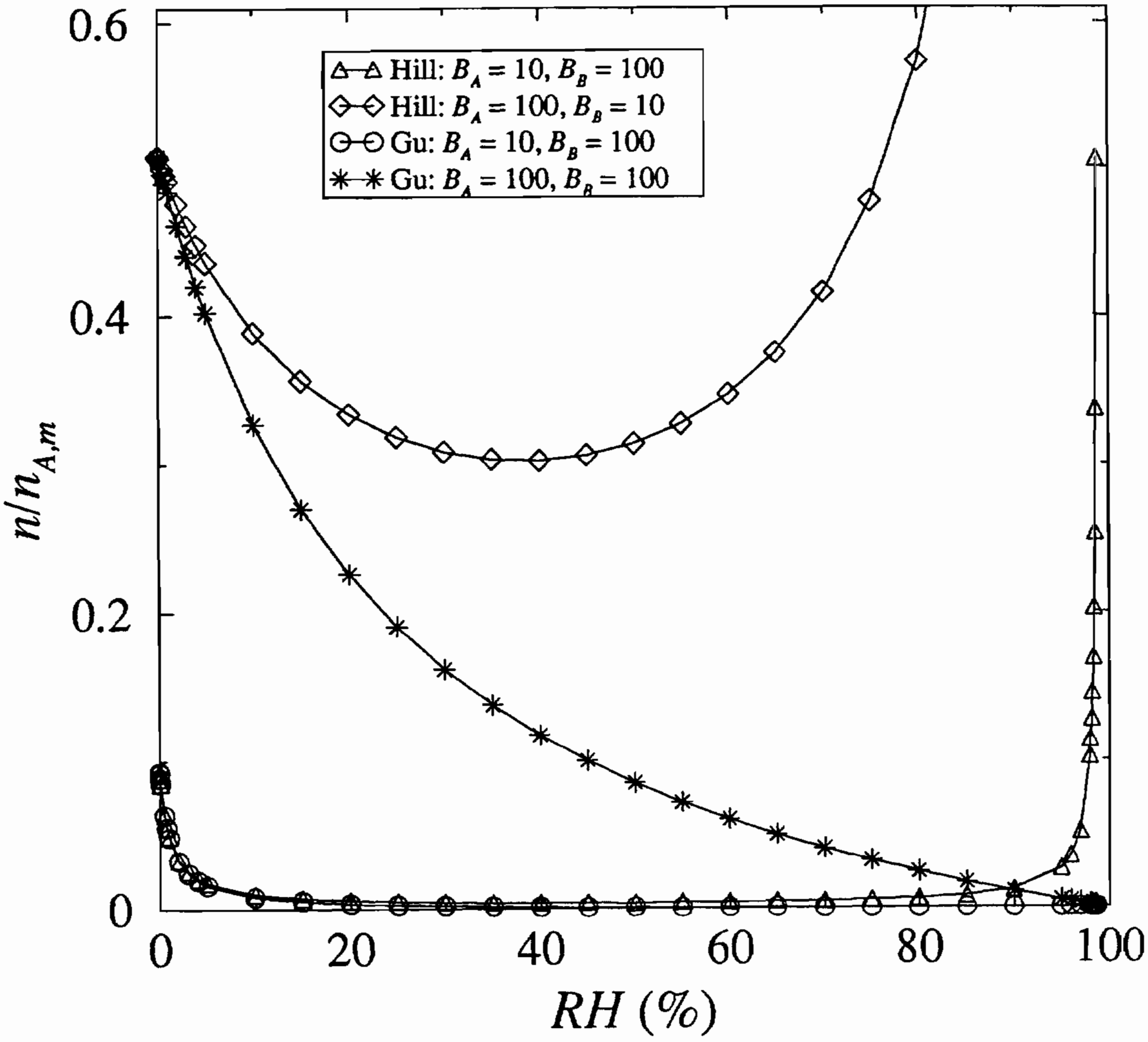

Fig. 4.2. A comparison of the Hill (1946) and Gu (1981) approach to gas/solid adsorption from a binary mixture of SOC and H_2O. The relative partial pressure of SOC (X_A) is fixed at 0.01, and $n/n_{A,m}$ is given as a function of RH (X_B).

gas/particle partitioning might be due to the effects of variable relative humidity. In order to critically examine this study, we need to understand the basis from which Thibodeaux *et al.* (1991) begin. They start with Equation 38 of Hill (1946), which is:

$$\frac{n_A}{n_{A,m}} = \frac{X_A[B_A(1 - X_B) + B_B X_B]}{(1 - X_A - X_B)[1 + X_A(B_A - 1) + X_B(B_B - 1)]} \qquad (4.4)$$

where the definitions of the variables are the same as given above.

The only difference between Equation 4.2 and Equation 4.4 (Hill, 1946, Equation 17a and 38, respectively) is that the derivation of Equation 4.4 uses a separate term for the composition of the first layer adsorbed to the surface, and then assumes the same composition for the rest of the adsorbed layers, and Equation 4.2 assumes the more special case that all layers have the same composition. Because the first layer of molecules adsorbed to a surface with any functionality will most likely be different than subsequent layers, Equation 4.4 is a more suitable approximation. Thibodeaux *et al.* (1992) then assume that in the case of A = SOC and B = H_2O, $X_A << X_B$. This is reasonable because the *RH* is always going to be higher than the relative partial pressure of an SOC in ambient air, and so the surface concentration of A molecules will generally be much lower than that of H_2O. Equation 4.4 can then be simplified to involve X_A multiplied by a function of X_B:

$$n_A = n_{A,m} B_A X_A \left[\frac{1 + (B_B/B_A - 1)X_B}{1 + (B_B - 2)X_B - (B_B - 1)X_B^2}\right] \qquad (4.5)$$

Figs. 4.3(a,b) illustrate the comparison between Equations 4.2, 4.4, and 4.5 for the same conditions as Fig. 4.1. Fig. 4.3(a) shows the case when $B_A > B_B$, when sorption of the SOC is strong relative to water, and Fig 4.3(b) shows the case when $B_A < B_B$, when sorption of H_2O is strong relative to the SOC. In Fig. 4.3(a), the strong binding of the SOC results in a decrease in coverage for Equation 4.4 and Equation 4.5 when *RH* > 20%, compared with Equation 4.2. This is most likely due to the assumption in

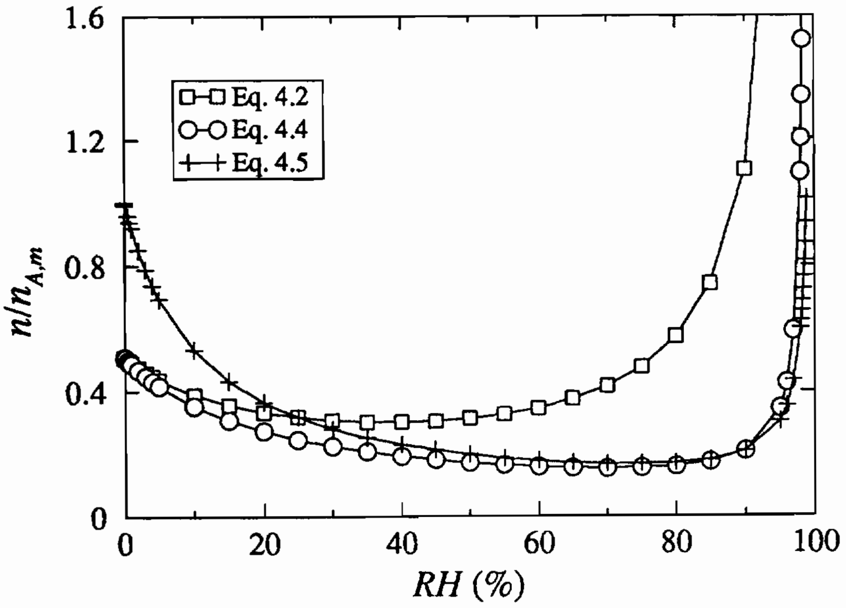

Fig. 4.3(a). A comparison of isotherms given by Eq. 4.2, Eq. 4.4, and Eq. 4.5 with $B_A = 100$ and $B_B = 10$ for each isotherm. The relative partial pressure of SOC (X_A) is fixed at 0.01, and $n/n_{A,m}$ is given as a function of RH (X_B).

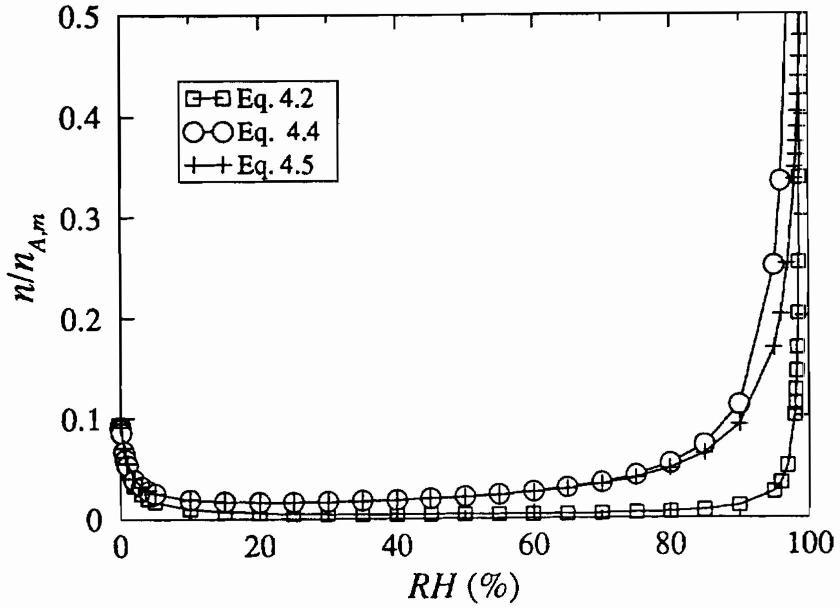

Fig. 4.3(b). A comparison of isotherms given by Eq. 4.2, Eq. 4.4, and Eq. 4.5 with $B_A = 10$ and $B_B = 100$ for each isotherm. The relative partial pressure of SOC (X_A) is fixed at 0.01, and $n/n_{A,m}$ is given as a function of RH (X_B).

Equation 4.2 that all layers have the same composition as the first layer. The term that describes the first layer composition depends on B_A, and so the larger B_A is, the more influence the first layer will have. Note also that Equation 4.4 becomes equivalent to Equation 4.5 when $RH >> p_A/p^o$, which follows from the assumption of Thibodeaux *et al.* (1991). In contrast, Fig. 4.2(b), with $B_B > B_A$, shows how the dominance of H_2O molecules in the first layer decreases the sorption of SOC. Overall, the strong binding of water is predicted to dampen adsorption of the SOC tremendously. A final point is that all three curves in Fig. 4.2(b) converge when X_B is large because of the large amount of B present.

4.1.3 K_p and the multicomponent adsorption theories

If the partition coefficient K_p is expressed in m^3 µg^{-1}, Equation 4.5 can be related to K_p according to

$$K_p = \frac{10^6 n_A}{\frac{p_A M}{RT}} \tag{4.6}$$

where n_A = amount adsorbed (g g^{-1}); M = molecular weight (g/mol); R is the gas constant (m^3 atm mol^{-1} K^{-1}). Substitution of Equation 4.5 into 4.6, and expressing X_A as p_A/p^o yields:

$$K_p = \frac{n_{A,m} B_A R T f_H(X_B)}{p^o{}_A M_A} \tag{4.7}$$

where $n_{A,m}$ (g g^{-1}) = amount in monolayer coverage which equals A_{TSP} (cm^2 µg^{-1}) $\cdot N_s$ (mol cm^{-2}) $\cdot M_A \cdot 10^6$ (µg g^{-1}). The quantity, $f_H(X_B)$, represents the bracketed term brackets in Equation 4.5; $f_H(X_B)$ can be thought of as the term that alters the value of K_p from the single component BET model given in Equation 3.1 to one that accounts for co-adsorption of component B. In a similar manner, Thibodeaux *et al.* (1991) presented a Langmuir-isotherm-based, two component model with the resulting expression:

$$K_p = \frac{n_{A,m} B_A RT}{p^o_A M_A} \left[\frac{1}{1 + B_B X_B}\right] \tag{4.8}$$

Figure 4.4(a,b) compares the approach of Equation 4.7, the Langmuir-based approach of Equation 4.8, and the Gu (1981) approach, all in K_p format. Pyrene is chosen as the model SOC compound (M_A = 202, and N_s = 1.965 × 10^{-10} mol cm^{-2}); the same B_A and B_B values as in Fig. 4.2 are chosen. Fig. 4.4(a,b) shows that predicted gas/solid partitioning for pyrene does not change with *RH* very significantly over much of the range of most ambient *RH* values (15%-80%). In addition, we note that the behavior in Fig. 4.4(a) is similar for all three equations due to the greater attraction of pyrene for the surface relative to water ($B_A > B_B$). Fig. 4.4(b), however, shows a large difference between the Thibodeaux *et al.* (1991) curve and the other two at *RH* values above 20%, with pyrene partitioning eventually increasing with increasing *RH*. Thibodeaux *et al.* (1991) argue that the multicomponent BET-based isotherm (Equation 4.7) makes more sense physically than the Langmuir-based approach, and that at high *RH* one can expect increased partitioning due to dissolution of the SOC into the adsorbed water.

4.2 Analysis of Yamasaki *et al.* (1982) Data in Terms of *RH*

The Yamasaki *et al.* (1982) study has been referred to extensively in this thesis due to the extent and quality of the data it presents. Yamasaki (1990) kindly provided our research group with the hourly relative humidity data for the air sampling periods. This data has been summarized in Table 4.1. Two different averages are provided there. The first represents a 24 hour average over each sampling period and the second represents an average of the last three readings, representing the average for the last 2 hours of the sampling period. Pilinis *et al.* (1989) indicate that ambient aerosols respond to changes in *RH* very quickly so that if for instance, rain was falling during the last few hours of the test, then the 2 hour average *RH* might be more appropriate to use rather than the whole 24 hour average.

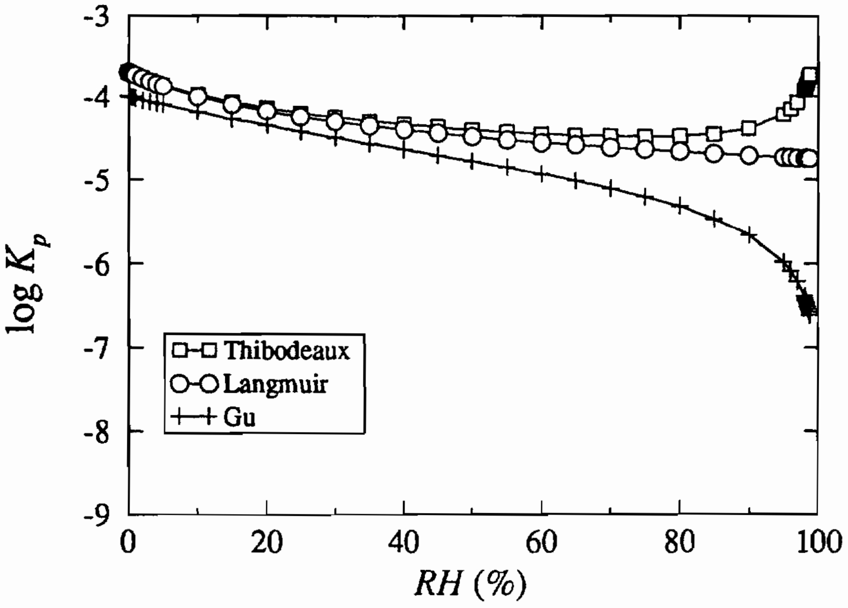

Fig 4.4(a). Predicted values of log K_p for pyrene as a function of RH based on the approaches of Thibodeaux, Langmuir, and Gu. In all cases B_A = 100, B_B = 10, and X_A = 0.01 for pyrene.

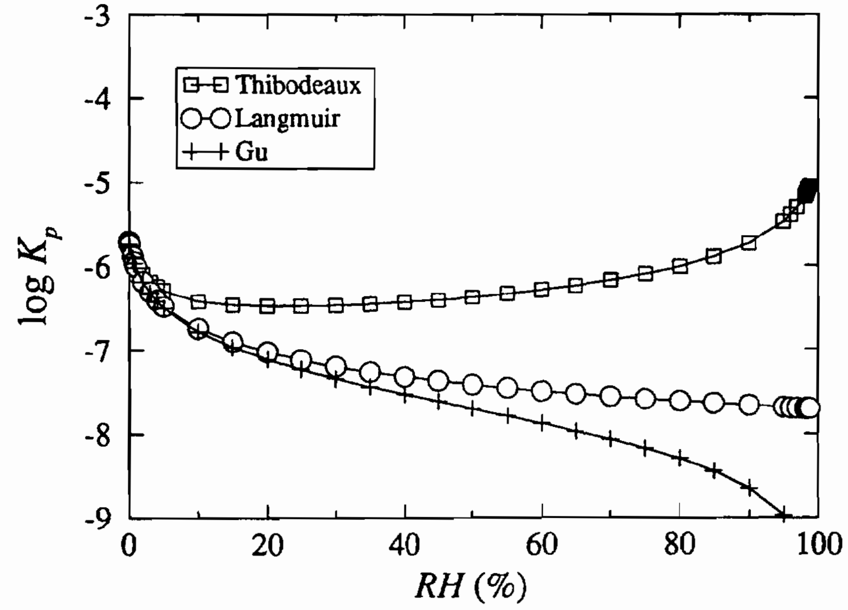

Fig 4.4(b). Predicted values of log K_p for pyrene as a function of RH based on the approaches of Thibodeaux, Langmuir, and Gu. In all cases B_A = 10, B_B = 100, and X_A = 0.01 for pyrene.

Table 4.1 Yamasaki *et al.* (1982) temperature and *RH* values for each sampling event.

Sampling Date	T(°C)	24 hr mean *RH*	Last 2 hr mean *RH*
07-Nov-77	20	86.76%	90.33%
21-Nov-77	13	71.42%	72.00%
06-Dec-77	10	68.56%	77.00%
14-Dec-77	12	66.27%	81.67%
26-Dec-77	7	61.54%	62.50%
12-Jan-78	8	70.12%	88.67%
19-Jan-78	6	54.08%	72.00%
08-Feb-78	6	54.92%	69.00%
22-Feb-78	5	59.32%	69.00%
08-Mar-78	12	45.32%	69.33%
22-Mar-78	7	71.56%	58.33%
05-Apr-78	13	66.20%	96.33%
19-Apr-78	16	75.80%	81.33%
11-May-78	16	88.84%	82.33%
17-May-78	18	93.72%	96.00%
01-Jun-78	21	42.24%	43.33%
14-Jun-78	26	77.63%	78.33%
05-Jul-78	30	68.78%	72.50%
13-Jul-78	27	85.63%	85.67%
19-Jul-78	30	78.64%	78.67%
02-Aug-78	29	94.96%	84.00%
16-Aug-78	30	89.79%	87.67%
28-Aug-78	28	81.04%	81.33%
13-Sep-78	17	76.83%	87.00%
28-Sep-78	21	90.46%	97.00%
12-Oct-78	18	55.32%	65.00%
25-Oct-78	21	81.88%	84.33%
08-Nov-78	16	79.44%	79.00%

Because of the range of temperature values observed during the various sampling events, and the strong temperature dependence of K_p, the data was sorted by increasing temperature. Figure 4.5 is the corresponding bar chart for the data. From Fig. 4.5, four different temperature values were chosen which had three or more temperature values within a ±1 °C range. We can then compare three or more log *(F/TSP)/A* values for each temperature. The temperatures selected were 6.8, 12.5, 20.4, and 28.9 °C. Figures 4.6 to 4.9 show log *(F/TSP)/A* vs. *RH* plots for each of these temperature values for six different PAH homologues: methyl-phenanthrene and methyl-anthracene; fluoranthene; pyrene; benzo[*a*]fluorene and benzo[*b*]fluorene; chrysene and benz[*a*]anthracene; benzo[*b*]fluoranthene, benzo[*j*]fluoranthene and benzo[*k*]fluoranthene. Since these data were collected between Osaka and Tokyo which are on the coast of Japan, there are not many low humidity values, the lowest being 42% *RH*. However, a few observations can be made in light of the earlier discussion of multicomponent adsorption theory. Firstly, there does not seem to be much effect of *RH* on the gas/particle partitioning process over the range of *RH* values encountered by Yamasaki *et al.* (1982). The 20.4 °C data (Fig. 4.7) has the widest spread of *RH* values and shows no consistent trend for the log *(F/TSP)/A* values of the PAHs. Certainly, there is no increase in log *(F/TSP)/A* at the high values of *RH* as the Thibodeaux *et al.* (1991) theory might predict. Furthermore, there is no decrease in log *(F/TSP)/A* at the higher *RH* values, as the Gu (1981) curve predicts. Thibodeaux *et al.* (1991) emphasize strongly the increase in sorption due to high *RH*, saying that the SOC can in effect dissolve into the layers of adsorbed water. Certainly, Fig. 4.6 through Fig. 4.9 do not support that conclusion. These results are consistent with those of Cotham and Bidleman (1992), who found that partitioning to UPM was not influenced noticeably by changes in *RH*. In that work, UPM was collected on a glass fiber filter and then exposed to gas phase organochlorine compounds at several ambient *RH* values (30%-70%) and a high *RH* value (>95%). At 20 °C, the resulting measured K_p values were not significantly different.

Another way to consider the Yamasaki *et al.* (1982) data is to realize that the BET constant for a PAH on UPM (B_A) is most likely large relative to the BET

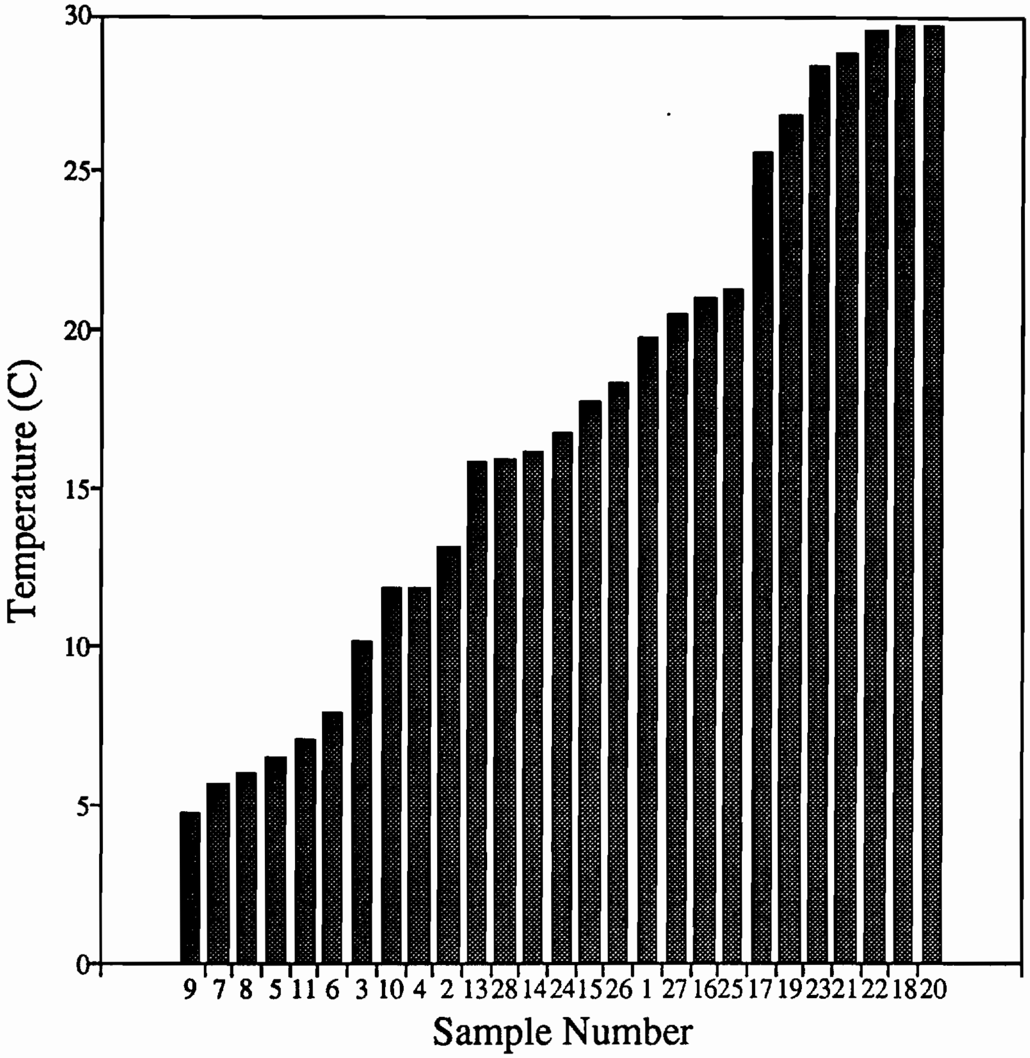

Fig. 4.5. A chart of the temperature (°C) values for the Yamasaki *et al.* (1982) samples. Samples were taken bi-weekly from November 1977 to November 1978.

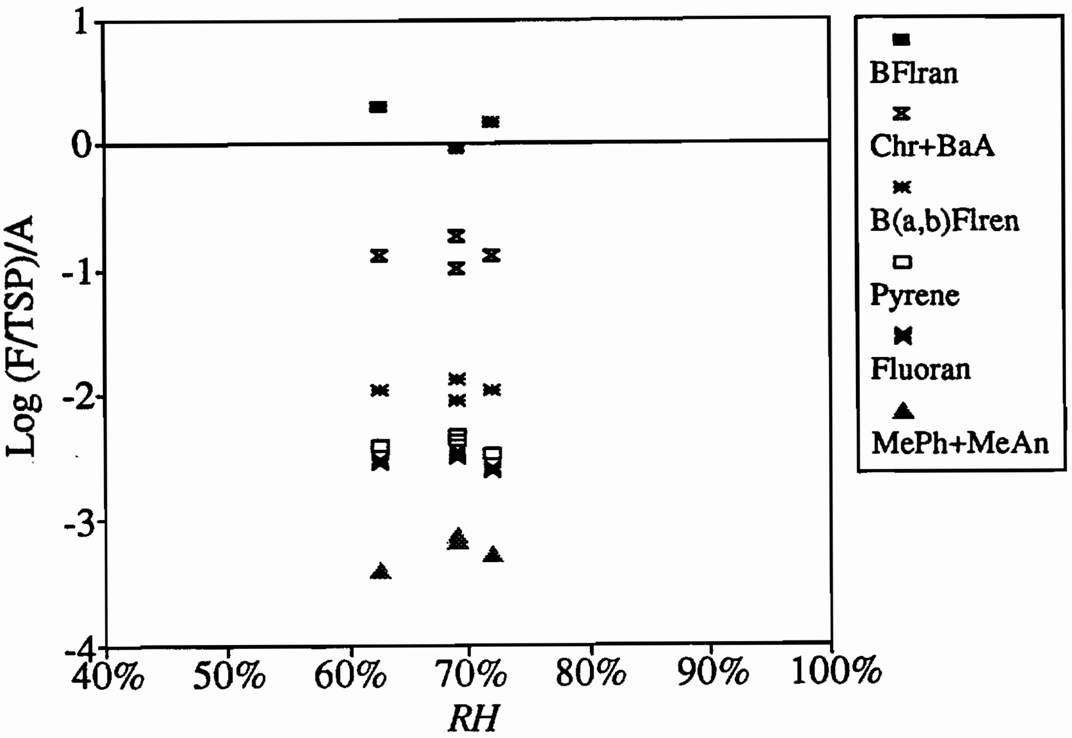

Fig. 4.6 Log *(F/TSP)/A* vs *RH* for PAHs on UPM as collected by Yamasaki *et al.* (1982). t = 6.8 ± 1 °C. BFlran = benzofluoranthene, Chr+BaA = chrysene and benz[*a*]anthracene, B(a,b)Flren = benzo[*a*]fluorene and benzo[*b*]fluorene, Fluoran = fluoranthene, MePh+MeAn = methyl phenanthrene and methyl anthracene.

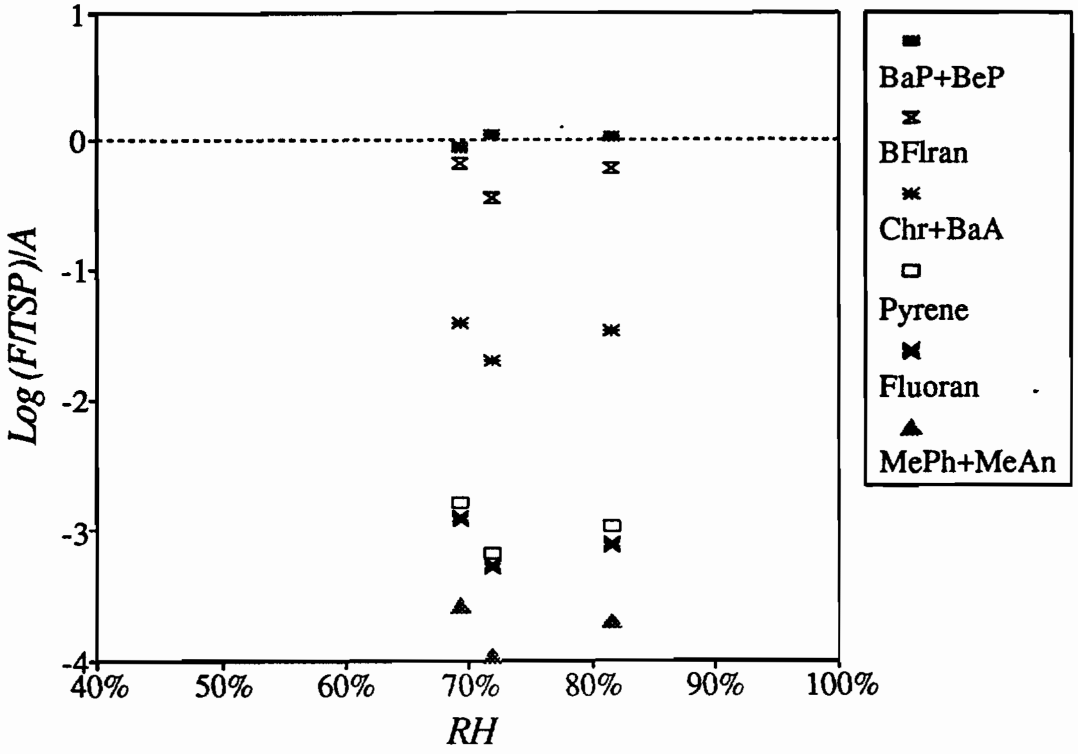

Fig. 4.7 Log *(F/TSP)/A* vs *RH* for PAHs on UPM as collected by Yamasaki *et al.* (1982). *t* = 12.5 ± 1 °C. BFlran = benzofluoranthene, Chr+BaA = chrysene and benz[*a*]anthracene, B(a,b)Flren = benzo[*a*]fluorene and benzo[*b*]fluorene, Fluoran = fluoranthene, MePh+MeAn = methyl phenanthrene and methyl anthracene.

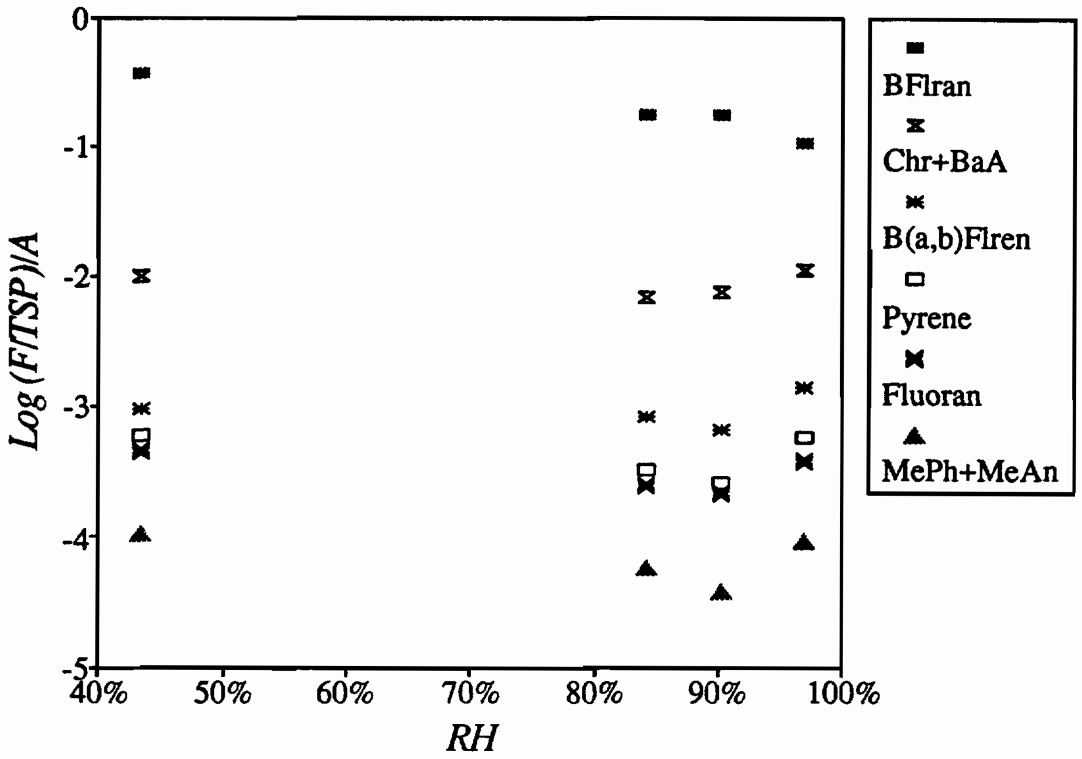

Fig. 4.8 Log *(F/TSP)/A* vs *RH* for PAHs on UPM as collected by Yamasaki *et al.* (1982). *t* = 20.4 ± 1 °C. BFlran = benzofluoranthene, Chr+BaA = chrysene and benz[*a*]anthracene, B(a,b)Flren = benzo[*a*]fluorene and benzo[*b*]fluorene, Fluoran = fluoranthene, MePh+MeAn = methyl phenanthrene and methyl anthracene.

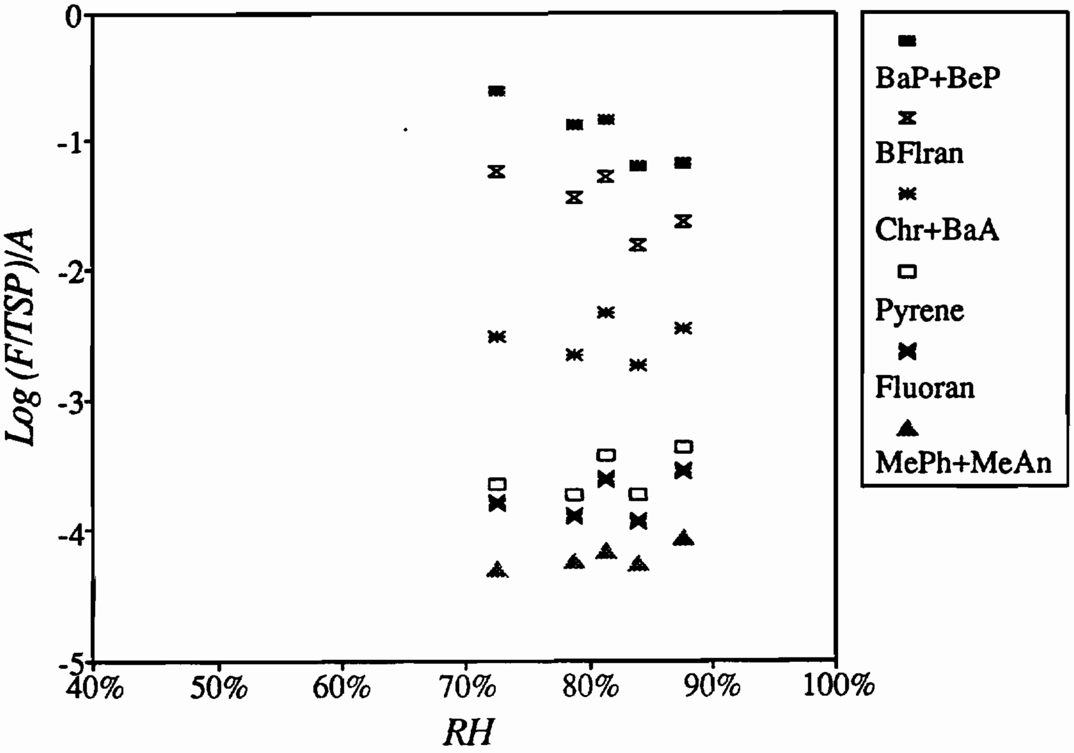

Fig. 4.9 Log *(F/TSP)/A* vs *RH* for PAHs on UPM as collected by Yamasaki *et al.* (1982). *t* = 28.9 ± 1 °C. BFlran = benzofluoranthene, Chr+BaA = chrysene and benz[*a*]anthracene, B(a,b)Flren = benzo[*a*]fluorene and benzo[*b*]fluorene, Fluoran = fluoranthene, MePh+MeAn = methyl phenanthrene and methyl anthracene.

constant for H_2O (B_B). This can be expected due to the presence of soot carbon in such an aerosol. Then, Fig. 4.4(a), with $B_A > B_B$, is more likely to describe the behavior of UPM equilibrating with a mix of gas phase H_2O and SOC than Fig. 4.4(b). If one considers the range of *RH* from 40% to 90+ % in Fig 4.4(a), all the curves remain relatively flat as well as equivalent because most of the change occurs between 0 and 20% *RH*.

In summary, several interesting theoretical approaches exist for examining gas/solid partitioning of SOCs in the presence of *RH*, but it is not clear at this point if any one of them is more valid than the other. The BET constant for each component has such a strong influence on the behavior that using the correct BET value is very important to the success of any one of the theories in predicting behavior. *RH* effects have always been a source of uncertainty in published ambient gas/particle studies. For the first time in the literature, *RH* effects on the partitioning of PAHs to UPM as measured by Yamasaki *et al.* (1982) are examined. Over the range of *RH* values encountered by Yamasaki *et al.* (1982), there does not seem to be any dependence of log *(F/TSP)/A* on *RH* for PAHs on UPM. Thibodeaux *et al.* (1991) attribute variations in published field measurements of log *(F/TSP)/A* values to changes in *RH*. Their conclusion is not supported by the analysis of the Yamasaki dataset provided here. Furthermore, any attempt to measure *RH* influence on gas/solid partitioning should include experiments at low *RH* because all of the multicomponent adsorption theories predict an increase in adsorption of SOC as *RH* decreases from 20% - 0%. A series of gas/solid partitioning experiments done at low values of *RH* is discussed in Chapter 5.

CHAPTER 5

AN EXPERIMENTAL APPROACH TO GAS/SOLID PARTITIONING

The previous four chapters have discussed the relative importance of different sources of difficulty in determining K_p values from measured values of *(F/TSP)/A* (e.g., uncontrolled variations in *T*, *RH*, and contamination level during sampling, sampling artifacts, and kinetic effects on contaminant sorption). Because of these difficulties, this work sought to develop and use a carefully-controlled experimental system to examine gas-solid adsorption of some model SOCs to a well-characterized model particulate material. By controlling *T*, *RH*, SOC concentration, and the nature of the sorbing phase, the system removes many of the variabilities inherent in field studies of gas/particle partitioning.

5.1 Materials and Methods

5.1.1 Selection of SOCs

N-alkanes and PAHs were chosen to represent as wide a range of vapor pressure as was considered experimentally feasible. There was a need to balance analytical sensitivity and the time required to reach equilibrium. In particular, at low gas phase concentrations, compounds with high p_L^o values will not sorb strongly enough to the model solid phase to be measured accurately. Conversely, compounds with low p_L^o would have taken many weeks to come to equilibrium given the amount of solid phase chosen for each experiment. The six *n*-alkanes selected were: heptadecane, nonadecane, eicosane, heneicosane, docosane, and tricosane (Ultra Scientific, Foxboro, MA). The PAHs selected were 2-methyl phenanthrene, fluoranthene, pyrene, benzo[*b*]fluorene, benz[*a*]anthracene and benzo[*b*]fluoranthene (Sigma Chemicals). Unfortunately, the benzo[*b*]fluoranthene was so non-volatile that it was not possible to generate a measurable gas concentration using the system.

5.1.2 Selection of Model Sorbent Material

The model particulate material that was studied is not a finely-divided particulate material like APM, but the quartz fiber filter (QFF) that is often used to collect samples of APM. The QFF was used as a surrogate particulate material for the following reasons:

1) The crystal structure of QFF closely resembles crystalline quartz. Quartz has been identified by X-ray and infrared (IR) spectroscopic techniques as an important constituent of airborne dust (e.g., see Pierroti *et al.*, 1978 and Sowelim *et al.*, 1980, 1983). Quartz has also been found in many samples collected at selected sites of the EPA Inhalable Particle Network (Davis *et al.*, 1984).

2) The size of the fibers that make up the filters is close to that of the airborne particulate matter, around 1 μm in diameter.

3) The fibers of a QFF are non-porous, and therefore the surface area available for partitioning should be calculatable in an unambiguous manner.

4) The fibers making up a QFF are solid, and therefore will not provide a second, <u>ab</u>sorptive partitioning mechanism.

5) The QFFs can be baked at high temperature and thus will have very low blank levels of contamination by the target compounds.

Fig. 5.1 shows a scanning electron micrograph of a clean QFF. At 30,000 × magnification, the surface still appears smooth.

5.1.3 Design of Apparatus

The initial design of the apparatus used to expose the QFF to the SOCs was based on that of the apparatus of Foreman and Bidleman (1987) and Cotham and Bidleman (1992) (see Figs 5.2(a,b)). The design of the system used for this research is shown in Fig. 5.3. In both Figs 5.2(a,b) and 5.3, the filters are mounted in filter holders and exposed to an air stream containing gas phase concentrations of the desired sorbates.

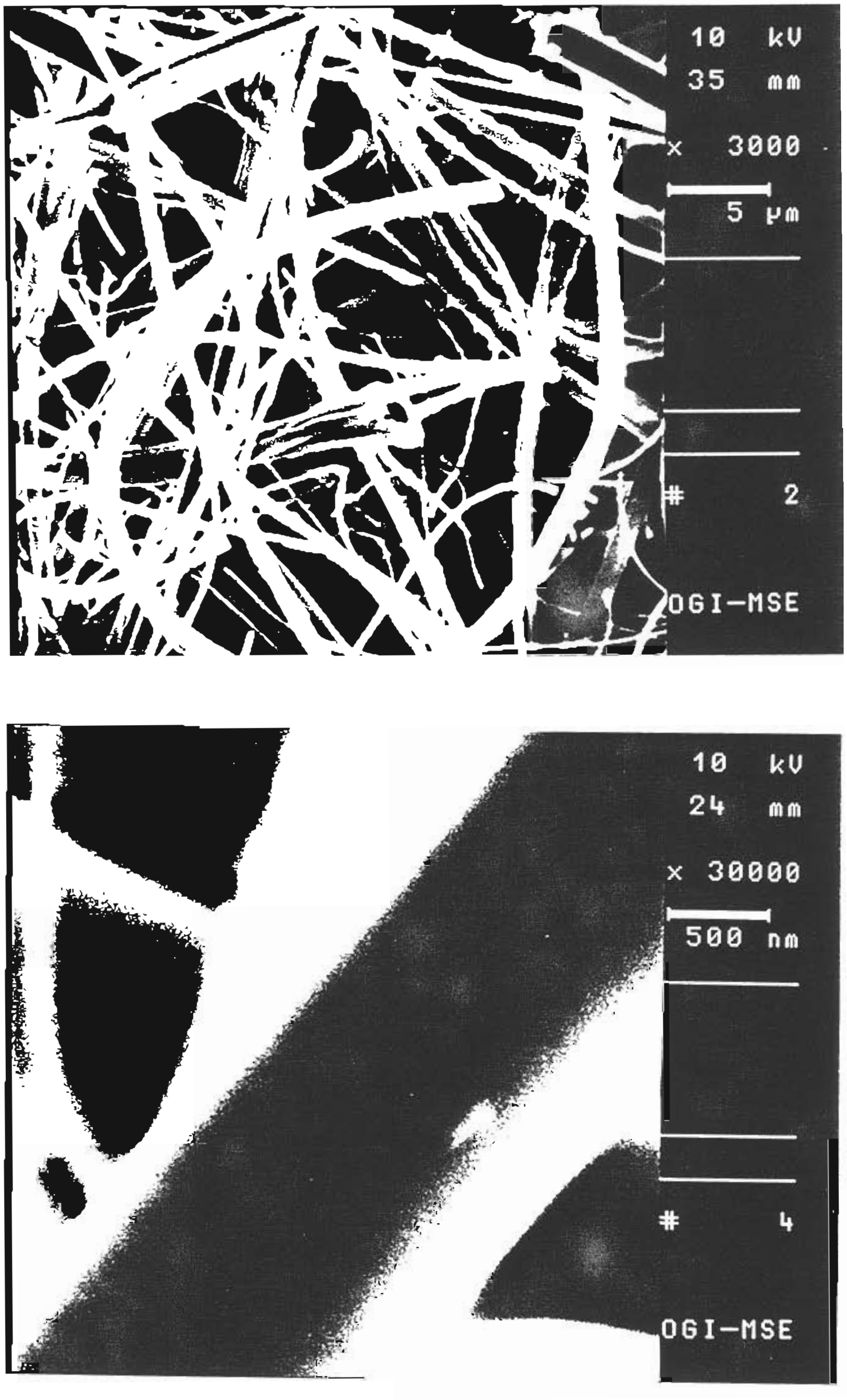

Fig. 5.1 Scanning electron microgaphs of QFF. a) 3000 magnification; b) 30,000 magnification. Scales are on the right.

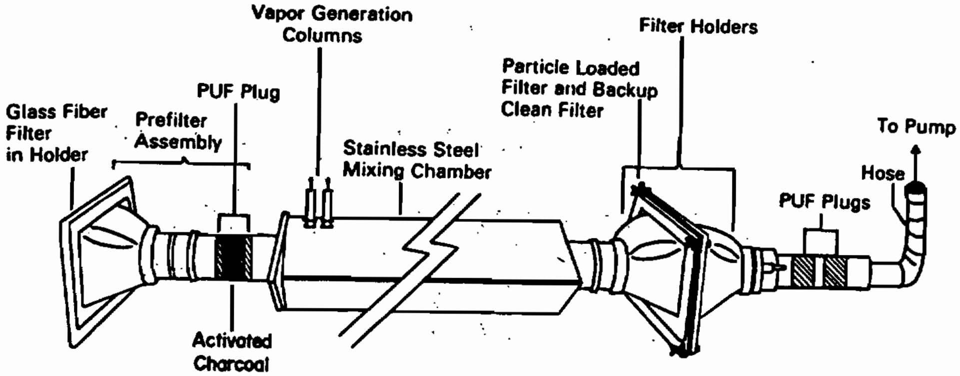

Fig. 5.2 (a) The Foreman-Bidleman apparatus for studying gas/particle partitioning of PAHs and organochlorines to UPM. Temperature determined by room temperature. (reprinted from Foreman and Bidleman, 1987).

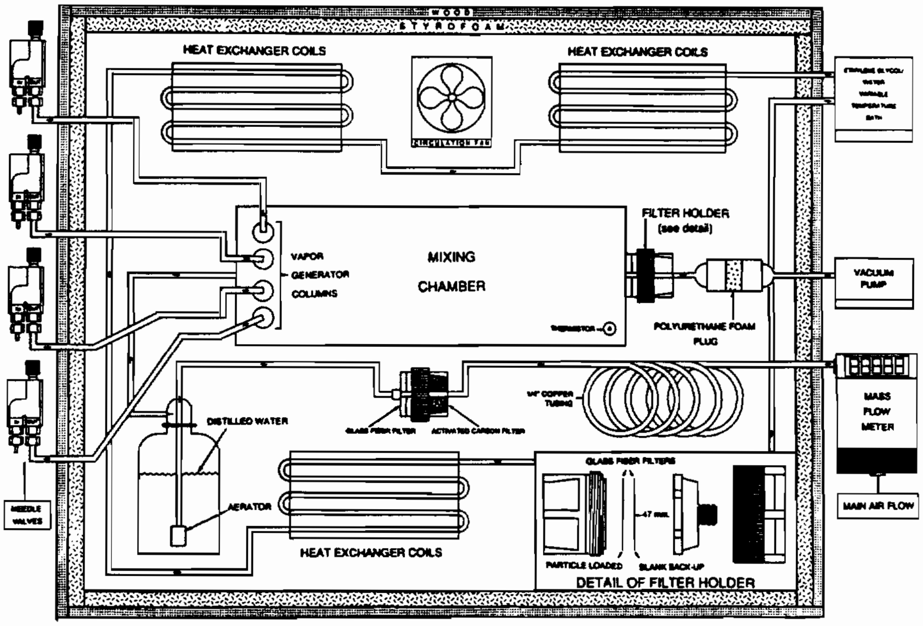

Fig. 5.2 (b) The Cotham-Bidleman apparatus for studying gas/particle partitioning of PAHs and organochlorines to UPM. Temperature controlled. (reprinted from Cotham and Bidleman, 1992).

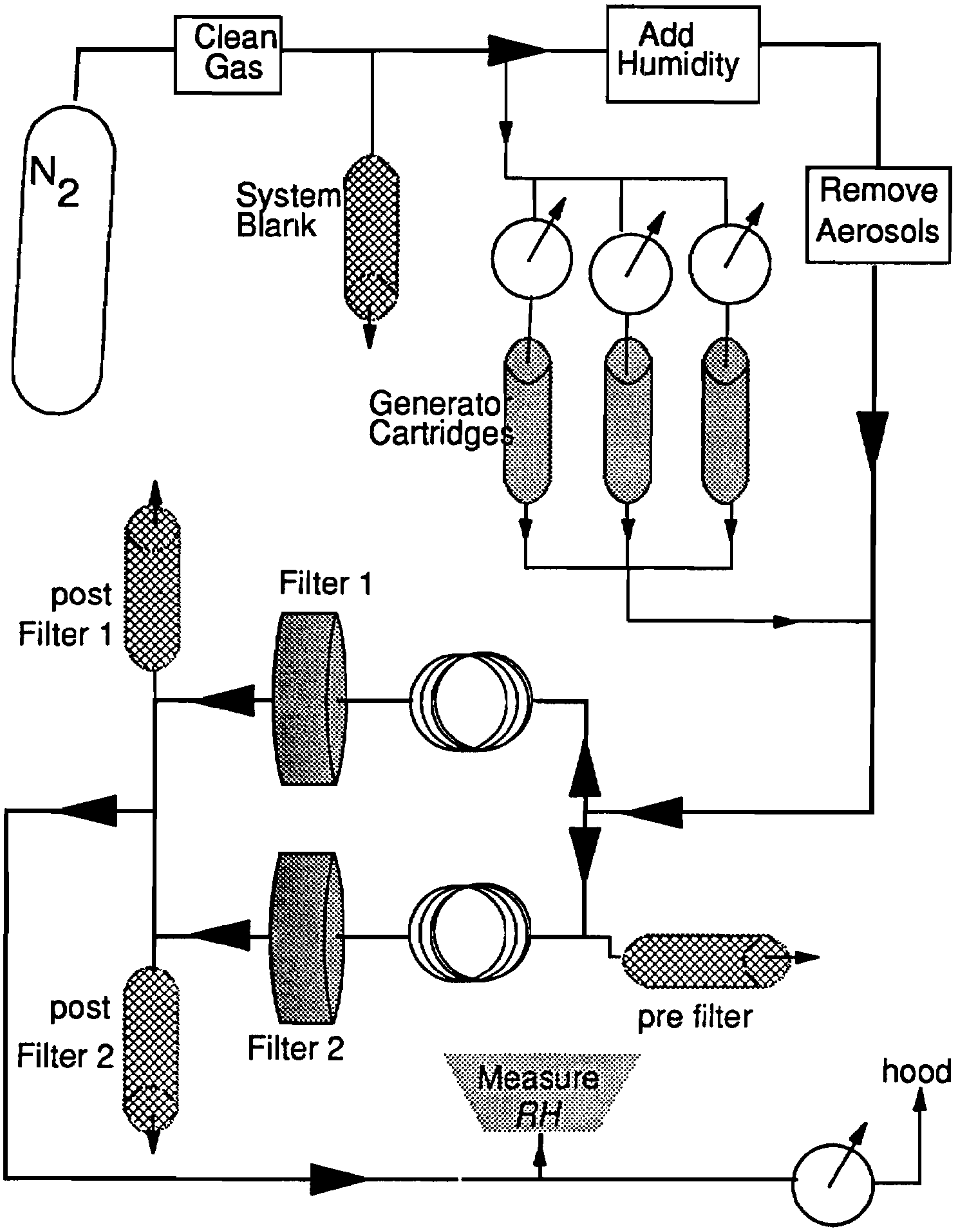

Fig. 5.3. Experimental apparatus used in this study. Arrows indicate flow direction. ATD indicates Tenax-filled adsorption/thermal desorption (ATD) cartridges.

The experimental concentrations of the SOCs were generated by passing air over glass beads coated with the sorbate compounds. The gas stream was then equilibrated with the model sorbent. The concentrations in the gas phase, c_g (ng m^{-3}), and the concentrations associated with the solid phase, c_s (ng µg^{-1}), were then measured and a partitioning coefficient (c_s/c_g, m^3 µg^{-1}) for each compound determined. The two variables c_g and c_s are distinguished from *A* and (*F/TSP*) because c_g is a laboratory, not an ambient, air concentration, and c_s is a laboratory measurement of gas-solid sorption to a solid, not a particulate-associated concentration divided by *TSP*. *T* and *RH* are controlled in both our system and the Cotham-Bidleman system. There are several important differences in the two designs, however. To begin with, Bidleman and co-workers used a negative pressure system using laboratory air for the air stream, and this system operates under positive pressure using the boil-off gas from a liquid N_2 dewar. This system also has two filter holders mounted in parallel, allowing the exposure of duplicate samples. Finally, c_g is measured using adsorption/thermal desorption (ATD) cartridges in our system upstream and downstream of the filter holders, and Bidleman and co-workers measured by sorption to a PUF plug downstream of the filter. The PUF plug was analyzed using solvent extraction. We feel that these design differences incorporated into our system are important improvements. The use of liquid N_2 boil-off for a gas source ensures that the substrate is exposed to very clean "air" because any SOCs in the liquid N_2 would remain in the cold dewar rather than volatilizing. The use of parallel streams allows a determination of experimental reproducibility. By measuring c_g upstream and downstream of the filter, a test for equilibrium with the filter can be carriaed out prior to termination of the experiment. Finally, in our system, the ATD method is a less time-consuming and solvent-intensive method for determining c_g than is PUF extraction.

5.1.4 Components and Operation of the Apparatus

This section describes the specific components that make up the system in Fig. 5.2 as well as its operation. The N_2 stream comes from a 160 liter dewar (Air Products, Allentown, PA) and is controlled by a Matheson regulator (model 3104, Secaucus, NJ). The flow passes through a large molecular sieve/activated carbon column (Chemical

Research Services, IL), and is then split three ways. A small part of the flow goes through an ATD cartridge filled with Tenax (Alltech, Deerfield, IL) in order to measure any background concentrations of analyte. The second part of the flow is sent through a humidification system consisting of two stainless steel impingers filled with de-ionized water and heated from below with heating mantles. The third portion of the flow goes through a flow box constructed with four rotameters (Brooks, Hatfield, PA) and four needle valves (Nupro, Solon, OH), and then on to three sets of sorbate generator cartridges and a dry gas makeup inlet. The flow box allows control of the flow through each set of generator cartridges and for the dry gas makeup. For instance, the flow through the cartridges containing the low p_L^o compounds is very high relative to the flow through the cartridges containing the high p_L^o compounds. This ensures that the gas concentrations of all compounds are within two orders of magnitude.

The sorbate generator cartridges as well as the ATD cartridges used with the above apparatus were of Pyrex glass with a bed length, inside and outside diameter of 8.25, 0.95 and 1.27 cm, respectively. The overall cartridge length was no more than 11.4 cm. The sorbate generator cartridges were filled with 0.5 mm glass beads (Glasperlen, Germany) that were sonicated in acetone/hexane and oven-dried prior to use. To coat the glass beads with sorbate, a 20 mg ml^{-1} methylene chloride solution of the sorbates was prepared and added to a 250 ml round bottom (RB) flask with ≈5 g of the glass beads. The methylene chloride was then removed using a rotary evaporator, and the glass beads, now coated with the sorbate compounds, were then funneled into the pre-baked cartridges. A small amount of glass wool used to keep them in the cartridge. Three sets of two cartridges each were prepared. The first set contained those compounds with the highest p_L^o values, heptadecane, nonadecane and 2-methyl phenanthrene. The second set contained those compounds with mid-range p_L^o values, eicosane, heneicosane, fluoranthene, pyrene and benzo[*b*]fluorene. The third set contained the compounds with the lowest p_L^o values, docosane, tricosane, benz[*a*]anthracene and benzo[*b*]fluoranthene. The cartridges were connected to one another and to the apparatus using 1/4 in (0.64 cm) i.d. Swagelok (Solon, OH) fittings . Depending on the desired *RH*, the dry gas makeup may or may not have been used.

The flows from the humidifiers and the sorbate cartridges are mixed and then split with half the flow going to each filter holder. A sampling port for an ATD cartridge is placed before the filter holders allowing a pre-filter concentration to be taken. Upstream of each filter holder a 15 cm length of 1/16 in (0.16 cm) o.d. stainless steel tubing is used as a flow restricter. The flow restricters ensure that unequal pressure drops across the two filter holders are made negligible, and that an equivalent amount of flow passes through each filter holder. The filter holders are 2.5 cm Gelman (Ann Arbor, MI) stainless steel filter holders modified to accept Swagelok connections. Teflon seals are used in the filter holder. The filter holders are cleaned with acetone/hexane and vacuum dried in an oven prior to use. Each QFF substrate is punched from a 20 × 25 cm sheet of Pallflex Corp. (Putnam, CT) QAOT-UP filter, baked at 550 °C, and inserted hot (≈100 °C) into the filter holder.

After flowing through the filters, a small amount of the flow on each of the two sides can be diverted through an ATD cartridge, so that the post-filter concentration can be obtained for each filter. Finally, the majority of the flow is sent through a rotameter (Dwyer Instruments, Michigan City, IN) and then into a fume hood. A tee in the exhaust allows measurement of the flow with a Precision Scientific (Chicago,IL) wet test meter, and a second tee allows measurement of *RH* with a dewpoint hygrometer (EG&G, Idaho Falls, ID.) The flow is set at 9 liters/min (lpm) which corresponds to a face velocity at each filter of 20 cm/sec. This face velocity is well within the range of normal hi-volume air sampling face velocities, and is about half the face velocity used by Hart and Pankow (1992) with their modified hi-vol apparatus. The whole apparatus is located inside of a environmental chamber (Environmental Growth Chamber, Inc.) modified to control temperature within ±0.2 °C using a Resistance Temperature Device (RTD) probe and controller (Omega Engineering, Stamford,CT).

5.1.5 Experimental Methods

The sorbate generator cartridges described above, were only prepared once for all of the experiments reported here; only small amounts of the sorbate compounds volatilized from the glass beads relative to the amounts with which the beads were coated.

The QFFs were prepared and the filter holders installed in the apparatus. Leak checks were done on the average of every third run; usually, no leaks were found. Once the filters were assembled, the box was equilibrated at 20 °C for two or more hours, the flow was started through the system at about 9 liters/min total flow, and the valves to the humidifier were slowly adjusted so that the desired humidity as measured by the dewpoint hygrometer was attained. For the high humidity experiments ($RH = 78\%$), the QFFs were pre-equilibrated for 12 hours with the humid airstream prior to the introduction of the gaseous sorbates. The flow through the sorbate generator cartridges was adjusted using the needle valves and rotameters. After ten or more days, the value of c_g upstream and downstream was determined by stopping the flow, connecting an ATD cartridge to each of the three sampling ports, and then re-starting the flow. Flow through the ATD cartridges was set at ~100 ml min^{-1} and monitored with a bubble flow meter at the beginning and end of the 18 hour sample period, resulting in a typical sample volume of ~100 L. The ATD cartridges were then analyzed, and the pre-filter and post-filter c_g values compared. If they were within 10% of the same value, the QFFs were considered to be at equilibrium with the gas phase, and the experiment was ended after taking an additional set of c_g measurements. The QFFs were then extracted and analyzed to determine their c_s values. The values of the RH, T, pressure drop and the flows were recorded daily during the length of the experiment, and adjustments were made when necessary.

5.1.6 Extraction and Analysis

5.1.6.1 QFF Extraction and Analysis

Each QFF was extracted with three 10 ml aliquots of methylene chloride (Burdick and Johnson) and the extracts reduced to 2 ml using a modified Kuderna-Danish (KD) method (Hart, 1989). The concentrated extracts were transferred quantitatively to pre-weighed 4 ml Reacti-vials (Pierce). Because of the clean nature of the apparatus, no additional sample cleanup, such as column chromatography, was necessary. The extracts were stored at -20 °C for < 24 hrs. Immediately prior to analysis, the extracts were blown down under N_2 to 200 µl, and 5 µl of 400 ng/µl phenanthrene *d*-10 (Cambridge

Isotopes, Cambridge, MA) solution was added as an internal standard. In addition to the two QFFs from each experiment, one oven blank QFF and two QFFs spiked with 10 µl of the stock solution containing the 12 sorbate compounds were extracted and analyzed for each experiment in order to determine recoveries. Table 5.1 summarizes the results of these recovery studies.

After blowdown, the samples were analyzed by capillary column gas chromatography/mass spectrometry (GC/MS) using on-column injection. The extracts were injected cool onto a 0.32 mm i.d., 0.25 µm film thickness DB-5 column (J&W Scientific, Folsom, CA) held at 70 °C inside of a Hewlett-Packard 5790A gas chromatograph (Palo Alto, CA) and interfaced to a Finnigan 4000 mass spectrometer/data system (MS/DS) (Sunnyvale, CA). The column was programmed from 70 °C - 175 °C at 25 °C/min, held for 2 minutes at 175 °C, and then programmed to 300 °C at 10 °C/min. The MS/DS was operated in the positive ion electron impact mode and scanned from 50 to 450 amu in 0.5 s intervals with the electron multiplier set at -1400 volts. The standard *m/z* values were used for quantitation.

5.1.6.2 ATD Cartridge Analysis

The ATD cartridges were backflush-desorbed using the method described in Hart *et al.* (1988) onto the same kind of GC column held at °0 C for 30 minutes at a desorption pressure of 30 psi. After the desorption, the pressure was reduced to the run pressure of 7 psi, and the GC oven was programmed to 175 °C at 25 °C/min, held for 2 min , then programmed to 300 °C at 10 °C/min. The MS conditions were identical to those used in the on-column runs.

Table 5.1 Results of spike recovery studies.

compound	Experiments through 021092[a] n=14 Average	s.d.	Experiments after 021092[b] n=14 Average	s.d.
n-alkanes				
heptadecane	71.5%	11.9%	90.3%	13.7%
nonadecane	79.9%	8.7%	98.9%	12.9%
eicosane	81.5%	10.0%	101.4%	12.8%
heneicosane	86.1%	10.3%	103.1%	11.7%
docosane	89.7%	11.0%	114.2%	15.1%
tricosane	93.1%	12.0%	114.5%	14.1%
PAHs				
2-methyl-phenanthrene	90.4%	15.4%	99.6%	14.7%
fluoranthene	91.1%	11.4%	102.5%	14.5%
pyrene	93.2%	10.4%	101.8%	14.7%
benz(*a*)anthracene	116.2%	14.4%	114.8%	18.2%
benzo[*b*]fluorene	116.2%	14.5%	105.3%	14.6%
benzo(*b*)fluoranthene	97.1%	13.8%	117.3%	16.5%

---

[a] The blowdown step in these extractions was too fast, resulting in a loss of heptadecane and nonadecane. The QFF extractions were corrected for the losses when recovery < 70%.

[b] The length of the blowdown step was increased significantly for these runs resulting in improved recoveries.

5.1.6.3 Quantitation

The compounds were quantified by comparing retention times, mass spectra, and mass intensities with those observed from injections of internal and external standard solutions. A five step procedure was followed:

1) External standard solutions were prepared bracketing the concentration ranges expected in the QFF extracts;

2) Retention times and mass spectra were recorded for the 12 compounds of interest and the internal standard;

3) Response curves for on-column and ATD were generated for each compound using the external standards (any standard which caused more than 10% scatter in the response curve was removed);

4) A response factor (*RF*) relative to the appropriate internal standard was calculated by the GC/MS/DS software according to:

$$RF = \frac{(area)(I.S.amt)}{(I.S.area)(amt)} \tag{5.1}$$

where *RF* = response factor and *I.S.* = internal standard; and

5) The scan numbers of the compound peaks were recorded, and the compound peaks in the sample and spike extracts were integrated using a program (QUSLRN) written by Pankow for the Finnigan's data system.

The corresponding concentrations were calculated by rearrangement of Eq. 5.1:

$$amt = \frac{(area)\,(I.S.amt)}{(I.S.area)\,(RF)} \tag{5.2}$$

giving the amounts. The total mass extracted from the QFF was thus used to determine c_s:

$$c_s = \frac{C_v M_{CH_2Cl_2}}{d_{CH_2Cl_2} M_F} \tag{5.3}$$

where C_v = concentration in vial (ng/µl), MCH_2Cl_2 = mass of CH_2Cl_2 in vial (g), dCH_2Cl_2 = density of CH_2Cl_2 (g/µl), and M_f = mass of QFF (µg).

The amount of SOC desorbed from the ATD cartridge determines c_g:

$$c_g = \frac{amount}{V_{ATD}} \cdot \frac{(P_{drop} + P_0)}{P_0} \tag{5.4}$$

where V_{ATD} = volume sampled with ATD cartridge (m^3), P_{drop} and P_0 are the pressure drop across the filter and the barometric pressure, respectively. The pressure drop correction is only needed when determining the c_g upstream of the filter.

5.1.6.4 Method quantitation limits

Because this study was carried out in a clean laboratory system using very clean "air" (N_2 boil-off), very low-level detection limits for the compounds in the samples was possible. In addition, with the exception of one experiment, the blank filters showed absolutely no response for any of the 12 compounds. Given that the peak area of the noise was ~0 for PAH each base peak (m/z = 192, 202, 228 and 252), and ~5-10 for *n*-alkane base peaks (m/z = 57), a quantitation limit of 35 - 70 area counts was determined to be acceptable. For instance, 2-methyl phenanthrene's base peak is m/z = 192 which is fairly uncommon. Since noise at m/z = 192 was absent, peak areas of 35 or more were considered quantifiable. This corresponds to about 0.3 ng μl^{-1} for the external standard injections. The lowest external standard used to construct the response lists was 0.48 ng μl^{-1}. Thus, while an amount as low as 0.3 ng μl^{-1} was not bracketed by the standards, it was also not far outside of that range.

5.2 Experimental Protocol

As noted above, the experimental work conducted here focuses on gas/solid adsorption by choosing a QFF as the sorbent material. The solid, crystalline structure of QFF makes any other sorption process unlikely. An important objective was to vary *RH* while keeping the rest of the variables constant. The multicomponent sorption theory in Chapter 4, predicts that sorption as a function of *RH* should change most rapidly between 0 and 30% *RH*. The efforts of this series of experiments therefore focused on this *RH* range, and also considered some very high *RH* values. Before proceeding, it should be noted that considerable effort was required to control the experimental conditions, especially the temperature. As a result, only the work involving the temperature-controlled box (as depicted in Fig. 5.3) will be discussed here.

The experiments conducted in the temperature-controlled box and discussed here included the following:

1) Four experiments at 10% *RH*;
2) Four experiments at 30% *RH*;
3) Two experiments at 6% *RH*;
4) Two experiments at 0.4% *RH*; and
5) Three experiments at 72-79% *RH*.

The first eight experiments were used to establish the reproducibility of the experimental system. The first one was conducted inside the box at 10% *RH* using a a Type J thermocouple temperature control instead of the more accurate RTD device. This resulted in changes on the order of ± 1.5 °C in temperature relative to the desired 20 °C. Therefore, after installation of the RTD controller, three more experiments were done at 10% *RH* for the sake of comparison. The values of 10% and 30% *RH* were chosen to bracket the expected range of *RH* required for monolayer coverage of water on the QFF. This is based on the single component BET equation (Eq. 4.1) choosing a range of values from 20 to 100 for the BET constant of water on quartz (Kang *et al.*, 1980). The 0.4% *RH* value was chosen to represent the low end of the experimental range for *RH* because it was not felt that any value extremely close to zero could be created and sustained in a reliable manner. Moreover, even *RH* values as low as 0.4% are probably never encountered in the ambient atmosphere.

5.3 Results and Discussion

This section is divided into several parts. The first part will present data for each of the *RH* values studied to illustrate the reproducibility and the degree of agreement found with the linear Langmuir adsorption theory of Pankow (1987, 1991). The second part will compare the PAH gas/solid sorption results from each experiment with the PAH gas/particle partitioning results of Yamasaki *et al.* (1982) in terms of log K_p vs. log p_L^o and in terms of log $K_{p,s}$ vs. log p_L^o. The third part will present results as a function of *RH* and in terms of multicomponent adsorption theory. Finally, a summary discussion will discuss implications of this work for global transport of SOCs, and possible further investigations with the experimental apparatus.

5.3.1 Results of Gas/Solid Sorption Experiments

5.3.1.1 Results of 10% *RH* Experiments

The first four experiments, designated 101691, 112691, 122091, and 010292, were conducted in the environmental chamber at ~10 % *RH* and 20 °C. As stated above, the first experiment was done with less precise temperature control. The results in this section are presented in terms of log c_s/c_g vs. log p_L^o. Each experiment yielded an *n*-alkane plot and a PAH plot. Each plot contains data for each of the two replicate QFFs, namely QFF #1 and QFF #2. Different symbols are used for the two QFFs. A single, simple linear regression (SLR) line for both QFFs is also plotted. Figs. 5.4 and 5.5 show log c_s/c_g vs. log p_L^o plots for each of the four experiments. Table 5.2 summarizes the values of m_r and b_r together with the corresponding standard deviations values. Because occasional mishaps resulted in the disqualification of one of the two QFFs, some experiments only have one set of points, and the SLR lines are based on data from only one QFF. The error bars represent the ± 1 standard deviation.

In several of the experiments, the QFF in the lower filter holder, QFF #2, did not reach equilibrium for benz[*a*]anthracene, tricosane and docosane, as determined by equal values for the upstream and downstream values of c_g. Error bars were not determined for those values of c_s/c_g. These QFF #2 points, however, were included because they tended to be very close to the corresponding *equilibrium* value of c_s/c_g for QFF #1. The reason

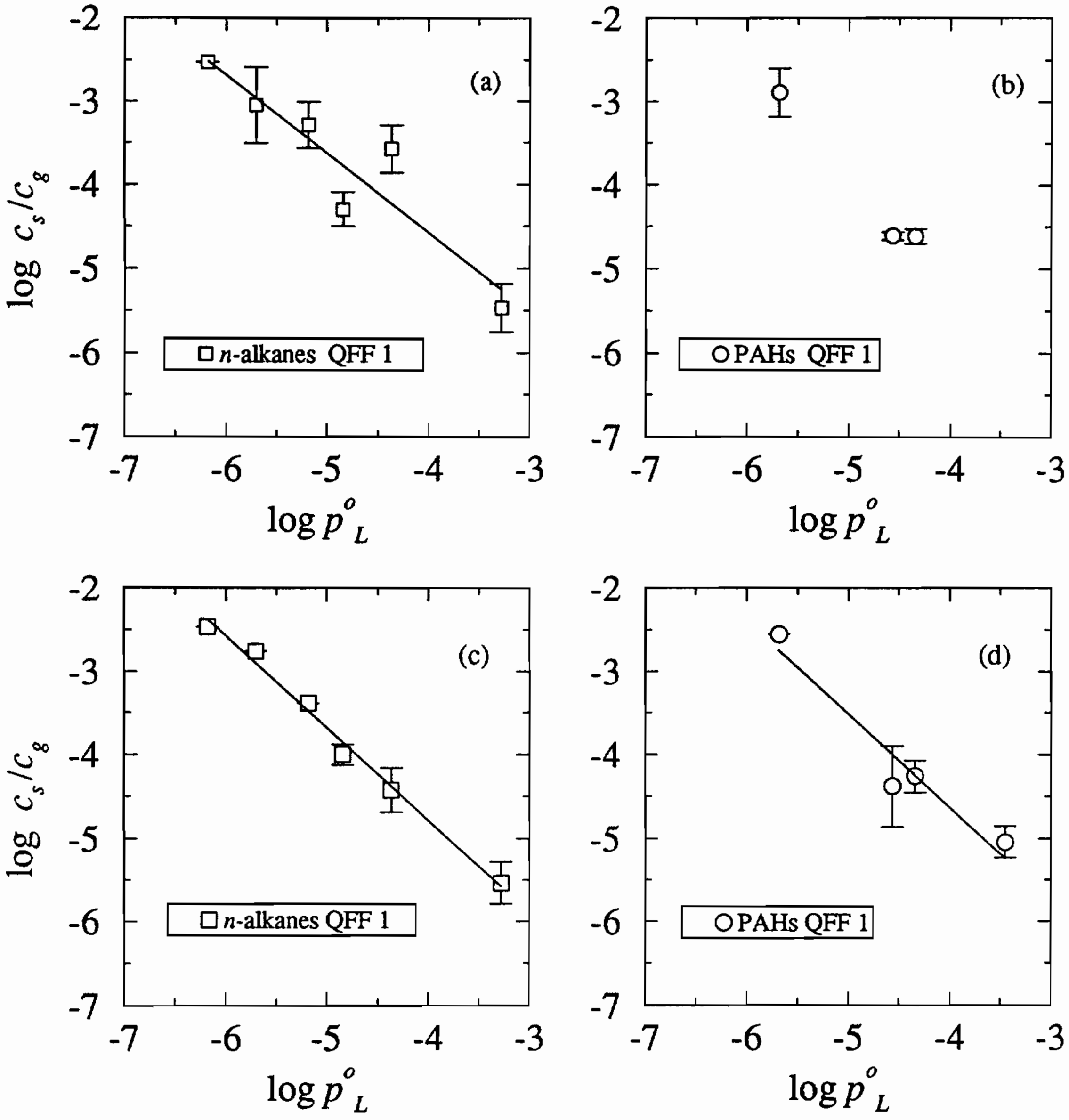

Fig. 5.4. Log c_s/c_g vs. log p^o_L plots for experiments 101691 **(a,b)** and 112691 **(c,d)**. Each line is a single SLR for all the points on each graph. m_r, b_r, and r^2 values given in Table 5.2.

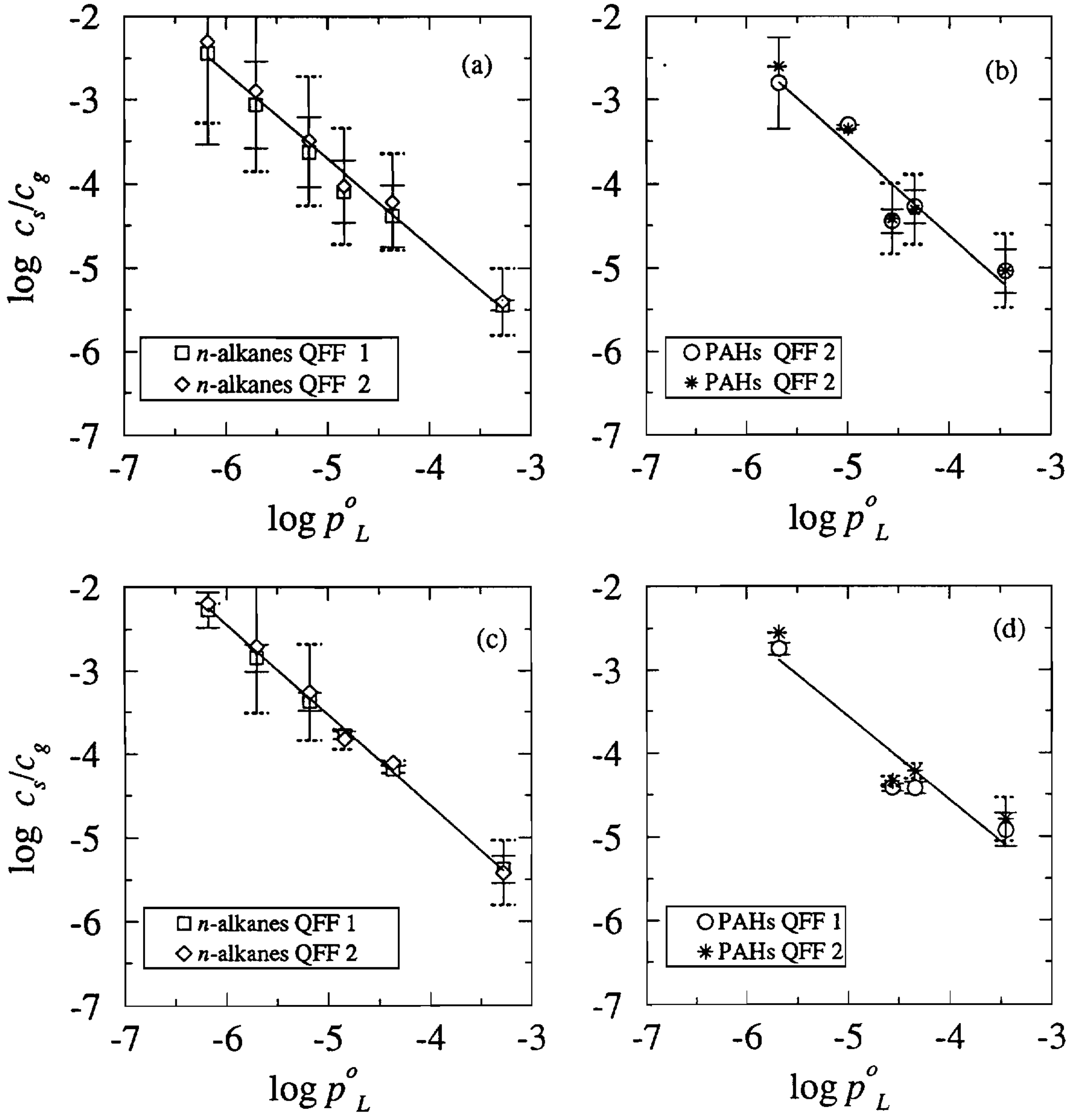

Fig. 5.5. Log c_s/c_g vs. log p^o_L plots for experiments 010292 (**a,b**) and 122091 (**c,d**). Each line is a single SLR for all the points on each graph. m_r, b_r, and r^2 values given in Table 5.2.

for the discrepancy between the upper and lower filter holders was not discovered until late in the study. It was found that if one side was blocked off, the measured pressure drops for each "side" of the flow were the same. However, when measured simultaneously, the flows through each side were significantly different, about 5.25 lpm through QFF #1 and 3.75 lpm through QFF #2. Thus, QFF #2 was exposed to 30% less volume of sorbate-laden N_2 than QFF #1. Based on the mass delivery volumes from Eq. 3.2, QFF #2 was close to equilibrium for most compounds when most experiments were terminated, hence the good agreement between log c_s/c_g values for QFF #1 and QFF #2 for all compounds. As summary plots, Fig. 5.6 gives the log c_s/c_g vs. log p_L^o plot for all QFFS from the four experiments error bars for the pooled standard deviations using a method as described by Davies and Goldsmith (1984, p. 45).

5.3.1.2 Results of 30% *RH* Experiments

Four separate experiments were done at ~30% *RH*, designated 011392, 012492, 021092, and 022592. In the 012492 experiment, QFF #2 was disqualified during the extraction so there are data for seven QFFs in this group. The results for the 30% *RH* experiments are given in Figs. 5.7 and 5.8. This set of experiments had lower relative standard deviations and was generally more consistent than the 10% *RH* experiments. The results are summarized in Table 5.3 and Fig. 5.9. Note that the b_r values are very similar, and that the m_r values are very close to -1.

5.3.1.3 Results of 6% *RH* Experiments

Two separate experiments were done using 6% *RH*, designated 032092 and 040392. No QFFs were lost, so there are four QFFs in this group. The results of the 6% *RH* experiments are shown in Fig. 5.10. Again, like the 30% *RH* experiments, this set had lower relative standard deviation values for c_s/c_g and generally good agreement between all four QFFs. The results summary appears in Table 5.4 and Fig. 5.11.

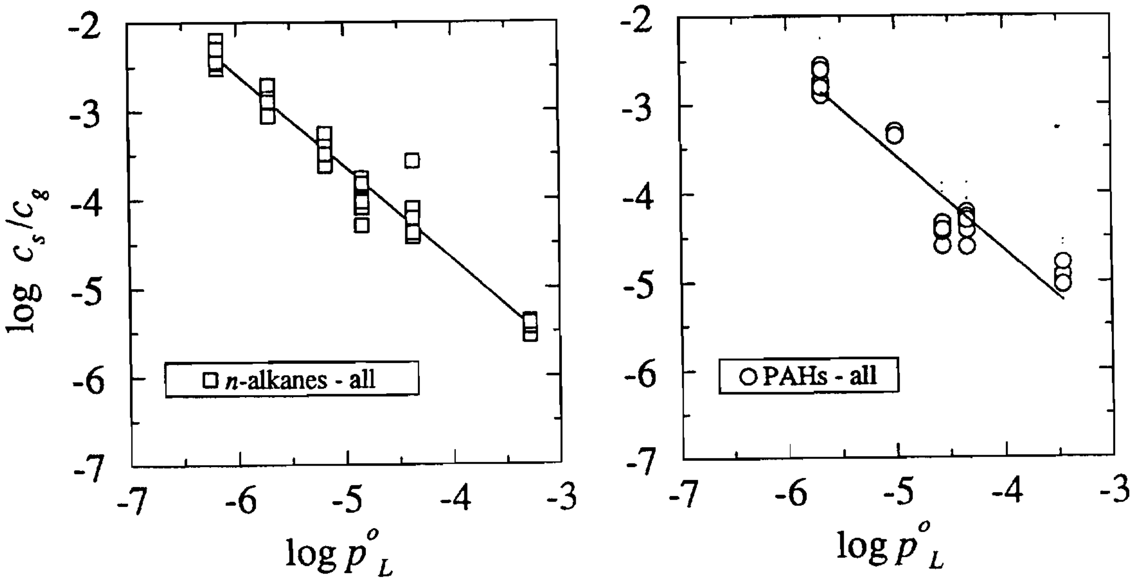

Fig. 5.6. Log c_s/c_g vs. log p^o_L plots for all of the 10% *RH* runs: 101691; 110691; 112691; 122091; and 010292. Each line is a single SLR for all of the sample points on each graph. m_r, b_r, and r^2 values given in Table 5.2.

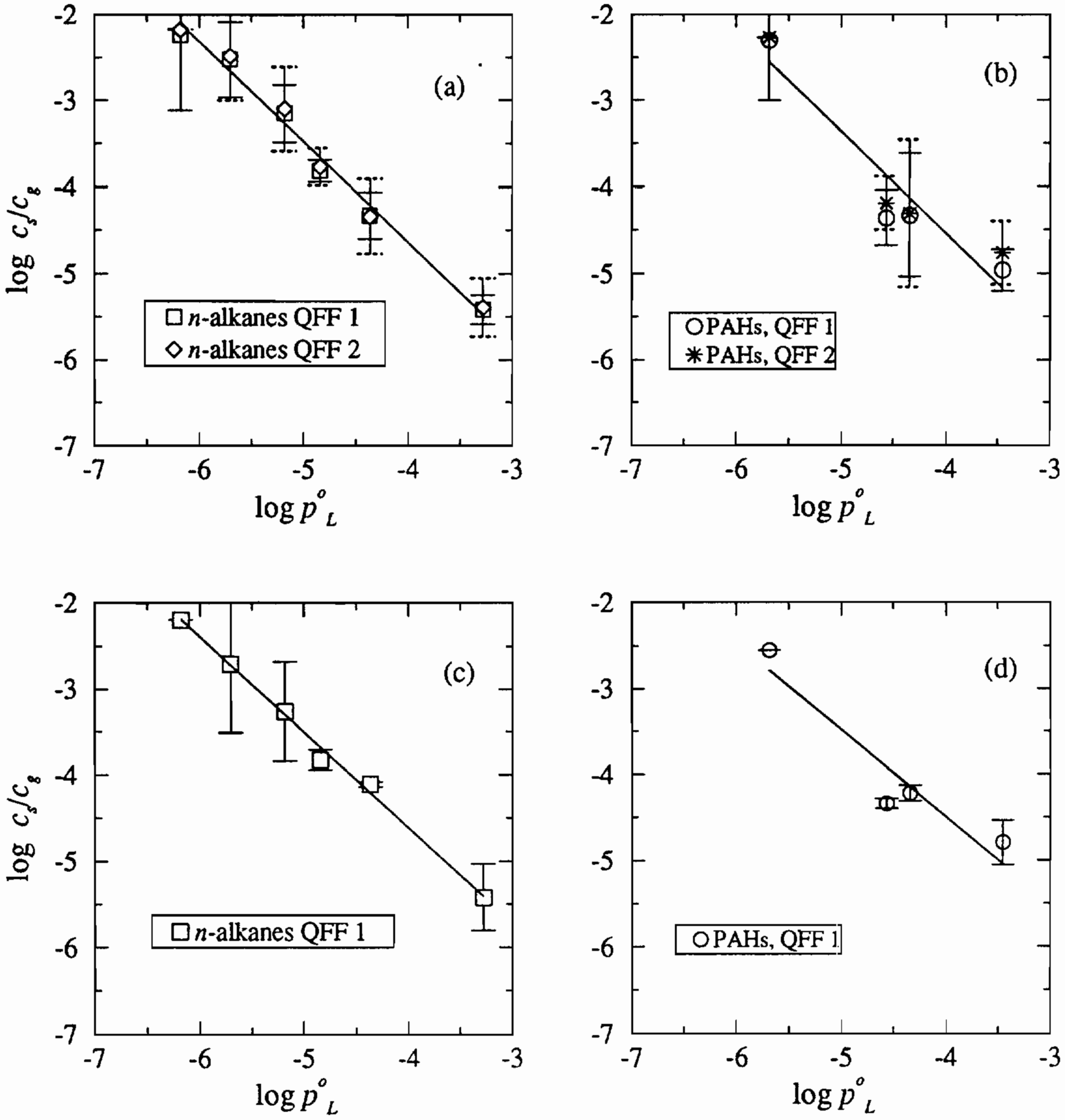

Fig. 5.7. Log c_s/c_g vs. log p^o_L plots for experiments 011392 **(a,b)** and 012492 **(c,d)**. Each line is a single SLR for all the points on each graph. m_r, b_r, and r^2 values given in Table 5.3.

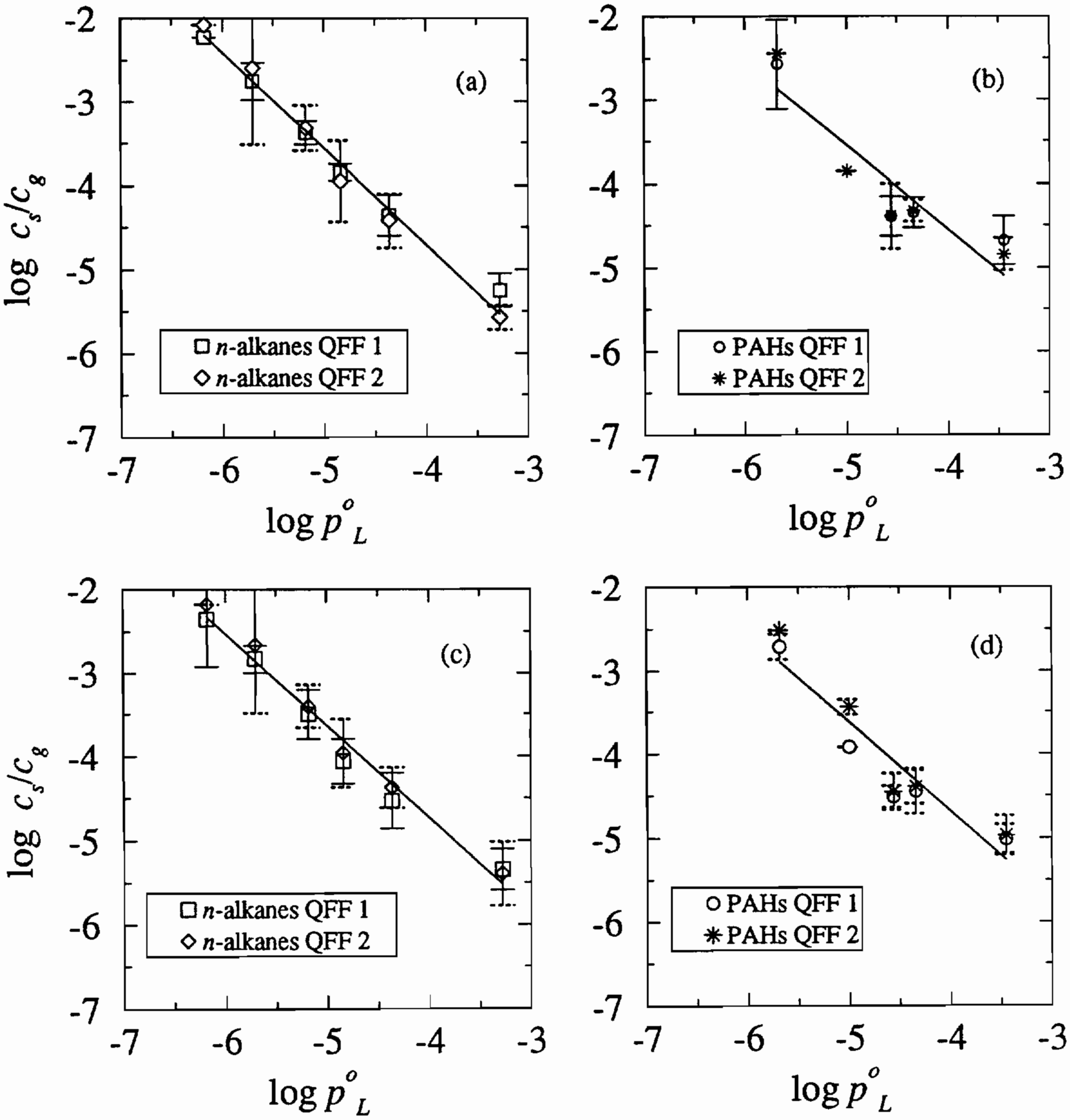

Fig. 5.8. Log c_s/c_g vs. log p^o_L plots for experiments 021092 (**a,b**) and 022592 (**c,d**). Each line is a single SLR for all the points on each graph. m_r, b_r, and r^2 values given in Table 5.3.

Table 5.2 m_r and b_r values for the 10% *RH* gas/particle partitioning experiments.

		n-alkanes			PAHs		
Run	QFF	m_r	b_r	r^2	m_r	b_r	r^2
101691	1	-0.94	-8.36	0.859	NA	NA	NA
110691	1	-1.08	-9.69	0.992	-1.08	-9.57	0.937
112691	2	-1.10	-9.19	0.991	-1.12	-9.10	1.935
122091	1,2	-1.08	-8.93	0.996	-1.00	-8.56	0.895
010292	1,2	-1.03	-8.87	0.986	-1.09	-8.96	0.923
All		-1.05	-8.97	0.917	-1.07	-8.82	0.854

Table 5.3 m_r and b_r values for the 30% *RH* gas/particle partitioning experiments.

		***n*-alkanes**			**PAHs**		
Run	**QFF**	m_r	b_r	r^2	m_r	b_r	r^2
011392	1,2	-1.16	-9.26	0.987	-1.17	-9.22	0.900
012492	1	-1.11	-9.03	0.995	-1.01	-8.53	0.897
021092	1,2	-1.14	-9.28	0.986	-1.00	-8.52	0.843
022592	1,2	-1.10	-9.11	0.981	-1.06	-8.94	0.887
All		-1.13	-9.19	0.982	-1.06	-8.82	0.869

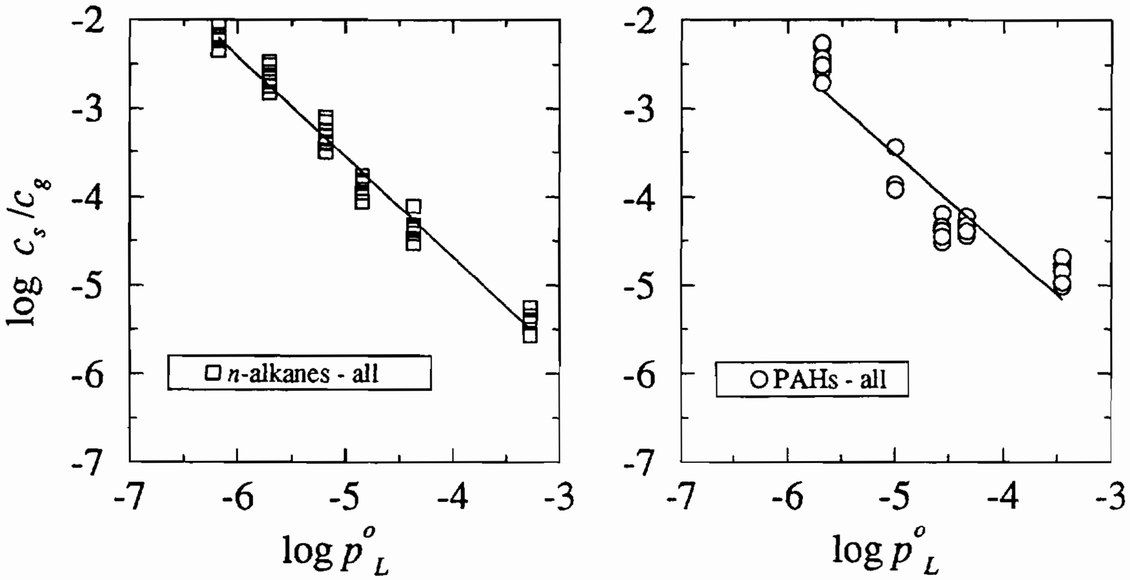

Fig. 5.9. Log c_s/c_g vs. log p^o_L plots for all of the 30% *RH* runs: 011392; 012492; 021092; and 022592 . Each line is a single SLR for all of the sample points on each graph. m_r, b_r, and r^2 values given in Table 5.3.

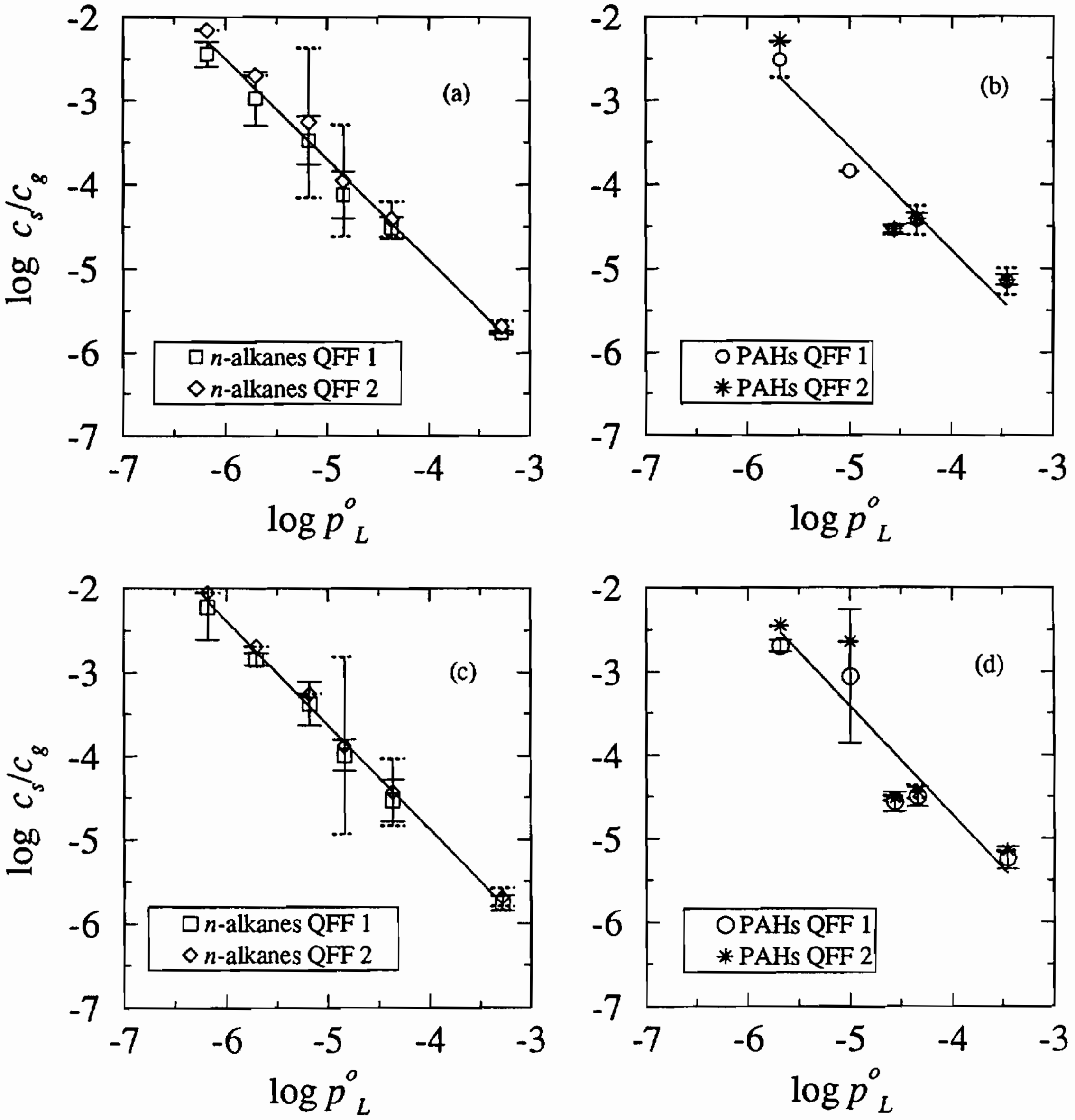

Fig. 5.10. Log c_s/c_g vs. log p^o_L plots for experiments 032092 (a,b) and 040392 (c,d). Each line is a single SLR for all the points on each graph. m_r, b_r, and r^2 values given in Table 5.4.

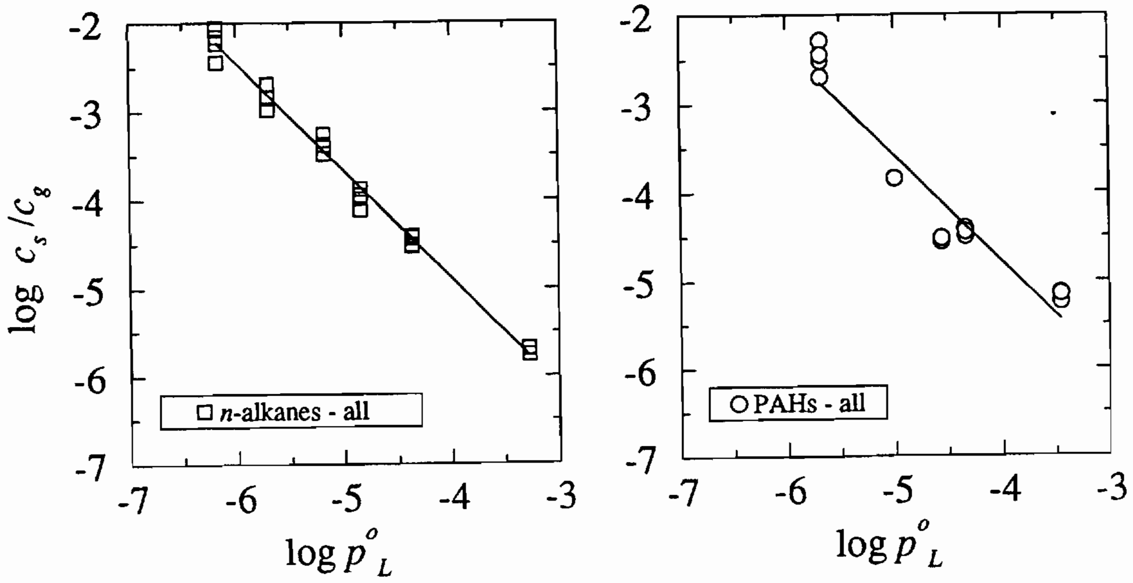

Fig. 5.11. Log c_s/c_g vs. log p^o_L plots for both of the 6% *RH* runs: 032092; and 040392. Each line is a single SLR for all of the sample points on each graph. m_r, b_r, and r^2 values given in Table 5.4.

5.3.1.4 Results of 0.4% *RH* Experiments

Two separate experiments, designated 042192 and 050792, were run at very low humidity. The experimental procedure was altered slightly in order to produce and then measure the *RH* accurately. At the beginning of an experiment, no flow was permitted through the humidifiers for four hours in order to remove any residual water remaining after assembling the system. The humidity was increased incrementally to avoid memory problems in the system if too much water was introduced to the flow. The *RH* was measured by allowing a small portion of the exit flow to go through a sorbent tube filled with Drierite ($CaSO_4$). The weight change divided by the volume gave the concentration of water in the air. The results were very reproducible. Blank Drierite tubes were run showing no weight gain. The mean *RH* for experiment 032092 was 0.37% and the mean *RH* for 040392 was 0.38%. The results of these experiments are shown in Fig. 5.12. These experiments gave low relative standard deviation values and showed excellent agreement. The data summary appears in Table 5.5 and Fig. 5.13.

5.3.1.5 Results of 78% *RH* Experiments

Three separate experiments, designated 052792, 061992, and 070892, were run at 78% *RH*. These experiments were run at the highest humidity that could be generated with the system. The high humidity was generated by routing all of the dilution flow through the humidifiers and heating the water in the first impinger. The QFFs were equilibrated with the humid air for 2 hours before the stream from the sorbate generator cartridges was turned on. The results are shown in Fig. 5.14, and summarized in Table 5.6 and Fig. 5.15. Note that only three compounds were measured during experiment 052792 because of difficulties with water condensing in the system. Nevertheless, it is clear that the c_f/c_g values are much lower for the high humidity experiments than the experiments at the other *RH* levels. In experiments 061992 and 070892, adjustments were made to the flow through the impingers, so that there was no condensed water observed in the filter holders or on the QFFs.

Table 5.4 m_r and b_r values for the 6% *RH* gas/particle partitioning experiments.

		n-alkanes			PAHs		
Run	**QFF**	m_r	b_r	r^2	m_r	b_r	r^2
032092	1,2	-1.19	-9.65	0.988	-1.21	-9.62	0.897
040392	1,2	-1.24	-9.85	0.994	-1.29	-9.89	0.854
All		-1.22	-9.75	0.990	-1.20	-9.58	0.908

Table 5.5 m_r and b_r values for the 0.4% *RH* gas/particle partitioning experiments.

		n-alkanes			PAHs		
Run	**QFF**	m_r	b_r	r^2	m_r	b_r	r^2
042192	1,2	-1.22	-9.70	0.978	-1.15	-9.25	0.925
050392	1,2	-1.15	-9.43	0.990	-1.09	-9.14	0.887
All		-1.16	-9.45	0.977	-1.12	-9.19	0.899

Table 5.6 m_r and b_r values for the 78% *RH* gas/particle partitioning experiments.

		n-alkanes			PAHs		
Run	QFF	m_r	b_r	r^2	m_r	b_r	r^2
052792	2	NA	NA	NA	NA	NA	NA
061992	1,2	-1.00	-9.84	0.946	-0.940	-9.14	0.933
070892	1,2	-1.02	-10.0	0.967	-0.979	-10.0	0.947
All		-1.02	-10.0	0.931	-0.959	-9.91	0.939

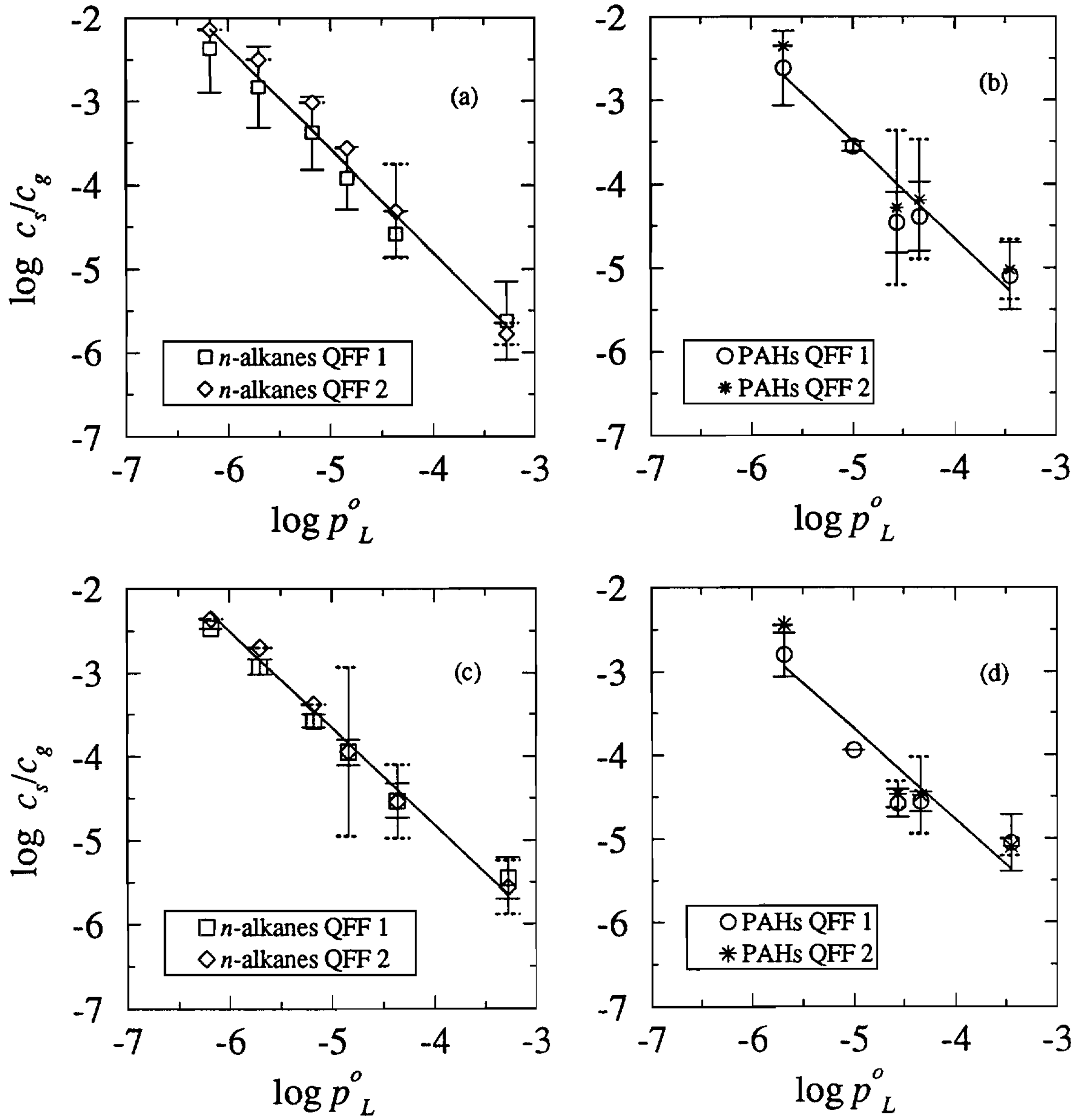

Fig. 5.12. Log c_s/c_g vs. log p^o_L plots for experiments 042192 (**a,b**) and 050792 (**c,d**). Each line is a single SLR for all the points on each graph. m_r, b_r, and r^2 values given in Table 5.5.

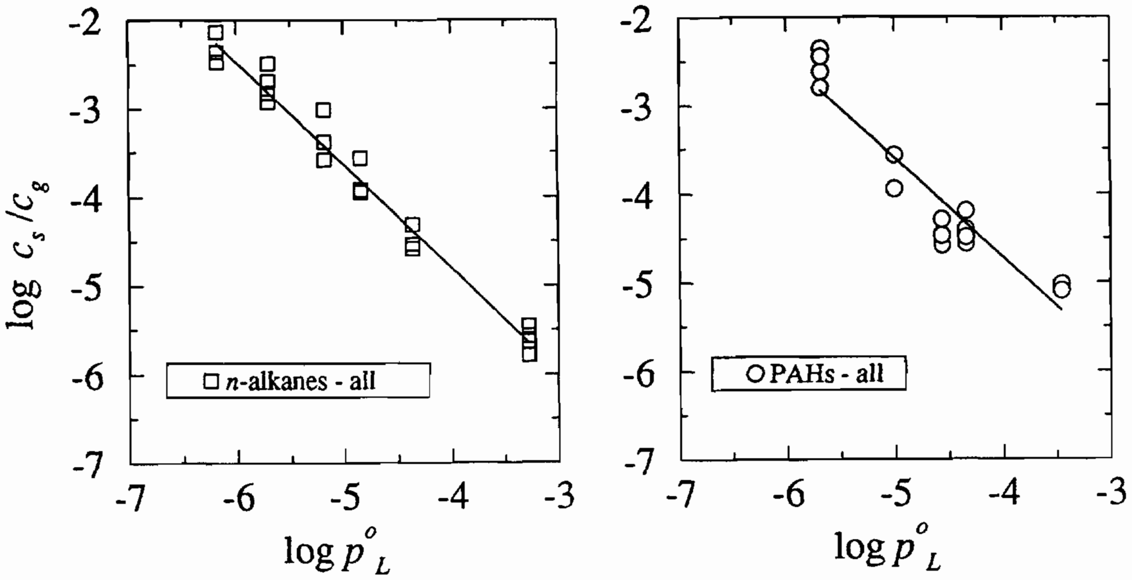

Fig. 5.13. Log c_s/c_g vs. log p^o_L plots for both of the 0.4% *RH* runs: 042192; and 050392. Each line is a single SLR for all of the sample points on each graph. m_r, b_r, and r^2 values given in Table 5.5.

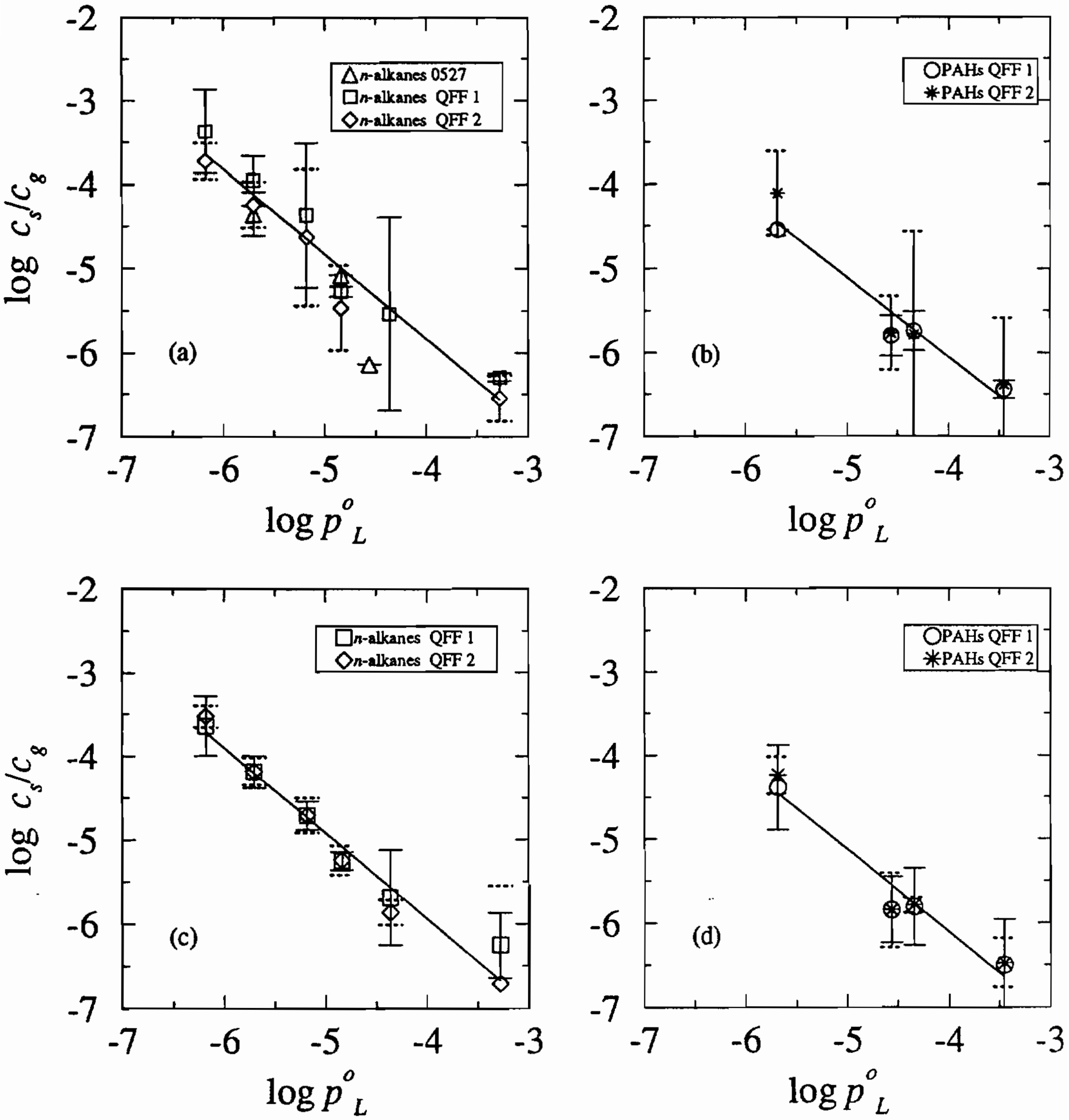

Fig. 5.14. Log c_s/c_g vs. log p^o_L plots for experiments 052792 (three points only), 061992 (a,b), and 070892 (c,d). Each line is a single SLR for all the points on each graph. m_r, b_r, and r^2 values given in Table 5.6.

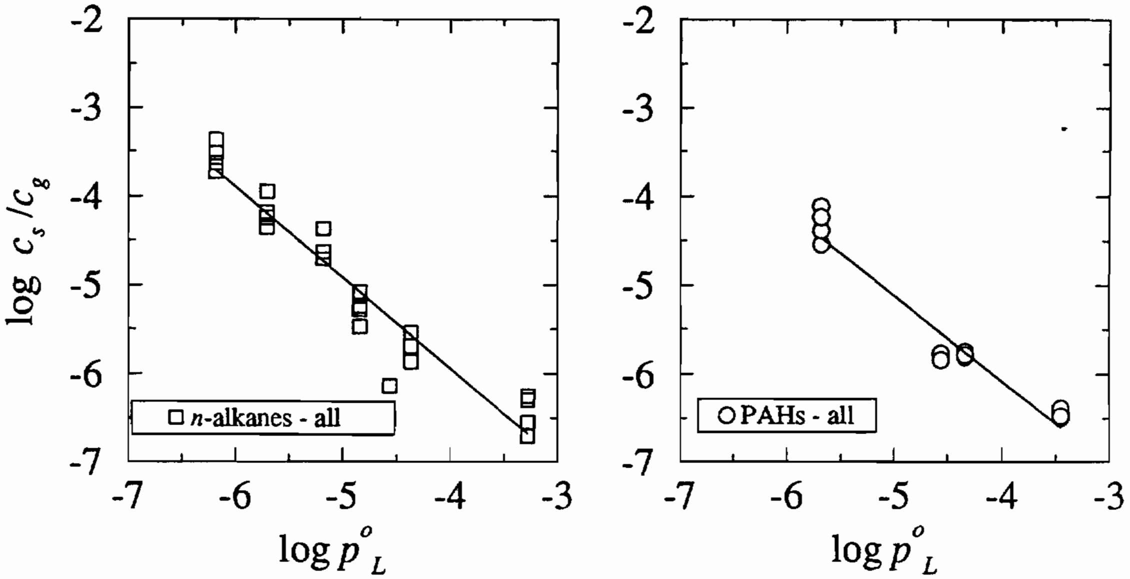

Fig. 5.15. Log c_s/c_g vs. log p^o_L plots for all of the 75% *RH* runs: 052792 (three points only); 061992; and 070892. Each line is a single SLR for all of the sample points on each graph. m_r, b_r, and r^2 values given in Table 5.6.

5.3.1.6 Summary Discussion of Gas/Solid Adsorption Results

Inspection of Tables 5.2-5.6 shows that the m_r values for the *n*-alkanes tend to be more negative than -1 (e.g., -1.1). For m_r to be equal to -1, Pankow (1987,1991) notes that $N_s e^{(Ql-Qv)}$ must essentially remain constant within the class of compounds. This condition may not be met here, since there is no *a priori* reason why $N_s e^{(Ql-Qv)}$ must remain constant. Another possible reason for the slightly steeper slopes could be in the analytical technique for measuring c_g. Adsorption/thermal desorption from Tenax is known to work less well with the less volatile SOCs. Therefore, if 100% desorption efficiency was not achieved for the low p_L^o compounds, then those values of log c_s/c_g would have a slight positive bias and the slope of the log c_s/c_g vs. log p_L^o line would become steeper. Although ATD desorption efficiency studies were determined early in this effort, it was not practical from a time standpoint to re-desorb each sample cartridge to make sure all of the low p_L^o compounds were completely desorbed. Overall, though, log c_s/c_g is highly correlated with log p_L^o, and thus the results seem to agree well with the simple, physical adsorption model for gas/solid partitioning.

5.3.2 A Look at the Influence of Surface Area

The influence of particle surface area on gas/solid partitioning is well-known. Storey and Pankow (1992) show that normalization for specific surface area (A_{TSP} for ambient particles) can improve the agreement between the partitioning of PAHs to monodisperse aerosols with that for the partitioning of PAHs to UPM. In Figs 5.16(a,c) - 5.22(a,c), the log c_s/c_g (of PAHs) vs. log p_L^o plots for each experiment are compared to SLR lines for log $(F/TSP)/A$ vs. log p_L^o of PAHs on UPM calculated from Pankow (1991). In Figs 5.16(b,d) - 5.22(b,d), the log $(c_s/c_g)_s$ vs. log p_L^o plots from each experiment are compared to the same SLR lines normalized to TSP_s. The $(c_s/c_g)_s$ values are defined by:

$$(c_s/c_g)_s = \frac{(c_s/c_g)}{10^2 A_{QFF}} \tag{5.5}$$

where A_{QFF} = the surface area of the QFF in cm^2 µg^{-1}. Thus $(c_s/c_g)_s$ has units of m^3 m^{-2} just as $(F/TSP_s)/A$ does. Using krypton adsorption, the A_{QFF} of the same brand and model quartz fiber filter was measured by Micromeritics (Norcross, GA) to be 0.022 ± .01 cm2 µg^{-1} (Turpin, 1992). TSP_s was taken to be 0.094 ± .03 cm^2 µg^{-1}, as obtained by Micromeritics for UPM collected in Portland by Sheffield (1992).

After normalization for surface area, there is remarkable agreement between the experimental points and the UPM-SLR line. While this agreement does not prove that simple, physical adsorption is the only important mechanism controlling gas/particle partitioning of SOCs in urban air, it does add support to the hypothesis that the mechanism is playing a significant role. Figures 5.16(b,d) - 5.22(b,d) have an important implication. If further work validates the close agreement between simple gas/solid adsorption experiments and the measured K_p values for SOC on APM, then only A_{TSP} and TSP for a given sample of APM would be necessary to predict partitioning behavior. Such a simplification would be extremely useful in developing models for the global fate and transport of these compounds.

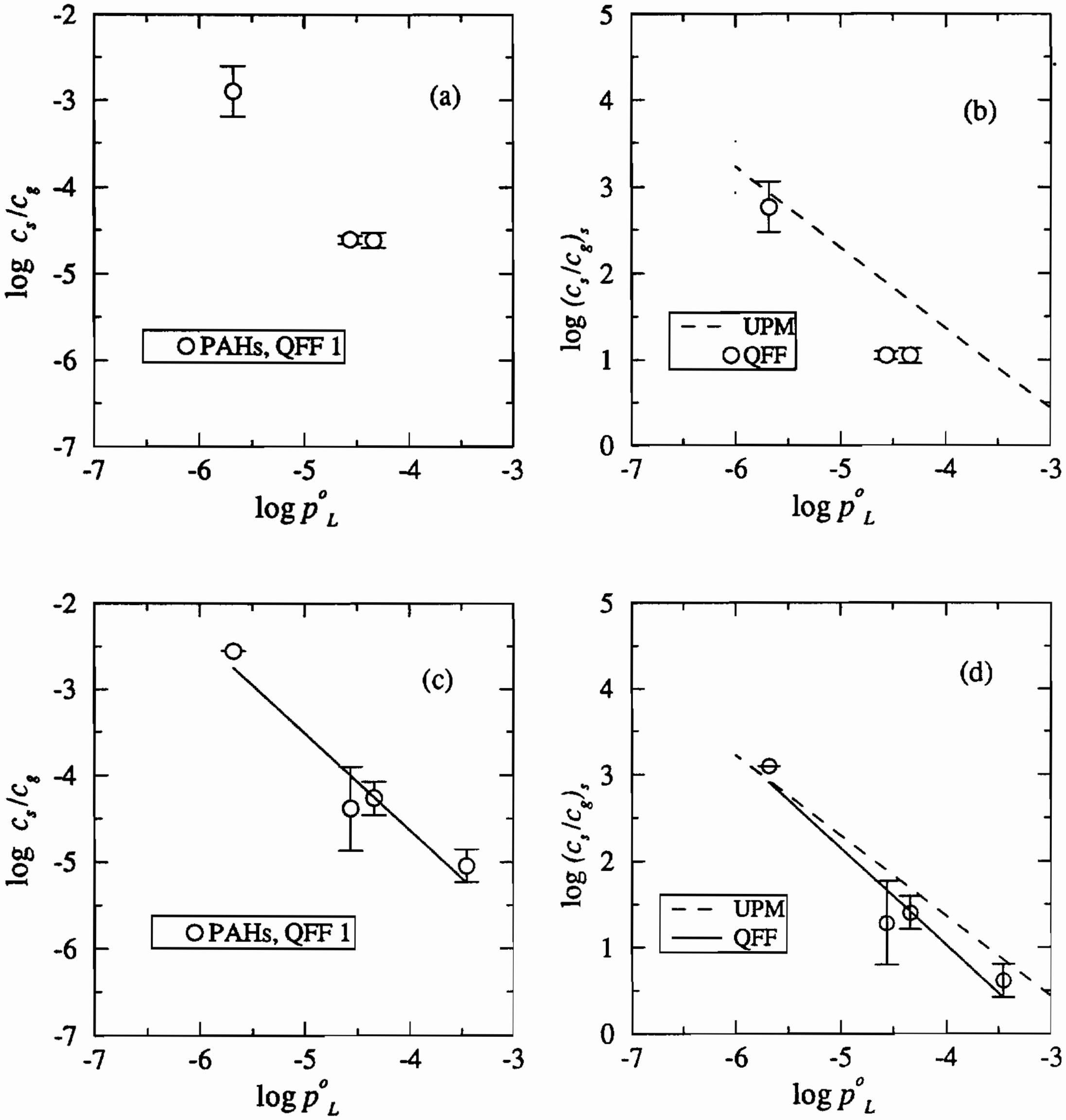

Fig. 5.16. Log c_s/c_g and log $(c_s/c_g)_s$ vs. log p^o_L of PAHs on QFF at 20 °C compared to UPM-SLR lines for log $(F/TSP)/A$ and log $(F/TSP_s)/A$ vs. log p^o_L of PAHs at 20 °C calculated using method of Pankow (1991). **(a,b)** experiment 101691; **(c,d)** experiment 112691. The regression lines through the experimental points were calculated using only the data points from the individual experiment. RH = 10% for both experiments.

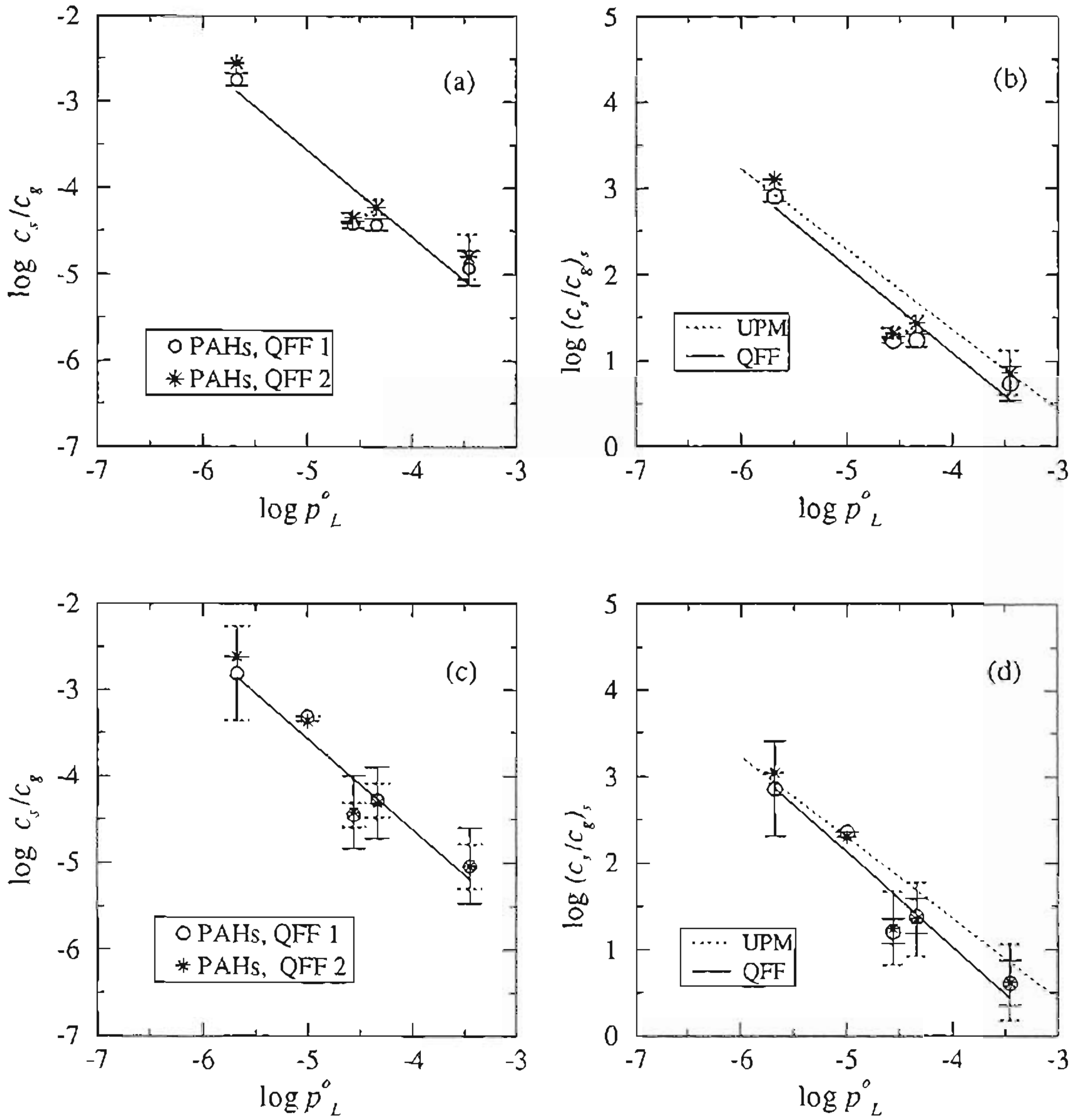

Fig. 5.17. Log c_s/c_g and log $(c_s/c_g)_s$ vs. log p^o_L of PAHs on QFF at 20 °C compared to UPM-SLR lines for log $(F/TSP)/A$ and log $(F/TSP_s)/A$ vs. log p^o_L of PAHs at 20 °C calculated using method of Pankow (1991). (a,b) experiment 122091; (c,d) experiment 010292. The regression lines through the experimental points were calculated using only the data points from the individual experiment. RH = 10% for both experiments.

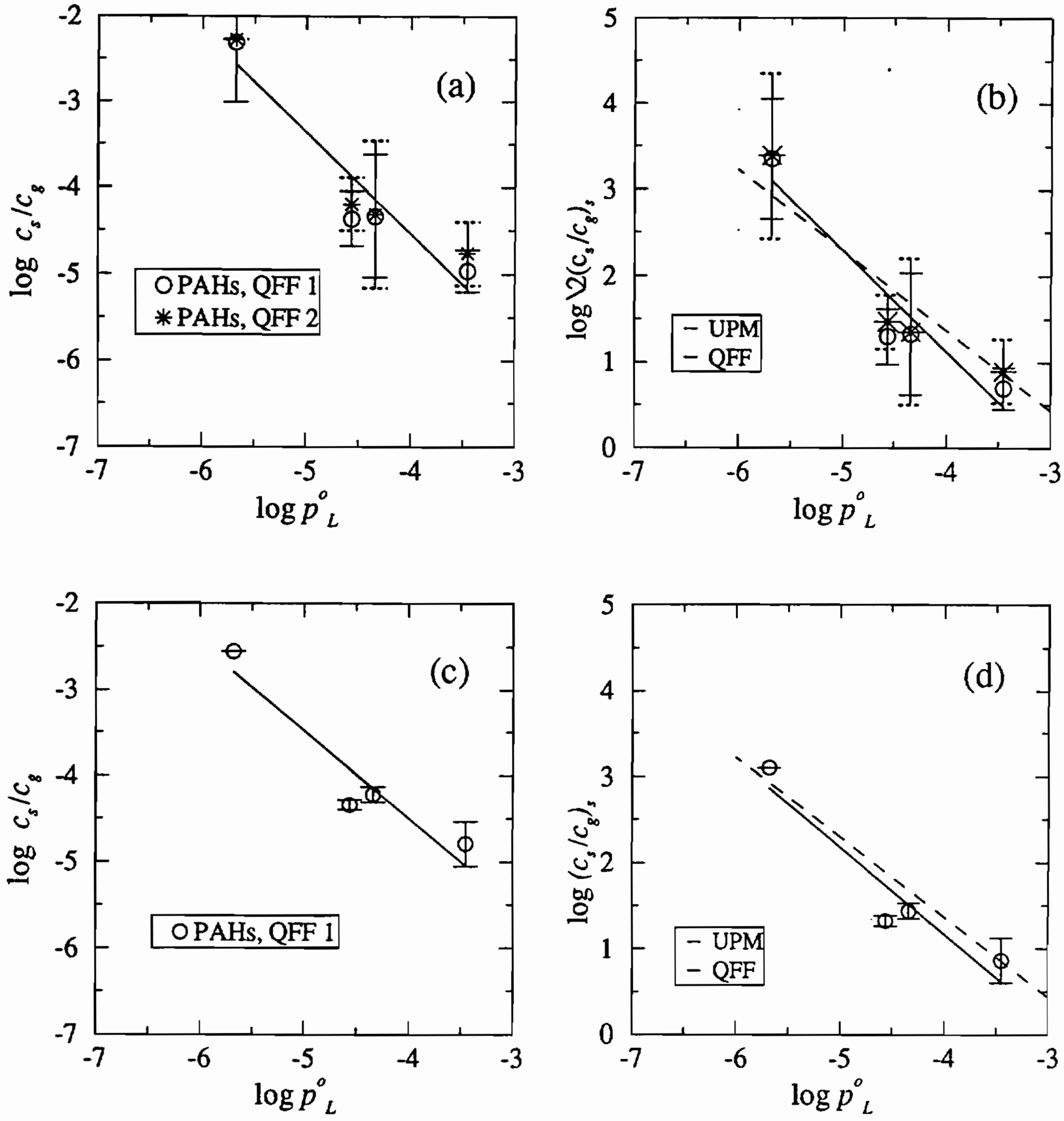

Fig. 5.18. Log c_s/c_g and log $(c_s/c_g)_s$ vs. log p^o_L of PAHs on QFF at 20 °C compared to UPM-SLR lines for log $(F/TSP)/A$ and log $(F/TSP_s)/A$ vs. log p^o_L of PAHs at 20 °C calculated using method of Pankow (1991). **(a,b)** experiment 011392; **(c,d)** experiment 012492. The regression lines through the experimental points were calculated using only the data points from the individual experiment. RH = 30% for both experiments.

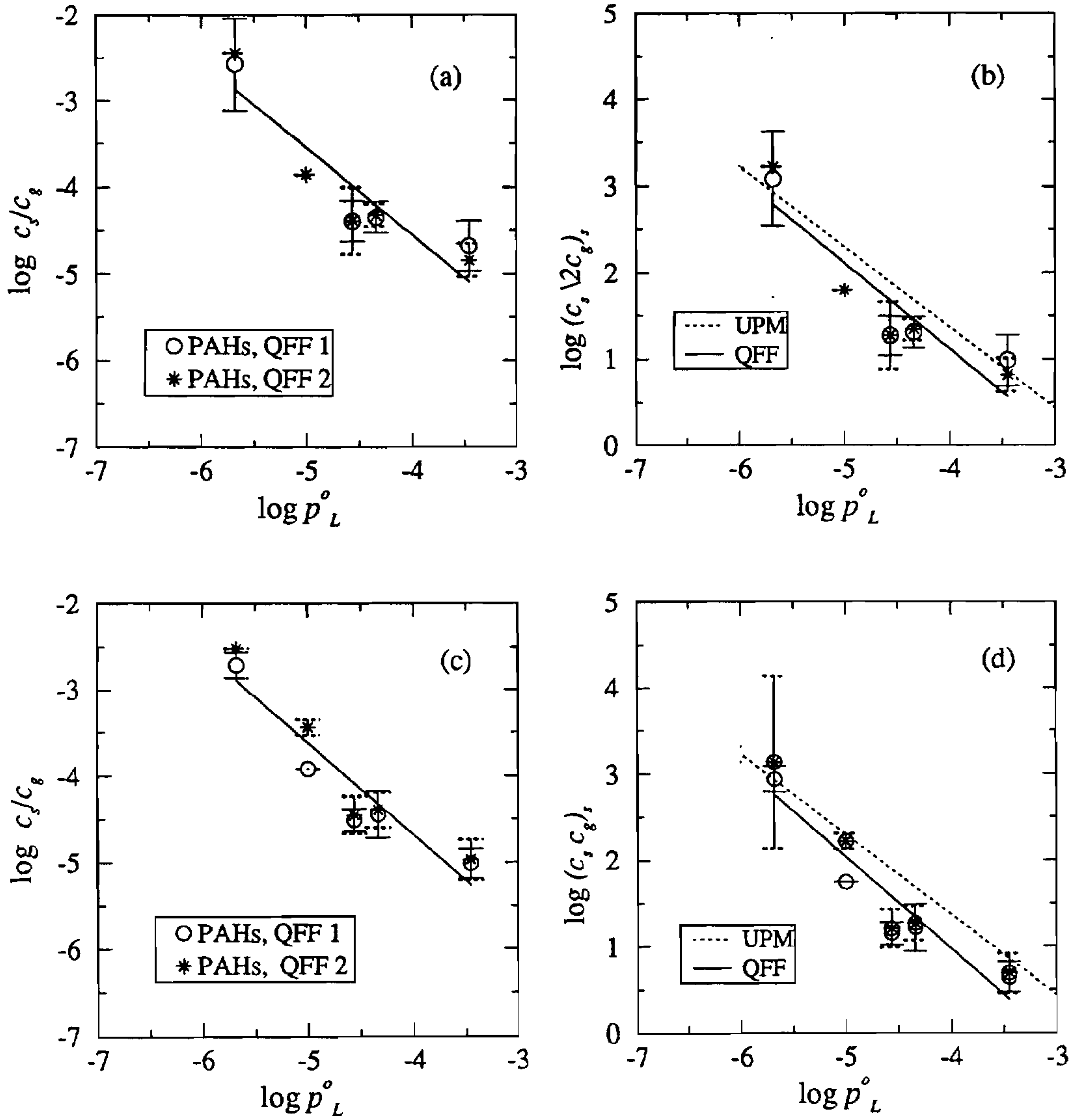

Fig. 5.19. Log c_s/c_g and log $(c_s/c_g)_s$ vs. log p_L^o of PAHs on QFF at 20 °C compared to UPM-SLR lines for log $(F/TSP)/A$ and log $(F/TSP_s)/A$ vs. log p_L^o of PAHs at 20 °C calculated using method of Pankow (1991). (a,b) experiment 021092; (c,d) experiment 022592. The regression lines through the experimental points were calculated using only the data points from the individual experiment. RH = 30% for both experiments.

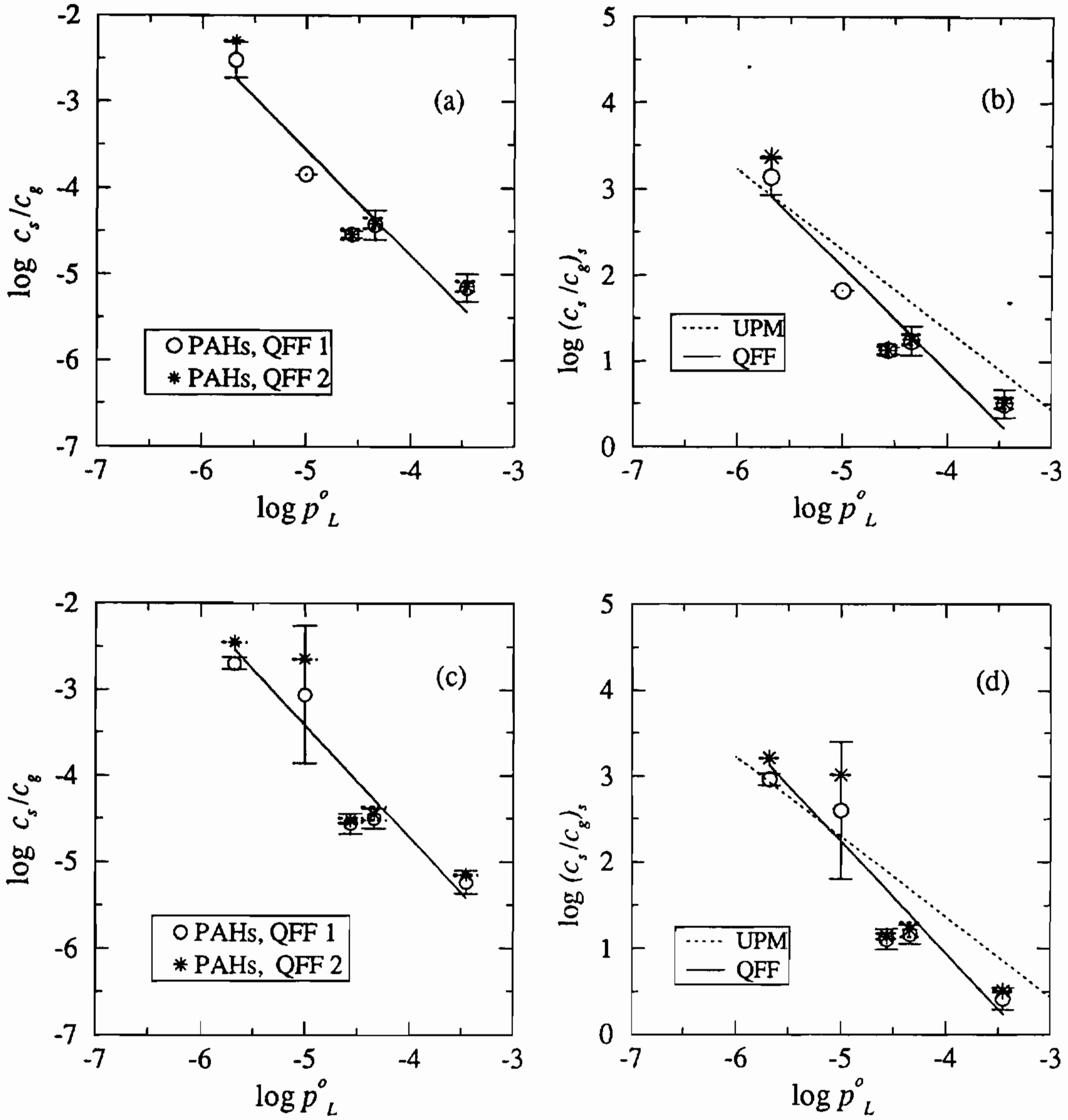

Fig. 5.20. Log c_s/c_g and log $(c_s/c_g)_s$ vs. log p^o_L of PAHs on QFF at 20 °C compared to UPM-SLR lines for log $(F/TSP)/A$ and log $(F/TSP_s)/A$ vs. log p^o_L of PAHs at 20 °C calculated using method of Pankow (1991). **(a,b)** experiment 032092; **(c,d)** experiment 040392. The regression lines through the experimental points were calculated using only the data points from the individual experiment. *RH* = 6% for both experiments.

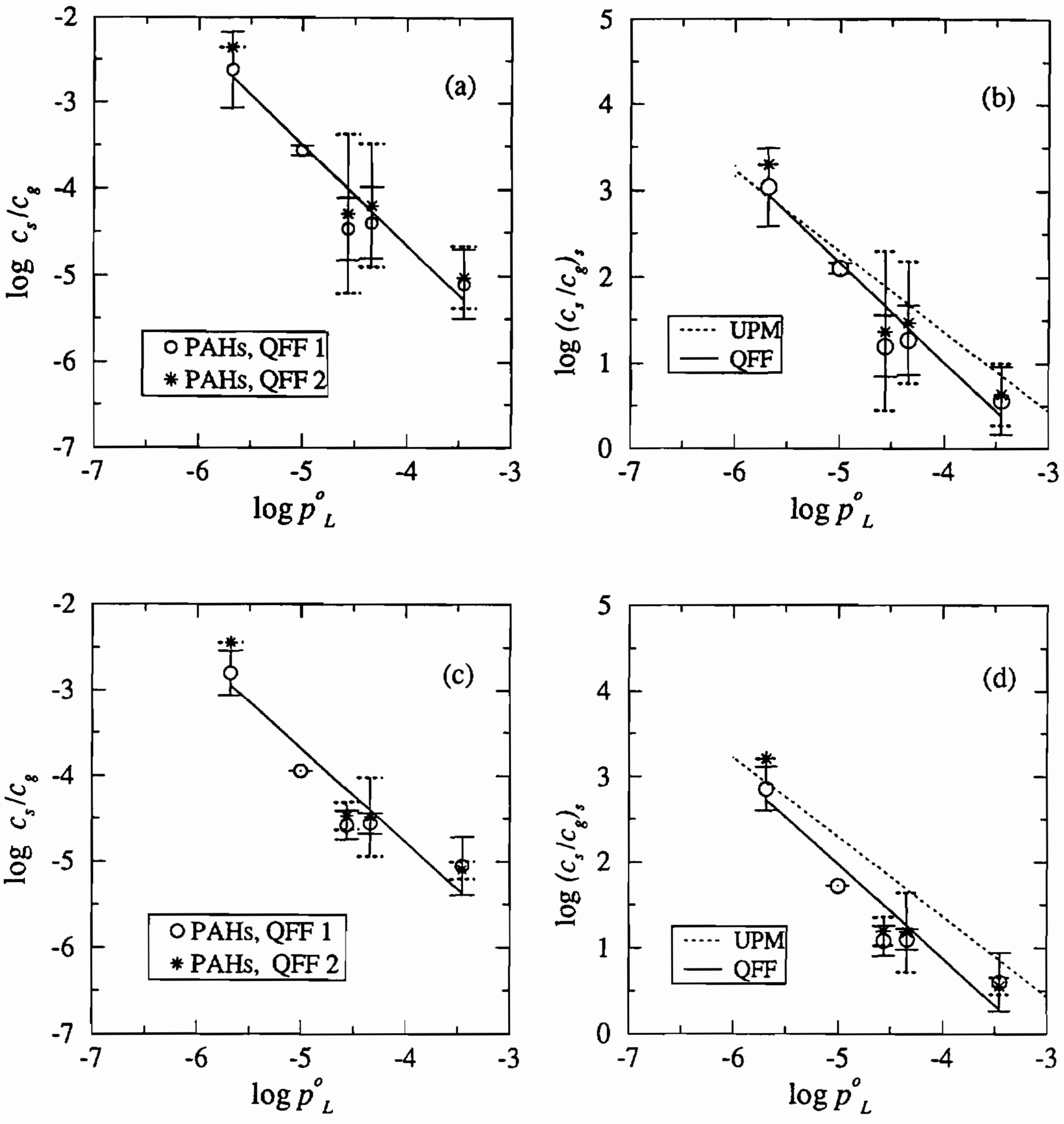

Fig. 5.21. Log c_s/c_g and log $(c_s/c_g)_s$ vs. log p^o_L of PAHs on QFF at 20 °C compared to UPM-SLR lines for log *(F/TSP)/A* and log *(F/TSP$_s$)/A* vs. log p^o_L of PAHs at 20 °C calculated using method of Pankow (1991). **(a,b)** experiment 042192; **(c,d)** experiment 050792. The regression lines through the experimental points were calculated using only the data points from the individual experiment. *RH* = 0.4% for both experiments.

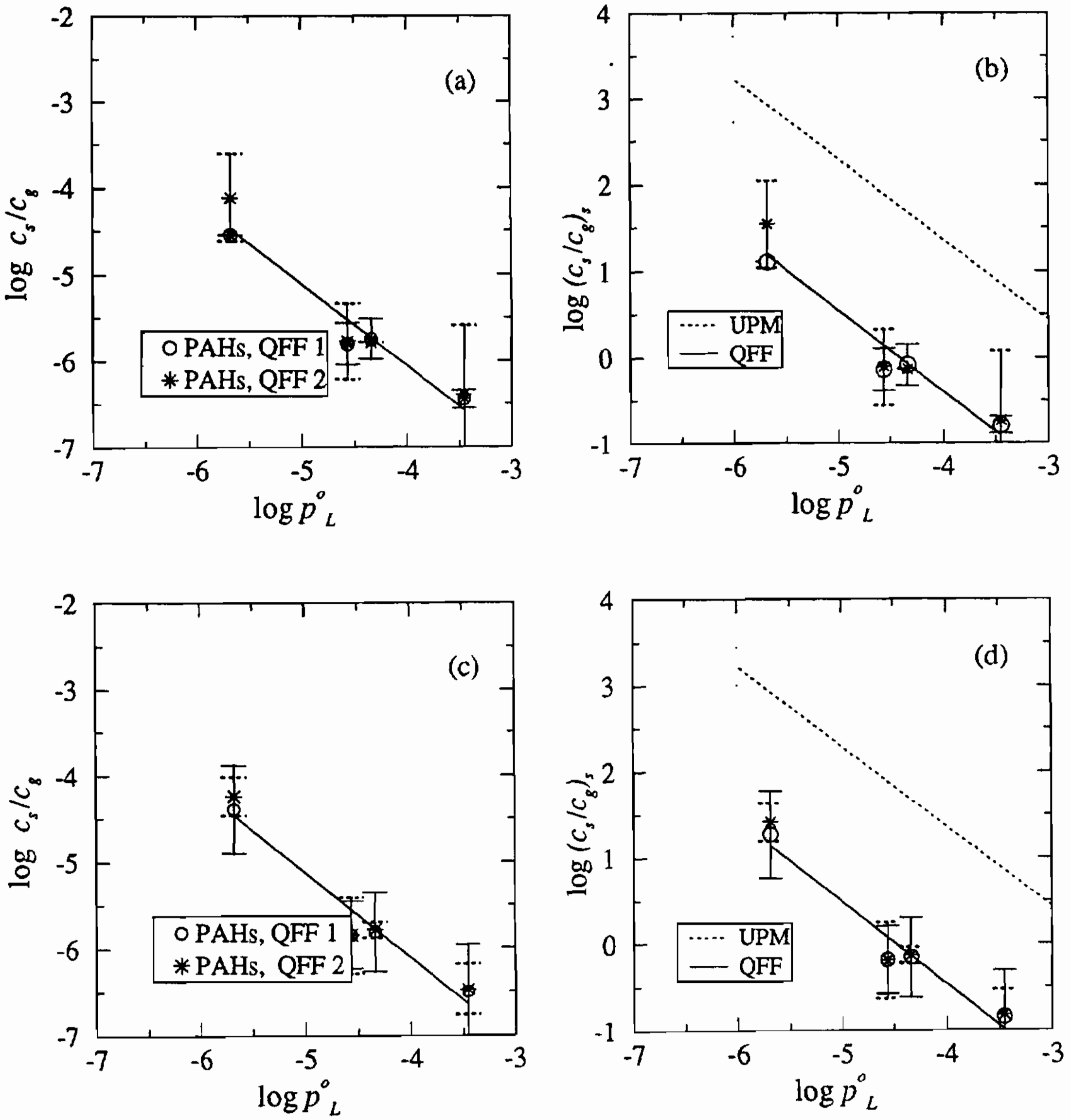

Fig. 5.22. Log c_s/c_g and log $(c_s/c_g)_s$ vs. log p_L^o of PAHs on QFF at 20 °C compared to UPM-SLR lines for log $(F/TSP)/A$ and log $(F/TSP_s)/A$ vs. log p_L^o of PAHs at 20 °C calculated using method of Pankow (1991). (a,b) experiment 061992; (c,d) experiment 070892. The regression lines through the experimental points were calculated using only the data points from the individual experiment. RH = 78% for both experiments.

5.3.3 Results in Terms of *RH*

By plotting the average log c_s/c_g values of individual compounds vs. *RH*, the effect of *RH* on sorption can be illustrated just as in Chapter 4. The results from the above experiments are presented in Figs. 5.23 and 5.24. Table 5.7 summarizes the average log c_s/c_g values for each *RH*, and also provides grand averages and pooled relative standard deviations for *RH* = 0.4%, 6%, 10% and 30%. There are important points to be made about this data. First, the log c_s/c_g values for all of the these runs for each compound are very similar, certainly within one standard deviation. Secondly, a student *t*-test (Table 5.8) was applied between average log c_s/c_g values for each of the four low *RH* values (e.g. *RH* = 0.4%, 6%, 10%, and 30%). With the exception of the two shaded values, no significant (>99% confidence level) difference between the values was found. The two exceptions are very close to the *t*-statistic for the 95% confidence level. Table 5.8 gives all of the *t*-statistics for the comparisons. Finally, a *t*-test on the mean log c_s/c_g values of all the "dry" *RH* experiments and the mean log c_s/c_g values for 78% *RH* experiments shows that the two means are significantly different for every compound. These *t*-statistics are shaded in the far right column of Table 5.8. For most of the compounds, there is a full order-of-magnitude difference between the c_s/c_g values.

The consistency of the experiments at 0.4%, 6%, 10% and 30% *RH* seems to indicate that the gas-solid adsorption *n*-alkanes and PAHs to QFF is independent of *RH* over the range for which there are a few layers of water or less on the surface. In Chapter 4, the theoretical work of Thibodeaux *et al.* (1991) on multicomponent adsorption would predict that the greatest *RH* effect on gas/particle partitioning in ambient air would be observed between 0 and 30% *RH*. However, the work presented here seems to indicate that adsorption of the compounds to the QFF is occurring independent of *RH* for these lower values. It should be noted that H_2O molecules may have been bound to the QFF surface after removal from the muffle furnace and installation in the filter holders. Therefore, it may be that the number of adsorbed water layers on the QFF at 0.4% *RH* was not very different than at 30% *RH*. The similarity in log c_s/c_g values for the different *RH* values is also consistent with the similarity in log *(F/TSP)/A* values observed by Yamasaki *et al.* (1982) for PAHs at different *RH*.

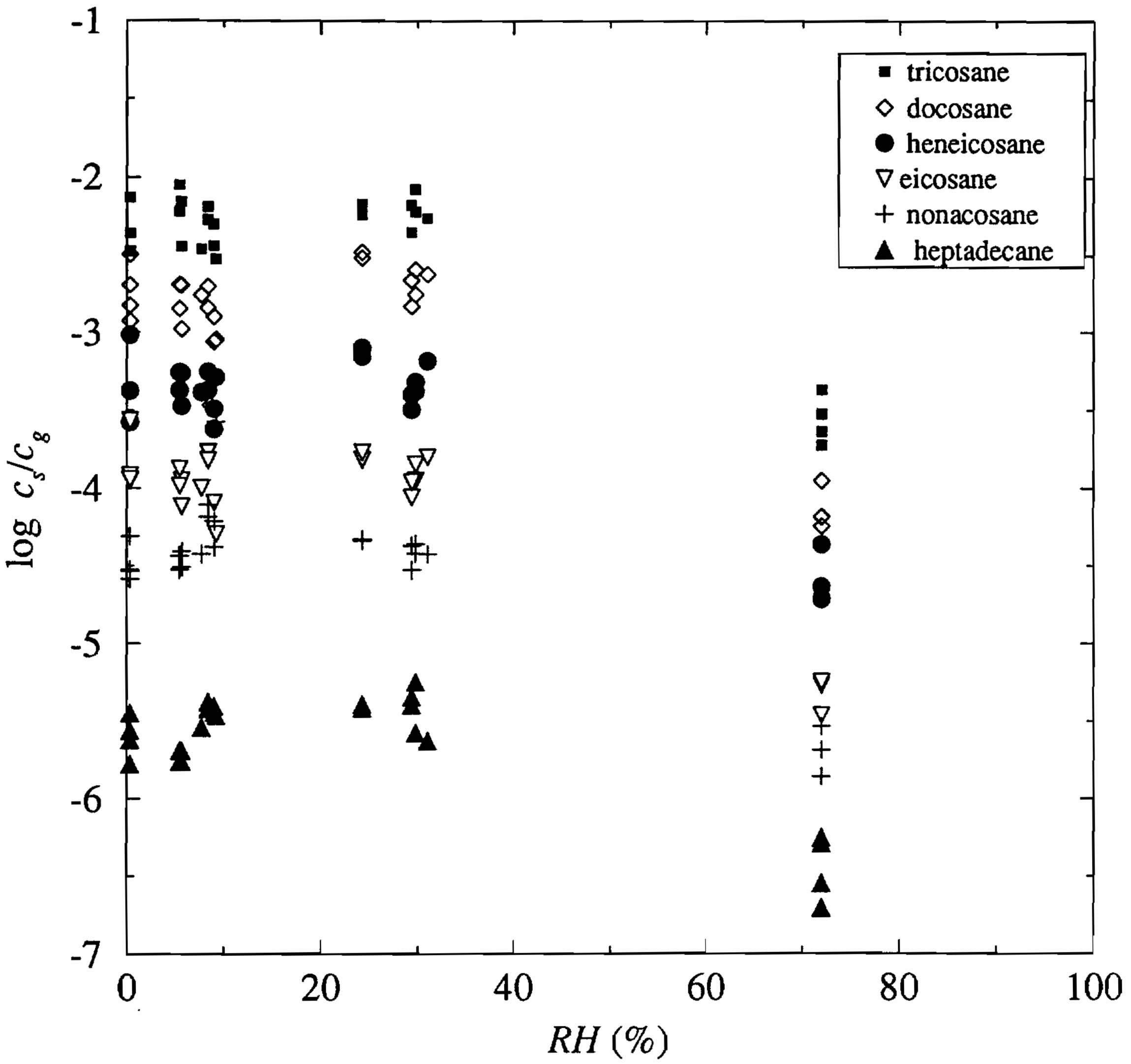

Fig. 5.23. Log c_s/c_g vs. *RH* for the *n*-alkanes. Error bars were omitted to reduce the complexity of the plot.

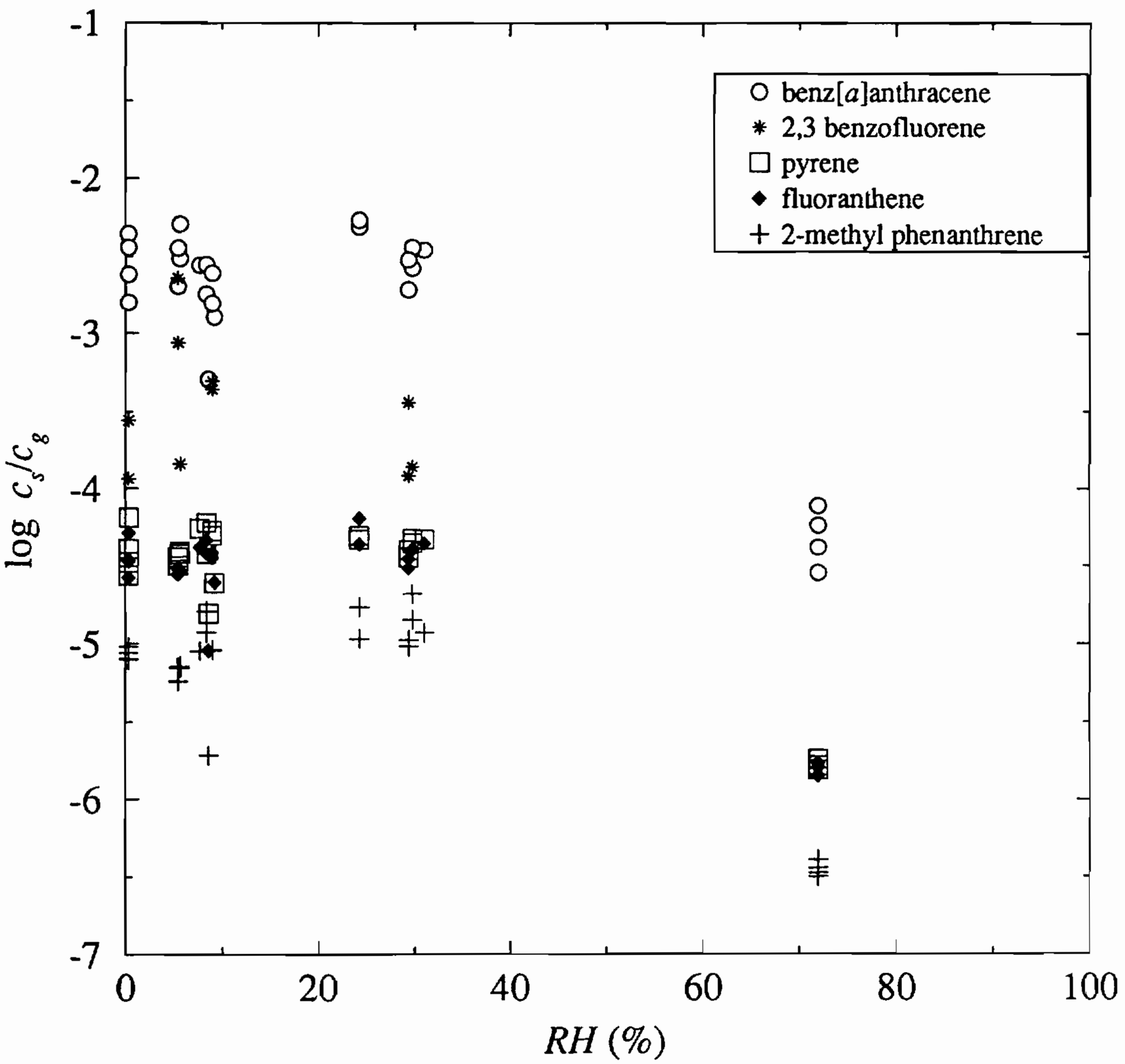

Fig. 5.24. Log c_s/c_g vs. *RH* for the PAHs. Error bars were omitted to reduce the complexity of the plot.

Table 5.7 Average log c_s/c_g values organized by *RH*.

compound	mean 10% log c_s/c_g	mean 25% log c_s/c_g	mean 6% log c_s/c_g	mean 0.4% log c_s/c_g	overall log c_s/c_g	overall r.s.d.	mean 75% log c_s/c_g	mean 75% r.s.d.
n-alkanes								
heptadecane	-5.54	-5.43	-5.73	-5.61	-5.55	0.26	-6.45	0.31
nonadecane	-4.26	-4.39	-4.47	-4.49	-4.38	0.33	-5.69	0.74
eicosane	-4.09	-3.88	-3.98	-3.84	-3.96	0.32	-5.26	0.28
heneicosane	-3.49	-3.29	-3.34	-3.34	-3.37	0.42	-4.60	0.19
docosane	-2.97	-2.64	-2.80	-2.74	-2.79	0.33	-4.18	0.27
tricosane	-2.46	-2.22	-2.22	-2.33	-2.32	0.38	-3.56	0.34
PAHs								
2-methyl-phenanthrene	-5.09	-4.87	-5.17	-5.07	-5.03	0.25	-6.45	0.36
fluoranthene	-4.52	-4.38	-4.54	-4.45	-4.47	0.32	-5.88	0.39
pyrene	-4.41	-4.35	-4.44	-4.40	-4.40	0.35	-5.78	0.30
benz(*a*)anthracene	-2.78	-2.47	-2.49	-2.55	-2.59	0.38	-4.32	0.43
benzo[*b*]fluorene	-3.33	-3.74	-3.18	-3.75	-3.64	0.28	0.00	0.00

Table 5.8 *t*-statistics for inter-experiment comparisons of log c_s/c_g values.

compound	6% vs. 0.4% *t*	10% vs. 0.4% *t*	30% vs. 0.4% *t*	10% vs. 6% *t*	30% vs. 6% *t*	10% vs. 30% *t*	all[‡] vs. 75% *t*
n-alkanes							
heptadecane	-0.75[**]	0.32	1.05	1.13	2.32	-0.75	6.09
nonadecane	0.08	0.95	0.45	0.98	0.42	0.75	5.51
eicosane	-0.28	-0.90	-0.18	-0.37	0.36	-1.22	7.55
heneicosane	-0.01	-0.31	0.20	-0.30	0.23	-0.74	4.03
docosane	-0.22	-0.76	0.33	-0.61	0.58	-1.30	7.52
tricosane	0.28	-0.28	0.27	-0.98	0.01	-0.57	6.06
PAHs							
2-methyl phenanthrene	-0.60	-0.13	1.21	0.56	2.38	-1.64	8.81
fluoranthene	-0.34	-0.29	0.31	0.10	1.16	-0.92	7.99
pyrene	-0.16	-0.05	0.18	0.26	0.38	-0.32	7.38
benz(a)anthracene	0.23	-0.66	0.19	-0.95	0.04	-0.93	7.15
benzo[*b*]fluorene	0.00	0.00	0.00	NA	-0.58	0.42	0.00

[‡] The average of all 0%, 5%, 10%, 30% *RH* runs

[**] $t_{.0025}$ = 2.01 - 2.25 for 5-25 degrees of freedom

The decrease in the c_s/c_g values at high *RH* values is more confusing. One way to analyze this result is to look at the amount of water present on the QFF at high *RH*. Several pre-baked QFFs were exposed to ~75% *RH* in a glove box for 24 hours. The *RH* was generated by a constant humidity method by placing a saturated solution of NH_4Cl and KNO_3 in the glove box (Sheffield, 1992). The filters were then weighed on a sensitive electrobalance (Cahn/Ventron, Cerritos, CA). By baking the filters at 300 °C, and re-weighing them immediately, the amount of H_2O adsorbed is found to be 6.42 ± .44 mg g^{-1}. Assuming that all of the QFF surface (2.2 m^2 g^{-1}) is available for sorption of water, n/n_m can be calculated:

$$\frac{n}{n_m} = \frac{\dfrac{6.42 \pm .44 mg\ H_2O}{g\ QFF} \bullet \dfrac{mol H_2O}{18{,}000 mg}}{\dfrac{1.6 \times 10^{-5} mol H_2O}{m^2} \bullet \dfrac{2.2 m^2}{g\ QFF}} = 10.2 \pm 0.69 \qquad (6.6)$$

This corresponds to about 10 monolayer equivalents of water. The measured n/n_m can then be compared to the value predicted by the BET equation, Eq. 4.1. For $X_A = 0.75$, Eq. 4.1 gives n/n_m values between 3.00 and 3.99, for $B_A = 1$ to 100. This difference in observed and predicted values for H_2O on the QFF surface is most likely due to a stronger binding mechanism than the physical adsorption that BET theory assumes.

There are two possible explanations to consider. The first is that the amount of water on the surface of the QFF is so large that the SOC is mostly partitioning to the *liquid* H_2O on the surface. Henry's Law governs this type of partitioning where a constant *H* (atm m^3 mol^{-1}) is defined as:

$$H = \frac{p_{SOC}}{\{SOC\}} \qquad (6.7)$$

where p_{SOC} = the partial pressure of the SOC (atm) and *{SOC}* = the activity of the SOC in water (mol m^{-3}). *H* values for many hydrocarbon SOCs have been tabulated by Mackay and Shiu (1982). The tabulated *H* values can be compared to *H* values calculated from experiments 061992 and 070892 which were done at RH = 78%. The conversions from c_g to p_{SOC} and c_s to $\{SOC\}$ (assuming that all of the compound associated with the QFF is dissolved in the water layers) are given below:

$$p_{SOC} = \frac{c_g RT}{10^9 M} \tag{5.8}$$

and

$$\{SOC\} = \frac{c_s}{W_{H_2O} 10^9 M} \tag{5.9}$$

where $R = 8.2 \times 10^{-5}$ (atm m^3 mol^{-1} K^{-1}); M (g mol^{-1}) and T (K) are defined previously; WH_2O = amount of water adsorbed to the QFF (m^3 μg^{-1}); and 10^9 converts ng to g. Table 5.9 gives the p_{SOC}, $\{SOC\}$, calculated H, and the Mackay and Shiu (1982) H values when available. There is a large difference in the calculated H and literature H values. This can be explained by the very high $\{SOC\}$ values found. These values exceed the known solubility limit of hexadecane by three orders-of-magnitude. Furthermore, it is unlikely that the ~10 monolayers of water over the whole surface of the QFF would behave like droplet of the same volume. Clearly, there is another sorption mechanism besides dissolution into the sorbed water, or there is more water present on the surface of the QFFs due to a higher RH then was measured. Although no water condensed on the filter was observed by the naked eye, droplets were observed to have formed in the glass manifold that mixes the sorbate-laden gas stream with the dilution gas stream.

The second explanation for the observed decrease in sorption of SOC with high RH is the loss of surface area due to the condensation of H_2O in micropores of the QFF. A decrease in surface area would result in a decline in adsorption and hence a lower c_s/c_g value. The Kelvin equation (Heimenz, 1986) predicts r (m), the radius of curvature of liquid in a capillary to be:

$$r = \frac{-M\gamma}{\rho RT \ln RH} \tag{5.10}$$

Table 5.9 Calculated Henry's Law constant for two 78% *RH* experiments.

	p_{soc}†† (atm)	{*SOC*} (mol m^{-3})	*H* (atm m^3 mol^{-1})	p_{soc}ᵃ (atm)	{*SOC*} (mol m^{-3})	*H* (atm m^3 mol^{-1})	*H* (lit.)‡‡ (atm m^3 mol^{-1})
n-alkanes	Experiment 061992			Experiment 070892			
heptadecane	1.9×10^{-10}	0.480	3.9×10^{-10}	1.94×10^{-10}	0.459	4.22×10^{-10}	1.49×10^{-5}
nonadecane	9.7×10^{-12}	NA	NA	9.87×10^{-12}	0.108	9.1×10^{-11}	NA
eicosane	5.9×10^{-12}	0.166	3.56×10^{-12}	9.6×10^{-12}	0.354	2.71×10^{-11}	2.88×10^{-6}
heneicosane	2.3×10^{-12}	0.483	4.72×10^{-12}	3.79×10^{-12}	0.473	8.01×10^{-12}	NA
docosane	2.74×10^{-12}	1.45	1.90×10^{-12}	3.76×10^{-12}	1.59	2.36×10^{-12}	NA
tricosane	2.43×10^{-13}	0.499	4.87×10^{-13}	3.1×10^{-13}	0.520	5.96×10^{-13}	NA
PAHs							
2-methyl phenanthrene	7.57×10^{-11}	0.189	4.00×10^{-10}	8.39×10^{-11}	0.181	4.64×10^{-10}	NA
fluoranthene	2.58×10^{-11}	0.275	9.73×10^{-11}	4.36×10^{-11}	0.421	1.04×10^{-10}	2.18×10^{-3}
pyrene	1.41×10^{-11}	0.157	8.98×10^{-11}	2.34×10^{-11}	0.246	9.53×10^{-11}	1.19×10^{-5}
benz(a)anthracene	8.84×10^{-13}	0.307	2.88×10^{-13}	1.44×10^{-12}	0.439	3.27×10^{-12}	1.97×10^{-7}

---

††Average of QFF #1 and #2

‡‡ From Mackay and Shiu, (1982).

where γ = surface tension (mJ m^{-2}); ρ = density of the liquid (kg m^{-3}); R = 8314 mJ mol^{-1} K^{-1}; and M = molecular weight (kg mol^{-1}). The values for water for γ, ρ and M are 72.8, 1000, and 0.018, respectively. At 20 °C, r = 2.17 nm, or a pore diameter of 4.33 nm. On a surface such as a QFF, a micropore would most likely appear as longitudinal cracks or scales on the fiber. In Fig. 5.1(b), the QFF does not appear to have any micropores at a resolution of ~20 nm. It is unfortunate that the SEM does not resolve any closer on this particular surface. The condensation in the hypothetical micropores is likely to occur only at some critical *RH*, because the capillary pressure would need to overcome the free energy of volatilization. The geometric surface area of the quartz fibers in a QFF (assuming a mean fiber diameter of 1 µm, and a fiber density of 2.65 g cm^{-3}) is 218 cm^2, and the BET surface area for a QFF is 638 cm^2. Thus, there does not appear to be enough surface area available in the hypothetical micropores to account for the large decrease in measured partitioning.

In summary, the reasons for the decrease in gas/solid partitioning at high *RH* are not clear. From the Henry's Law calculation, it is very unlikely that adsorption to the QFF surface is replaced by dissolution into the water layers as the gas/solid partitioning mechanism, unless there is more water present on the surface due to a higher *RH*. The presence of microporous structures that are filled at high *RH* could be the reason for a drop in partitioning. However, the filled micropores would have to account for a ten-fold decrease in surface area, and this does not seem possible.

5.4 Implications and Future Work

The gas/solid sorption of PAHs and *n*-alkanes to quartz, a model for APM mineral surfaces, has been measured under ambient conditions. No evidence for effects *RH* on gas/solid partitioning were found in this experiment and in the field studies of Yamasaki *et al.* (1982). The close relationship between log $(c_s/c_g)_s$ for PAHs in these experiments and log $(F/TSP_s)/A$ for PAHS on UPM from the Yamasaki *et al.* (1982) study suggests the significant importance of available surface area to the gas/particle partitioning process. One of the overall goals of this research has been to lay the groundwork for extrapolating our understanding of gas/particle partitioning in the urban atmosphere to gas/particle partitioning on a global or regional scale. This work makes an important contribution to that effort.

For future experimental work, the apparatus that has been designed and built that be used to look at a variety of other model APM. For instance, any type of material that can be mounted on a filter, or in the filter holder, can be studied. Some model APM that are important to study include: carbon (both soot and graphite), sea salt, and aluminosilicates. All of these materials are important components of global aerosols. By changing the generator cartridges, different types of SOC can be studied as well. Because the whole apparatus is inside of a temperature-controlled box, different temperature values can be used which can help determine Q_l values. Experiments such as these can broaden our understanding of the effects of different variables on determining K_p values from the measured values of $(F/TSP)/A$.

CHAPTER 6

SUMMARY DISCUSSION

An overview of current gas/particle partitioning theory has been presented with emphasis on recent research into the partitioning behavior of semivolatile organic compounds (SOCs) on urban particulate material (UPM). Further evidence has accumulated that a simple, physical adsorption mechanism can describe the gas/particle partitioning of SOCs to UPM. By examining laboratory measurements of PAH desorption from the aerosols of four pure materials (graphitic carbon, $NaCl_{(s)}$, alumina and silica), the temperature (T) dependence of the gas/solid partitioning coefficient (K_p) was compared to the T dependence of K_p for PAHs on UPM. Close agreement between UPM and graphitic carbon was obtained when corrections for specific surface area (A_{TSP}) were made. In addition to T dependence, the relationship between K_p and the sub-cooled liquid vapor pressure, p_L^o, was explored. Changes in environmental conditions such as T, particle characteristics, ambient SOC concentration and SOC sorption kinetics, as well as sampling artifacts, can vary the measured value of $(F/TSP)/A$ from the true value of K_p.

The potential effect of RH on gas/solid partitioning was explored in detail in terms of multicomponent adsorption theory. Although the theories would predict an increase in K_p with very low RH and very high RH, the available data from an urban study showed no RH effect on the measured K_p between 42% and 95% RH.

An experimental apparatus was designed and built for the determination of gas/solid partitioning of SOCs to model particulate materials under controlled conditions. The adsorption of *n*-alkanes and PAHs to a quartz surface, specifically a quartz fiber filter (QFF), was determined at 20 °C at different RH values. The gas phase concentrations and the adsorbed solid phase concentrations were used to determine values for the partitioning coefficient, c_s/c_g, which was then compared to measured K_p values for UPM.

After normalizing for A_{TSP}, the partitioning behavior of the model system was found to be very similar to the partitioning behavior of the UPM.

The apparatus was designed to minimize variability in T, RH, and SOC concentration in the gas. The model APM (i.e. QFF) was chosen because of its well-known size and surface characteristics. The whole apparatus was placed inside of a temperature-controlled box. The dilution air that the solid phase sees was purified N_2, which was humidified at a constant RH. The SOC concentration was determined by controlling the flow of N_2 over a coated substrate, which, due to the constant T, produces a constant concentration. The QFF substrate was punched from the same sheet of 25 × 20 cm filter paper and was baked at 550 °C to remove any organic contamination. In addition, the design of the apparatus makes it useful for investigating a wide variety of sorbents and gas phase SOCs.

Results showed that the SOC-QFF interaction fits the linear-Langmuir type behavior for physical adsorption of gases to surfaces as expected from the choice of the QFF as a solid. There was a strong linear relationship between log c_s/c_g and log p_L^o for both the *n*-alkanes and the PAHs. This study represents the first time a laboratory study of gas/particle partitioning has used a model APM with known characteristics, as well as the first time equilibrium between upstream and downstream concentrations of the APM was demonstrated. Furthermore, the close relationship between log $(c_s/c_g)_s$ for these experiments and log $(F/TSP_s)/A$ for the Yamasaki *et al.* (1982) study suggests the ability of simple, physical adsorption to model the gas/particle partitioning process in the atmospheric environment.

The experimental approach was first to measure the SOC-QFF gas-solid adsorption and then to examine a range of RH values and see what effect RH had on the adsorption process. The RH ranged between 0.4% and 78%. The distribution of RHs was weighted towards the drier end of the scale because theoretical calculations have predicted the greatest effect on adsorption occurring at low RH. Also, examination of RH influence on ambient air gas-particle partitioning revealed no obvious effects in the range 40% to 98% RH.

This study represents the first time *RH* effects on gas/solid partitioning were systematically examined. *RH* effects on log c_s/c_g were minimal for all *RH* values below 31%, although multicomponent adsorption theory would predict a large increase in SOC adsorption, *RH* values close to 0%. However, three experiments at high *RH*, 72-78%, show significantly less adsorption of SOCs. This effect may be explained by the loss of surface area due to the condensation of H_2O in the micropores of the QFF. A decrease in surface area would result in a decline in adsorption and hence a lower c_s/c_g value. The assumption of a non-porous surface for the QFF is still valid at lower *RH* because condensation in the micropores is likely to occur all at once at some critical *RH* when the capillary pressure overcomes the free energy of volatilization.

In light of the design of the apparatus and the results of this study, the following three areas of future work can be suggested: 1) gas/solid sorption experiments for the wide range of materials known to make up global APM; 2) a closer examination of the cause of decreased adsorption due to high *RH*; 3) use of materials that are not APM but participate in the global fate of SOCs such as plant cuticles, tree bark, and leaves (e.g. see Pankow, 1993).

CHAPTER 7
REFERENCES

Baker J. E. and Eisenreich S.J. (1990) Concentrations and fluxes of polycyclic aromatic hydrocarbons and polychlorinated biphenyls acors the air-water interface of Lake Superior. *Envir. Sci. Technol.*, **24**, 342-352.

Benner B. A. Jr., Gordon G. E. and Wise S. A. (1989) Mobile sources of aromatic hydrocarbons: A roadway tunnel study. *Envir. Sci. Technol.*, **23**, 1269-1278.

Bidleman T. F. (1988) Atmospheric Processes. *Envir. Sci. Technol.*, **22**, 361-367.

Bidleman T. F. (1990) Personal communication to J. F. Pankow.

Bidleman T. F., Billings W. N., and Foreman W. T. (1986) Vapor-particle partitioning of organic compounds: estimates from field collections. *Envir. Sci. Technol.*, **20**, 1038-1043.

Brunauer S., Emmett P. H., and Teller E. (1938). Adsorption of gases in multimolecular layers. *J. Am. Chem. Soc.*, **60**, 309-319.

Buchholz D., Rounds S. A., and Pankow J. F. (1993). Response of gas/particle partitioning of SOCs to changes in contaminant levels. *Atmos. Env.* in preparation.

Chiou C. T., and Shoup T. D. (1985). Soil sorption of organic vapors and effects of humidity on sorptive mechanism and capacity, *Envir. Sci. Technol.*, **19**, 1196-1200.

Cotham W. E. (1990) Chemical and physical processes affecting the transport and fate of semivolatile organic contaminants in the environment. Ph.D. Thesis. University of South Carolina.

Cotham W. E. and Bidleman T. F. (1992) Laboratory investigations of the partitioning of organochlorine compounds between the gas phase and atmospheric aerosols on glass-fiber filters. *Envir. Sci. Technol.*, **26**, 469-477.

Davies O.L. and Goldsmith P.L. (1984) *ed. Statistical Methods in Research and Production, 4th edition.* Longman, London and New York. 45.

Davis B. L., Johnson L. R., Stevens R. K., Courtney W. J., and Safriet D. W. (1984) The quartz content oand elemental composition of aerosols from selected sites of the EPA Inhalable Particulate Network. *Atmos. Env.*, **18**, 771-782.

Dennis J. M., Massey R. C., McWeeny D.J. and Watson D.H. (1983) Polycyclic aromatic hydrocarbons in the U.K. Diet. In *Polynuclear Aromatic Hydrocarbons: Formation, Metabolism and Measurement* . edited by Cooke M. and Dennis A. J. Battelle Press, Columbus, Ohio. 405-412

Duce R. A. and Gagosian R.B. (1982) The input of atmospheric n-C_{10} to n-C_{30} alkanes to the ocean. *J.Geophys. Res.* **87**, 7192-7200.

Eisenreich S. J., Looney B.B. and Thornton J.D. (1981) Airborne organic contaminants in the Great Lakes ecosystem. *Envir. Sci. Technol.*, **15**, 30-38.

Eitzer B. D. and Hites R. A. (1989) Polychlorinated dibenzo-*p*-dioxins and dibenzofurans in the ambient atmosphere of Bloomington, Indiana. *Envir. Sci. Technol.*, **23**, 1389-1395.

Foreman W. T., and Bidleman T. F. (1987) An experimental system for investigating vapor-particle partitioning of trace organic pollutants. *Envir. Sci. Technol.*, **21**, 869-875.

Foreman W. T. and Bidleman T. F. (1990) Semivolatile organic compounds in ambient air in Denver, Colorado. *Atmos. Environ.*, **24A**, 2405-2416.

Gregg S.J. and Sing K. S. W. (1967) *Adsorption, Surface Area and Porosity.* Academic Press, New York. p.36ff.

Gu T. (1981) BET-type equations for adsorption of mixed vapors of immiscible liquids. *J. Colloid Interface Sci.*, **82**, 584-585.

Gu T. (1982) The application of BET-type equations to adsorption of mixed vapors of miscible liquids. *J. Colloid Interface Sci.*, **88**, 599-601.

Hart K.M. (1989) A study of atmsopheric n-alkanes and PAHs and their distribution between the gaseous and particulate phases. Ph.D. Thesis. Oregon Graduate Institute.

Hart K. M., Isabelle L. M. and Pankow J.F. High-volume air sampler for particle and gas sampling. 1. design and gas sampling performance. *Envir. Sci. Technol.*, **26**, 1048–1052.

Hiemenz P.C. (1986) *Principles of colloid and surface chemistry, 2nd ed.* Marcel Dekker, New York. 302-307.

Hinckley D. A., Bidleman T. F., Foreman W. T., and Tuschall J. R. (1990) Determination of vapor pressures for nonpolar and semipolar organic compounds from gas chromatographic retention data. *J. Chem. Eng. Data*, **35**, 232-237.

Hill T.L. (1946) The theory of multimolecular adsorption from a mixture of gases. *J. Chem. Phys.*, **14**, 268-275.

Junge C. E. (1977) Basic considerations about trace constituents in the atmosphere as related to the fate of global pollutants. In *Fate of Pollutants in the Air and Water Environments.* Part I. edited by Suffet I. H. J. Wiley and Sons. New York. 7-26.

Kang Y., Skiles J.A., and Wightman J.P. (1980) Interaction of gaseous hydrogen chloride and water with oxide surfaces. 2. Quartz. *J. Phys. Chem.*, **84**, 1448-1453.

Langmuir I. (1918) The adsorption of gases on plane surfaces of glass, mica, and platinum". *J. Am. Chem. Soc.*, **40**, 1361-1402.

Ligocki M. P., and Pankow J. F. (1989) Measurements of the gas/particle distributions of atmospheric organic compounds. *Envir. Sci. Technol.*, **23**, 75-83.

Mackay D. and Shiu W. Y. (1982) Critical review of Henry's law constants for chemicals of environmental interest. *J.Phys. Chem. Ref. Data*, **10**, 1175-1199.

Masclet P., Pistikopoulos P., Beyne S. and Mouvier G. (1988) Long range transport and gas/particulate distribution of polycyclic aromatic hydrocarbons at a remote site in the Mediterranean Sea. *Atmos. Environ.*, **22**, 639-650.

McDow S. R. and Huntzicker J. J. (1990) Vapor adsorption artifact in the sampling of organic aerosol: face velocity effects. *Atmos. Environ.*, **24A**, 2563-2272.

McVeety B. D. and Hites R. A. (1988) Atmospheric deposition of polycyclic aromatic hydrocarbons to water surfaces: a mass balance approach. *Atmos. Environ.*, **22**, 511-536.

Medalia A.I., Rivin D., and Sanders D.R. (1983) A comparison of carbon black with soot. *Sci. Tot. Env.*, **31**, 1-22.

Niessner R. and Wilbring P. Ultrafine particles as trace catchers for polycyclic aromatic hydrocarbons: the photoelectric aerosol sensor as a tool for *in-situ* sorption and desorption studies. *Anal. Chem.* **61**, 708-714.

Olufsen B. (1980) Polynuclear aromatic hydrocarbons in Norwegian drinking water sources. In *Polynuclear Aromatic Hydrocarbons: Chemistry and Biological Effects* (edited by A. Bjorseth and A. J. Dennis), pp. 333-344. Battelle Press, Columbus, Ohio.

Pankow J. F. (1987) Review and comparative analysis of the theories on partitioning between the gas and aerosol particulate phases in the atmosphere. *Atmos. Environ.*, **21**, 2275-2283.

Pankow J. F. (1988) The calculated effects of non-exchangeable material on the gas-particle distributions of organic compounds. *Atmos. Environ.*, **22**, 1405-1409.

Pankow J. F. (1991) Common y-intercept and single compound regressions of gas-partitioning data vs. 1/T. *Atmos. Environ.*, **25A**, 2229-2239.

Pankow J. F. and Bidleman T.J. (1991) Effects of temperature, TSP, and percent non-exchangeable material in determining the gas/particle partitioning of organic compounds. *Atmos. Environ.*, **25A**, 2241-2249.

Pankow J. F. and Bidleman T.J. (1992) Interdependence of the slopes and intercepts from log-log correlations of measured gas-particle partitioning and vapor pressure. 1. Theory and analysis of available data. *Atmos. Environ.*, **26A**, 1071-1080.

Pankow J. F., Ligocki M. P., Rosen M. E., Isabelle L. M., and Hart K. M. (1988). Adsorption/thermal desorption with small cartridges for the determination of trace semivolatile organic compounds. *Anal. Chem.*, **60**, 40-47.

Patton G.W., Walla M.D., Bidleman T.F., and Barrie L.A. (1992) Polycyclic aromatic and organochlorine compounds in the atmosphere of northern Ellesmere Island, Canada. *J. Geophys. Res.*, in press.

Pennell K. D., Rhue R. D., Rao P. S. C., and Johnson C. T. (1992) Vapor-phase sorption of *p*-xylene and water on soils and clay minerals. *Envir. Sci. Technol.*, **26**, 756-762.

Pierotti D., Rasmussen L. E., and Rasmussen R. A. (1978). The Sahara as a possible sink for trace gases. *Geophysical Research Letters*, **5**, 1001-1004.

Pilinis C., Sienfeld J.H. and Grosjean D. (1989) Water content of atmospheric aerosols. *Atmos. Env.*, **23**, 1601-1606.

Ross *et al.* (1982) *Colloids and Surfaces*, **5**, 17-31.

Rounds S. A. and Pankow, J. F. (1990) Application of a radial diffusion model to describe gas/particle sorption kinetics. *Envir. Sci. Technol.*, **24**, 1378-1386.

Rounds S. A., Tiffany B., and Pankow J. F. (1993) Gas/particle sorption kinetics with an intraparticle diffusion model: desorption experiments. *Envir. Sci. Technol.*, in press.

Sheffield, A. (1992) Personal communication at the Oregon Graduate Institute.

Sowelim M.A. (1983). Characteristics of storm deposited dust at Cairo. *Atmos. Env.*, **17**, 145-149.

Storey J. M. E. and Pankow J. F. (1992a) Gas/particle partitioning of semi- volatile organic compounds to model atmospheric particulate materials. 1. Sorption to graphite, sodium chloride, alumina and silica particles under low humidity conditions. *Atmos. Environ.*, **26A**, 435-443.

Storey J. M. E. and Pankow J. F. (1992b) Overview of current gas/particle partitioning theory. In *Precipitation Scavenging and Atmosphere-Surface Exchange*, **1**, edited by Schwartz S.E. and Slinn W.G.N.. Hemisphere Publishing, Washington, D.C.

Tan Y. L. and Heit M. (1981) Analysis of polynuclear aromatic hydrocarbons in sediment cores from two remote Adirondack lake by high resolution gas chromatography/mass spectrometry. In *Chemical Analysis and Biological Fate: Polynuclear Aromatic Hydrocarbons* . edited by Cooke M. and Dennis A. J. Battelle Press, Columbus, Ohio. 561-570.

Thibodeaux L.J., Nadler K.C., Valsaraj K.T., and Reible, D.D. (1991) The effect of moisture on volatile organic chemical gas-to-particle partitioning with atmospheric aerosols - competitive adsorption theory. *Atmos. Environ.*, **25A**, 1649-1656.

Valsaraj K. T. and Thibodeaux L.J. (1988) Equilibirum adsorption of chemical vapors on surface soils, landfills, and landfarms - a review. *J. Hazardous Mtls*, **19**, 79-99.

Velinsky D. J. (1986). Atmospheric deposition of organic carbon to Chesapeake Bay", *Atmos. Environ.*, **20**, 941-947.

Whitby K., Husar R. and Liu, B. (1972) The aerosol size distribution of Los Angeles smog. *J. Coll. Int. Sci.*, **39**, 177-204.

Witz S., Eden R. W., Liu C. S., and Wadley M. W. (1988) Water content of collected aerosols in the south coast and southeast desert air basins. *J. Air Pollut. Control Assoc.*, **38**, 418-419.

Yamasaki, H., Kuwata, K., and Miyamoto, H. (1982) Effects of temperature on aspects of airborne polycyclic aromatic hydrocarbons. *Envir. Sci. Technol.*, **16**, 189-194.

Yamasaki, H., Kuwata, K., and Kuge, Y. (1984) Determination of vapor pressure of polycyclic aromatic hydrocarbons in the supercooled liquid phase and their adsorption on airborne particulate matter. *Nippon Kagaku Kaishi*, **8**, 1324-1329 (*Chemical Abstracts*, 101:156747p).

Zhang X. and McMurry P. H. (1991) Theoretical analysis of evaporaive losses of adsorbed or absorbed species during atmospheric aerosol sampling. *Envir. Sci. Tech.*, **25**, 456-469.

APPENDIX

The appendix contains information about each of the fourteen individual experiments reported here arranged in chronlogical order from 101691 to 070892. The general run conditions as well as specific gas and solid phase concentration are given.

Table A.1. Experiment 101691.

Run Characteristics: **Run 101691** (QFF #1, only)	T (°C)	RH (%)	tot.vol. (m3)	wt(mg) QFF#1	fore press. (in H2O)	back press. (in H20)
	20 ± 1.5	10	74.60	29.6	49	46

Compound	MW (g)	c_g (ng/m3)	c_s (ng/μg)	log c_s/c_g	r.s.d.	log $(c_s/c_g)_s$	log p_L^o (torr)
n-alkanes							
heptadecane	240	663.9	2.82×10^{-3}	-5.47	0.29	0.19	-3.27
nonadecane	268	21.8	5.36×10^{-3}	-3.58	0.29	2.08	-4.36
eicosane	282	182.8	1.04×10^{-2}	-4.29	0.20	1.37	-4.84
heneicosane	296	11.0	5.82×10^{-3}	-3.29	0.28	2.37	-5.18
docosane	310	55.2	5.33×10^{-2}	-3.05	0.46	2.61	-5.70
tricosane	324	7.6	2.29×10^{-2}	-2.52	1.90	3.13	-6.18
PAHs							
2-methyl phenanthrene	192	184.8	NA	NA	NA	NA	-3.45
fluoranthene	202	592.7	1.46×10^{-2}	-4.61	0.05	1.05	-4.56
pyrene	202	835.8	2.12×10^{-2}	-4.61	0.09	1.05	-4.34
benz(a)anthracene	228	20.5	2.79×10^{-2}	-2.89	0.29	2.76	-5.68
2,3 benzofluorene	216	NA	NA	NA	NA	NA	-5.00

Table A.2. Run data from 112691 experiment.

Run Characteristics: **Run 112691** (QFF #1, only)	T (°C)	RH (%)	tot.vol. (m3)	wt(mg) QFF#1	fore press. (in H2O)	back press. (in H20)
	20 ± 0.2	9.8	NA	29.4	49	46

Compound	MW (g)	c_g (ng/m3)	c_s (ng/µg)	log c_s/c_g	r.s.d.	log $(c_s/c_g)_s$	log p_L^o (torr)
n-alkanes							
heptadecane	240	1248.2	3.58×10^{-3}	-5.54	0.25	0.12	-3.27
nonadecane	268	57.9	2.19×10^{-3}	-4.42	0.26	1.23	-4.36
eicosane	282	54.7	5.52×10^{-3}	-4.00	0.12	1.66	-4.84
heneicosane	296	20.0	8.24×10^{-3}	-3.39	1.08	2.27	-5.18
docosane	310	62.7	1.10×10^{-1}	-2.76	1.09	2.90	-5.70
tricosane	324	10.2	3.53×10^{-2}	-2.46	2.07	3.20	-6.18
PAHs							
2-methyl phenanthrene	192	407.3	3.68×10^{-3}	−5.04	0.19	0.61	-3.45
fluoranthene	202	71.6	2.98×10^{-3}	-4.38	0.49	1.28	-4.56
pyrene	202	42.3	2.32×10^{-3}	-4.26	0.19	1.40	-4.34
benz(a)anthracene	228	20.9	5.79×10^{-2}	-2.56	1.49	3.10	-5.68
2,3 benzofluorene	216	NA	NA	NA	NA	NA	-5.00

Table A.3. Run data from 122091 experiment.

Run Characteristics: Run **122091** (QFF #1)	T (°C)	RH (%)	tot.vol. (m3)	wt(mg) QFF#1	wt(mg) QFF#2	fore press. (in H2O)	back press. (in H20)
	20 ± 0.2	9.5	174.2	29.2	28.9	22	18

Compound	MW (g)	c_g (ng/m3)	c_s (ng/µg)	log c_s/c_g	r.s.d.	log $(c_s/c_g)_s$	log p_L^o (torr)
n-alkanes							
heptadecane	240	576.5	2.40×10^{-3}	-5.38	0.16	0.28	-3.27
nonadecane	268	21.5	1.41×10^{-3}	-4.18	0.04	1.47	-4.36
eicosane	282	16.5	2.80×10^{-3}	-3.77	0.05	1.89	-4.84
heneicosane	296	20.4	8.67×10^{-3}	-3.37	0.11	2.29	-5.18
docosane	310	42.5	6.07×10^{-2}	-2.84	0.16	2.81	-5.70
tricosane	324	4.52	2.39×10^{-2}	-2.27	0.21	3.38	-6.18
PAHs							
2-methyl phenanthrene	192	171.8	2.04×10^{-3}	-4.92	0.20	0.73	-3.45
fluoranthene	202	39.9	1.52×10^{-3}	-4.42	0.04	1.24	-4.56
pyrene	202	22.5	8.53×10^{-4}	-4.42	0.07	1.24	-4.34
benz(a)anthracene	228	18.1	3.25×10^{-2}	-2.75	0.07	2.91	-5.68
2,3 benzofluorene	216	2.9	NA	NA	NA	NA	-5.00

(QFF #2)	MW (g)	c_g (ng/m3)	c_s (ng/µg)	log c_s/c_g	r.s.d.	log $(c_s/c_g)_s$	log p_L^o (torr)
n-alkanes							
heptadecane	240	583.4	2.22×10^{-3}	-5.42	0.39	0.24	-3.27
nonadecane	268	21.7	1.70×10^{-3}	-4.11	0.03	1.54	-4.36
eicosane	282	17.6	2.66×10^{-3}	-3.82	0.12	1.84	-4.84
heneicosane	296	17.1	9.52×10^{-3}	-3.25	0.58	2.40	-5.18
docosane	310	29.7	5.86×10^{-2}	-2.71	0.80	2.95	-5.70
tricosane	324	3.5	2.24×10^{-2}	-2.19	1.07	3.47	-6.18
PAHs							
2-methyl phenanthrene	192	172.5	2.78×10^{-3}	-4.79	0.26	0.87	-3.45
fluoranthene	202	40.5	1.87×10^{-3}	-4.34	0.06	1.32	-4.56
pyrene	202	22.9	1.37×10^{-4}	-4.22	0.09	1.44	-4.34
benz(a)anthracene	228	11.0	3.07×10^{-2}	-2.56	1.42	3.10	-5.68
2,3 benzofluorene	216	NA	NA	NA	NA	NA	-5.00

Table A.4. Run data from 010292 experiment.

Run Characteristics: **Run 010292** (QFF #1)	T (°C)	RH (%)	tot.vol. (m3)	wt(mg) QFF#1	wt(mg) QFF#2	fore press. (in H2O)	back press. (in H20)
	20 ± 0.2	9.4	156.0	29.07	28.62	21.5	18.5

Compound	MW (g)	c_g (ng/m3)	c_s (ng/μg)	log c_s/c_g	r.s.d.	log $(c_s/c_g)_s$	log p_L^o (torr)
n-alkanes							
heptadecane	240	553.9	1.98×10^{-3}	-5.45	0.06	0.21	-3.27
nonadecane	268	24.9	1.04×10^{-3}	-4.38	0.37	1.28	-4.36
eicosane	282	18.1	1.47×10^{-3}	-4.09	0.37	1.57	-4.84
heneicosane	296	67.3	1.61×10^{-3}	-3.62	0.41	2.04	-5.18
docosane	310	78.9	6.91×10^{-2}	-3.06	0.52	2.60	-5.70
tricosane	324	7.60	2.75×10^{-2}	-2.44	1.09	3.22	-6.18
PAHs							
2-methyl phenanthrene	192	180.7	1.64×10^{-3}	−5.04	0.26	0.62	-3.45
fluoranthene	202	53.0	1.89×10^{-3}	-4.45	0.14	1.21	-4.56
pyrene	202	29.4	1.57×10^{-3}	-4.27	0.20	1.38	-4.34
benz(a)anthracene	228	29.3	4.60×10^{-2}	-2.80	0.55	2.85	-5.68
2,3 benzofluorene	216	1.9	9.55×10^{-4}	-3.31	1.33	2.35	-5.00

(QFF #2)	MW (g)	c_g (ng/m3)	c_s (ng/μg)	log c_s/c_g	r.s.d.	log $(c_s/c_g)_s$	log p_L^o (torr)
n-alkanes							
heptadecane	240	656.6	2.59×10^{-3}	-5.40	0.40	0.25	-3.27
nonadecane	268	28.8	1.76×10^{-3}	-4.21	0.57	1.44	-4.36
eicosane	282	22.6	2.14×10^{-3}	-4.03	0.69	1.63	-4.84
heneicosane	296	58.6	1.89×10^{-2}	-3.49	0.77	2.17	-5.18
docosane	310	59.7	7.55×10^{-2}	-2.90	0.95	2.76	-5.70
tricosane	324	6.0	3.01×10^{-2}	-2.30	0.00	3.36	-6.18
PAHs							
2-methyl phenanthrene	192	208.5	1.91×10^{-3}	−5.04	0.44	0.62	-3.45
fluoranthene	202	61.5	2.38×10^{-3}	-4.41	0.42	1.24	-4.56
pyrene	202	34.3	1.69×10^{-3}	-4.31	0.42	1.35	-4.34
benz(a)anthracene	228	18.7	4.56×10^{-2}	-2.61	0.00	3.05	-5.68
2,3 benzofluorene	216	1.8	8.06×10^{-4}	-3.36	1.35	2.30	-5.00

Table A.5. Run data from 011392 experiment.

Run Characteristics: Run 011392 (QFF #1)	T (°C)	RH (%)	tot.vol. (m3)	wt(mg) QFF#1	wt(mg) QFF#2	fore press. (in H2O)	back press. (in H20)
	20 ± 0.2	26.7	146.5	27.31	29.23	21	17

Compound	MW (g)	c_g (ng/m3)	c_s (ng/μg)	log c_s/c_g	r.s.d.	log $(c_s/c_g)_s$	log p°_L (torr)
n-alkanes							
heptadecane	240	793.1	3.03×10^{-3}	-5.43	0.17	0.24	-3.27
nonadecane	268	32.6	1.53×10^{-3}	-4.33	0.27	1.33	-4.36
eicosane	282	13.0	1.99×10^{-3}	-3.81	0.13	1.84	-4.84
heneicosane	296	43.9	3.10×10^{-2}	-3.15	0.33	2.51	-5.18
docosane	310	42.7	1.29×10^{-1}	-2.52	0.44	3.14	-5.70
tricosane	324	7.10	4.02×10^{-2}	-2.24	0.87	3.41	-6.18
PAHs							
2-methyl phenanthrene	192	266.5	2.89×10^{-3}	–4.96	0.24	0.69	-3.45
fluoranthene	202	49.0	2.13×10^{-3}	-4.36	0.32	1.30	-4.56
pyrene	202	25.8	1.21×10^{-3}	-4.33	0.71	1.33	-4.34
benz(a)anthracene	228	15.6	7.68×10^{-2}	-2.31	0.70	3.35	-5.68
2,3 benzofluorene	216	NA	NA	NA	NA	NA	-5.00

(QFF #2)	MW (g)	c_g (ng/m3)	c_s (ng/μg)	log c_s/c_g	r.s.d.	log $(c_s/c_g)_s$	log p°_L (torr)
n-alkanes							
heptadecane	240	741.6	3.01×10^{-3}	-5.39	0.34	0.27	-3.27
nonadecane	268	33.0	1.52×10^{-3}	-4.34	0.43	1.32	-4.36
eicosane	282	14.4	2.46×10^{-3}	-3.77	0.22	1.89	-4.84
heneicosane	296	43.8	3.50×10^{-2}	-3.10	0.49	2.56	-5.18
docosane	310	41.0	1.36×10^{-1}	-2.48	0.52	3.18	-5.70
tricosane	324	6.2	4.13×10^{-2}	-2.18	1.32	3.48	-6.18
PAHs							
2-methyl phenanthrene	192	249.8	4.32×10^{-3}	–4.76	0.37	0.90	-3.45
fluoranthene	202	49.3	3.19×10^{-3}	-4.19	0.31	1.47	-4.56
pyrene	202	26.0	1.28×10^{-3}	-4.31	0.85	1.35	-4.34
benz(a)anthracene	228	14.3	7.69×10^{-2}	-2.27	0.96	3.39	-5.68
2,3 benzofluorene	216	NA	NA	NA	NA	NA	-5.00

Table A.6 Run data from 012492 experiment.

Run Characteristics: **Run 012492** (QFF #1, only)	T (°C)	RH (%)	tot.vol. (m3)	wt(mg) QFF#1	fore press. (in H2O)	back press. (in H20)
	20 ± 0.2	30.6	145.2	29.81	22	18

Compound	MW (g)	c_g (ng/m3)	c_s (ng/µg)	log c_s/c_g	r.s.d.	log $(c_s/c_g)_s$	log p_L^o (torr)
n-alkanes							
heptadecane	240	691.22	1.63×10^{-3}	-5.63	0.11	0.03	-3.27
nonadecane	268	29.3	1.10×10^{-3}	-4.42	0.11	1.23	-4.36
eicosane	282	15.3	2.45×10^{-3}	-3.80	0.11	1.86	-4.84
heneicosane	296	47.0	3.11×10^{-2}	-3.18	0.10	2.48	-5.18
docosane	310	49.7	1.18×10^{-1}	-2.62	0.34	3.03	-5.70
tricosane	324	6.1	3.31×10^{-2}	-2.26	0.00	3.39	-6.18
PAHs							
2-methyl phenanthrene	192	234.9	2.78×10^{-3}	–4.93	0.03	0.73	-3.45
fluoranthene	202	73.7	3.27×10^{-3}	-4.35	0.07	1.30	-4.56
pyrene	202	37.2	1.76×10^{-3}	-4.33	0.26	1.33	-4.34
benz(a)anthracene	228	19.7	6.86×10^{-2}	-2.46	0.49	3.20	-5.68
2,3 benzofluorene	216	NA	NA	NA	NA	NA	-5.00

Table A.7. Run data from 021092 experiment.

Run Characteristics: **Run 021092** (QFF #1)	T (°C)	RH (%)	tot.vol. (m3)	wt(mg) QFF#1	wt(mg) QFF#2	fore press. (in H2O)	back press. (in H20)
	20 ± 0.2	29.8	145.2	28.77	29.37	22	18

Compound	MW (g)	c_g (ng/m3)	c_s (ng/μg)	$\log c_s/c_g$	r.s.d.	$\log\ (c_s/c_g)_s$	$\log p_L^o$ (torr)
n-alkanes							
heptadecane	240	533.1	3.02×10^{-3}	-5.25	0.20	0.41	-3.27
nonadecane	268	30.0	1.32×10^{-3}	-4.36	0.24	1.30	-4.36
eicosane	282	42.4	6.08×10^{-3}	-3.84	0.10	1.81	-4.84
heneicosane	296	46.1	1.94×10^{-2}	-3.38	0.14	2.28	-5.18
docosane	310	80.8	1.4210^{-1}	-2.75	0.22	2.90	-5.70
tricosane	324	8.1	4.82×10^{-2}	-2.22	1.42	3.43	-6.18
PAHs							
2-methyl phenanthrene	192	163.9	3.46×10^{-3}	-4.68	0.29	0.98	-3.45
fluoranthene	202	169.4	6.87×10^{-3}	-4.39	0.23	1.27	-4.56
pyrene	202	85.3	3.81×10^{-3}	-4.35	0.18	1.31	-4.34
benz(a)anthracene	228	25.5	6.79×10^{-2}	-2.57	0.54	3.08	-5.68
2,3 benzofluorene	216	4.2	NA	0.00	0.00	NA	-5.00

(QFF #2)	MW (g)	c_g (ng/m3)	c_s (ng/μg)	$\log c_s/c_g$	r.s.d.	$\log\ (c_s/c_g)_s$	$\log p_L^o$ (torr)
n-alkanes							
heptadecane	240	574.5	1.52×10^{-3}	-5.58	0.15	0.08	-3.27
nonadecane	268	33.1	1.26×10^{-3}	-4.42	0.32	1.24	-4.36
eicosane	282	45.8	5.17×10^{-3}	-3.95	0.48	1.71	-4.84
heneicosane	296	45.6	2.20×10^{-2}	-3.32	0.27	2.34	-5.18
docosane	310	63.3	1.61×10^{-1}	-2.59	0.92	3.06	-5.70
tricosane	324	6.9	5.81×10^{-2}	-2.08	2.27	3.58	-6.18
PAHs							
2-methyl phenanthrene	192	174.0	2.51×10^{-3}	-4.84	0.19	0.82	-3.45
fluoranthene	202	176.8	7.23×10^{-3}	-4.39	0.39	1.27	-4.56
pyrene	202	85.6	4.08×10^{-3}	-4.32	0.13	1.34	-4.34
benz(a)anthracene	228	19.5	7.06×10^{-2}	-2.44	1.50	3.22	-5.68
2,3 benzofluorene	216	4.0	5.49×10^{-4}	-3.86	1.01	1.80	-5.00

Table A.8. Run data from 022592 experiment.

Run Characteristics: Run 022592 (QFF #1)	T (°C)	RH (%)	tot.vol. (m3)	wt(mg) QFF#1	wt(mg) QFF#2	fore press. (in H2O)	back press. (in H20)
	20 ± 0.2	29.4	NA	29.73	29.13	21	17

Compound	MW (g)	c_g (ng/m3)	c_s (ng/µg)	log c_s/c_g	r.s.d.	log $(c_s/c_g)_s$	log p_L^o (torr)
n-alkanes							
heptadecane	240	581.8	2.62×10^{-3}	-5.35	0.24	0.31	-3.27
nonadecane	268	43.8	1.30×10^{-3}	-4.53	0.33	1.13	-4.36
eicosane	282	67.3	5.91×10^{-3}	-4.06	0.27	1.60	-4.84
heneicosane	296	51.2	1.65×10^{-2}	-3.49	0.30	2.16	-5.18
docosane	310	88.0	1.30×10^{-1}	-2.83	0.16	2.83	-5.70
tricosane	324	9.4	4.18×10^{-2}	-2.35	0.57	3.30	-6.18
PAHs							
2-methyl phenanthrene	192	270.9	2.62×10^{-3}	-5.01	0.17	0.64	-3.45
fluoranthene	202	248.3	7.63×10^{-3}	-4.51	0.13	1.14	-4.56
pyrene	202	124.9	4.51×10^{-3}	-4.44	0.27	1.21	-4.34
benz(a)anthracene	228	34.1	6.54×10^{-2}	-2.72	0.15	2.94	-5.68
2,3 benzofluorene	216	3.8	4.59×10^{-4}	-3.91	1.03	1.74	-5.00

(QFF #2)	MW (g)	c_g (ng/m3)	c_s (ng/µg)	log c_s/c_g	r.s.d.	log $(c_s/c_g)_s$	log p_L^o (torr)
n-alkanes							
heptadecane	240	583.9	2.35×10^{-3}	-5.40	0.38	0.26	-3.27
nonadecane	268	44.4	1.90×10^{-3}	-4.37	0.24	1.29	-4.36
eicosane	282	67.2	7.38×10^{-3}	-3.96	0.41	1.70	-4.84
heneicosane	296	51.4	2.05×10^{-2}	-3.40	0.26	2.26	-5.18
docosane	310	67.7	1.48×10^{-1}	-2.66	0.82	3.00	-5.70
tricosane	324	7.5	4.97×10^{-2}	-2.18	1.65	3.48	-6.18
PAHs							
2-methyl phenanthrene	192	279.6	2.98×10^{-3}	-4.97	0.23	0.69	-3.45
fluoranthene	202	256.5	9.01×10^{-3}	-4.45	0.22	1.20	-4.56
pyrene	202	129.3	5.20×10^{-3}	-4.40	0.20	1.26	-4.34
benz(a)anthracene	228	25.0	7.52×10^{-2}	-2.52	1.00	3.14	-5.68
2,3 benzofluorene	216	3.8	1.38×10^{-3}	-3.44	0.09	2.22	-5.00

Table A.9. Run data from 032092 experiment.

Run Characteristics: Run 032092 (QFF #1)	T (°C)	RH (%)	tot.vol. (m3)	wt(mg) QFF#1	wt(mg) QFF#2	fore press. (in H2O)	back press. (in H20)
	20 ± 0.2	6.5	271.9	28.98	28.90	21	17

Compound	MW (g)	c_g (ng/m3)	c_s (ng/μg)	log c_s/c_g	r.s.d.	log $(c_s/c_g)_s$	log p_L^o (torr)
n-alkanes							
heptadecane	240	1306.1	2.25e-03	-5.76	0.02	-0.11	-3.27
nonadecane	268	42.8	1.32e-03	-4.51	0.13	1.15	-4.36
eicosane	282	47.2	3.62e-03	-4.12	0.28	1.54	-4.84
heneicosane	296	28.2	9.48e-03	-3.47	0.29	2.18	-5.18
docosane	310	82.4	8.69e-02	-2.98	0.32	2.68	-5.70
tricosane	324	9.7	3.47e-02	-2.44	0.15	3.21	-6.18
PAHs							
2-methyl phenanthrene	192	345.5	2.43e-03	-5.15	0.16	0.50	-3.45
fluoranthene	202	195.4	5.71e-03	-4.53	0.04	1.12	-4.56
pyrene	202	94.7	3.56e-03	-4.43	0.17	1.23	-4.34
benz(a)anthracene	228	16.7	5.08e-02	-2.52	0.21	3.14	-5.68
2,3 benzofluorene	216	6.3	9.11e-04	-3.84	1.08	1.82	-5.00

(QFF #2)	MW (g)	c_g (ng/m3)	c_s (ng/μg)	log c_s/c_g	r.s.d.	log $(c_s/c_g)_s$	log p_L^o (torr)
n-alkanes							
heptadecane	240	1305.6	2.67e-03	-5.69	0.07	-0.03	-3.27
nonadecane	268	39.9	1.57e-03	-4.41	0.21	1.25	-4.36
eicosane	282	36.0	4.05e-03	-3.95	0.66	1.71	-4.84
heneicosane	296	18.9	1.04e-02	-3.26	0.89	2.40	-5.18
docosane	310	45.5	9.16e-02	-2.70	1.46	2.96	-5.70
tricosane	324	5.5	3.82e-02	-2.16	1.65	3.50	-6.18
PAHs							
2-methyl phenanthrene	192	378.3	2.74e-03	-5.14	0.06	0.52	-3.45
fluoranthene	202	194.2	5.66e-03	-4.54	0.06	1.12	-4.56
pyrene	202	93.0	3.64e-03	-4.41	0.06	1.25	-4.34
benz(a)anthracene	228	10.0	5.08e-02	-2.29	2.06	3.37	-5.68
2,3 benzofluorene	216	0.0	7.50e-04	0.00	0.00	NA	-5.00

Table A.10. Run data from 040392 experiment.

Run Characteristics: **Run 040392** (QFF #1)	T (°C)	RH (%)	tot.vol. (m3)	wt(mg) QFF#1	wt(mg) QFF#2	fore press. (in H2O)	back press. (in H20)
	20 ± 0.2	6.5	163.8	28.98	29.67	18.5	14.5

Compound	MW (g)	c_g (ng/m3)	c_s (ng/μg)	log c_s/c_g	r.s.d.	log $(c_s/c_g)_s$	log p_L^o (torr)
n-alkanes							
heptadecane	240	1810.5	3.11e-03	-5.76	0.09	-0.11	-3.27
nonadecane	268	65.3	1.94e-03	-4.53	0.25	1.13	-4.36
eicosane	282	71.8	7.43e-03	-3.99	0.19	1.67	-4.84
heneicosane	296	32.8	1.39e-02	-3.37	0.26	2.28	-5.18
docosane	310	57.8	8.21e-02	-2.85	0.07	2.81	-5.70
tricosane	324	5.8	3.48e-02	-2.22	0.39	3.44	-6.18
PAHs							
2-methyl phenanthrene	192	591.7	3.41e-03	-5.24	0.13	0.42	-3.45
fluoranthene	202	316.7	8.79e-03	-4.56	0.12	1.10	-4.56
pyrene	202	158.7	5.04e-03	-4.50	0.11	1.16	-4.34
benz(a)anthracene	228	22.1	4.46e-02	-2.70	0.07	2.96	-5.68
2,3 benzofluorene	216	1.8	1.56e-03	-3.06	0.80	2.60	-5.00

(QFF #2)	MW (g)	c_g (ng/m3)	c_s (ng/μg)	log c_s/c_g	r.s.d.	log $(c_s/c_g)_s$	log p_L^o (torr)
n-alkanes							
heptadecane	240	1881.9	3.82e-03	-5.69	0.11	-0.03	-3.27
nonadecane	268	62.2	2.31e-03	-4.43	0.40	1.23	-4.36
eicosane	282	61.0	8.13e-03	-3.88	1.06	1.78	-4.84
heneicosane	296	26.3	1.45e-02	-3.26	1.33	2.40	-5.18
docosane	310	39.4	8.05e-02	-2.69	1.60	2.97	-5.70
tricosane	324	3.8	3.36e-02	-2.05	2.25	3.61	-6.18
PAHs							
2-methyl phenanthrene	192	621.5	4.38e-03	-5.15	0.01	0.51	-3.45
fluoranthene	202	328.9	9.98e-03	-4.52	0.03	1.14	-4.56
pyrene	202	161.3	5.82e-03	-4.44	0.08	1.21	-4.34
benz(a)anthracene	228	13.0	4.63e-02	-2.45	2.14	3.21	-5.68
2,3 benzofluorene	216	0.8	1.79e-03	-2.64	1.13	3.01	-5.00

Table A.11. Run data from 042192 experiment.

Run Characteristics: Run 042192 (QFF #1)	T (°C)	RH (%)	tot.vol. (m3)	wt(mg) QFF#1	wt(mg) QFF#2	fore press. (in H2O)	back press. (in H20)
	20 ± 0.2	0.35	177.2	29.70	29.76	19.5	15.5

Compound	MW (g)	c_g (ng/m3)	c_s (ng/μg)	log c_s/c_g	r.s.d.	log $(c_s/c_g)_s$	log p_L° (torr)
n-alkanes							
heptadecane	240	1701.0	4.04e-03	-5.62	0.47	0.03	-3.27
nonadecane	268	69.4	1.82e-03	-4.58	0.27	1.08	-4.36
eicosane	282	102.7	1.24e-02	-3.92	0.37	1.74	-4.84
heneicosane	296	50.6	2.12e-02	-3.38	0.44	2.28	-5.18
docosane	310	68.5	1.02e-01	-2.83	0.49	2.83	-5.70
tricosane	324	7.4	3.23e-02	-2.36	0.53	3.30	-6.18
PAHs							
2-methyl phenanthrene	192	627.2	5.01e-03	-5.10	0.40	0.56	-3.45
fluoranthene	202	454.0	1.57e-02	-4.46	0.36	1.20	-4.56
pyrene	202	210.9	8.60e-03	-4.39	0.41	1.27	-4.34
benz(a)anthracene	228	23.8	5.71e-02	-2.62	0.45	3.04	-5.68
2,3 benzofluorene	216	4.6	1.28e-03	-3.56	0.06	2.10	-5.00

(QFF #2)	MW (g)	c_g (ng/m3)	c_s (ng/μg)	log c_s/c_g	r.s.d.	log $(c_s/c_g)_s$	log p_L° (torr)
n-alkanes							
heptadecane	240	1625.5	2.69e-03	-5.78	0.13	-0.12	-3.27
nonadecane	268	49.4	2.42e-03	-4.31	0.56	1.35	-4.36
eicosane	282	64.1	1.74e-02	-3.57	2.10	2.09	-4.84
heneicosane	296	28.3	2.73e-02	-3.01	2.31	2.64	-5.18
docosane	310	36.8	1.18e-01	-2.50	2.45	3.16	-5.70
tricosane	324	5.4	3.99e-02	-2.13	2.57	3.53	-6.18
PAHs							
2-methyl phenanthrene	192	497.0	4.73e-03	-5.02	0.36	0.64	-3.45
fluoranthene	202	331.2	1.71e-02	-4.29	0.92	1.37	-4.56
pyrene	202	145.5	9.48e-03	-4.19	0.71	1.47	-4.34
benz(a)anthracene	228	11.7	5.15e-02	-2.36	2.80	3.30	-5.68
2,3 benzofluorene	216	0.0	8.18e-04	0.00	0.00	NA	-5.00

Table A.12. Run data from 050792 experiment.

Run Characteristics: **Run 050792**	T (°C)	RH (%)	tot.vol. (m3)	wt(mg) QFF#1	wt(mg) QFF#2	fore press. (in H2O)	back press. (in H20)
(QFF #1)	20 ± 0.2	0.37	188.4	28.37	29.68	20	16

Compound	MW (g)	c_g (ng/m3)	c_s (ng/µg)	log c_s/c_g	r.s.d.	log $(c_s/c_g)_s$	log p_L^o (torr)
n-alkanes							
heptadecane	240	2701.0	9.52e-03	-5.45	0.25	0.20	-3.27
nonadecane	268	111.4	3.33e-03	-4.52	0.21	1.13	-4.36
eicosane	282	69.9	7.84e-03	-3.95	0.15	1.71	-4.84
heneicosane	296	34.5	9.12e-03	-3.58	0.08	2.08	-5.18
docosane	310	56.2	6.68e-02	-2.93	0.09	2.73	-5.70
tricosane	324	5.7	1.92e-02	-2.48	1.24	3.18	-6.18
PAHs							
2-methyl phenanthrene	192	824.7	7.25e-03	-5.06	0.34	0.60	-3.45
fluoranthene	202	265.5	7.03e-03	-4.58	0.17	1.08	-4.56
pyrene	202	145.1	3.99e-03	-4.56	0.12	1.10	-4.34
benz(a)anthracene	228	17.5	2.78e-02	-2.80	0.26	2.86	-5.68
2,3 benzofluorene	216	3.1	3.63e-04	-3.94	1.55	1.72	-5.00

(QFF #2)	MW (g)	c_g (ng/m3)	c_s (ng/µg)	log c_s/c_g	r.s.d.	log $(c_s/c_g)_s$	log p_L^o (torr)
n-alkanes							
heptadecane	240	2422.2	6.58e-03	-5.57	0.32	0.09	-3.27
nonadecane	268	91.1	2.67e-03	-4.53	0.44	1.12	-4.36
eicosane	282	52.0	5.98e-03	-3.94	1.01	1.72	-4.84
heneicosane	296	23.7	9.96e-03	-3.38	1.39	2.28	-5.18
docosane	310	36.0	7.26e-02	-2.70	1.65	2.96	-5.70
tricosane	324	4.7	2.03e-02	-2.36	1.72	3.30	-6.18
PAHs							
2-methyl phenanthrene	192	741.2	5.84e-03	-5.10	0.10	0.55	-3.45
fluoranthene	202	236.4	8.03e-03	-4.47	0.16	1.19	-4.56
pyrene	202	131.5	4.35e-03	-4.48	0.46	1.18	-4.34
benz(a)anthracene	228	9.0	3.25e-02	-2.44	1.88	3.21	-5.68
2,3 benzofluorene	216	2.2	0.00	0.00	0.00	NA	-5.00

Table A.13. Run data from 061992 experiment.

Run Characteristics: **Run 061992** (QFF #1)	T (°C)	RH (%)	tot.vol. (m3)	wt(mg) QFF#1	wt(mg) QFF#2	fore press. (in H2O)	back press. (in H20)
	20 ± 0.2	78	NA	28.99	29.20	17.5	13.5

Compound	MW (g)	c_g (ng/m3)	c_s (ng/µg)	log c_s/c_g	r.s.d.	log $(c_s/c_g)_s$	log p_L° (torr)
n-alkanes							
heptadecane	240	1829.7	9.33e-04	-6.29	0.05	-0.64	-3.27
nonadecane	268	102.6	2.98e-04	-5.54	1.15	0.12	-4.36
eicosane	282	65.6	3.52e-04	-5.27	0.06	0.39	-4.84
heneicosane	296	26.1	1.13e-03	-4.36	0.86	1.30	-5.18
docosane	310	31.6	3.53e-03	-3.95	0.30	1.71	-5.70
tricosane	324	3.3	1.43e-03	-3.37	0.50	2.29	-6.18
PAHs							
2-methyl phenanthrene	192	581.1	2.10e-04	-6.44	0.10	-0.79	-3.45
fluoranthene	202	204.7	3.26e-04	-5.80	0.24	-0.14	-4.56
pyrene	202	110.4	1.99e-04	-5.74	0.24	-0.09	-4.34
benz(a)anthracene	228	7.9	2.27e-04	-4.54	1.53	1.11	-5.68
2,3 benzofluorene	216	0.6	NA	NA	NA	NA	-5.00
(QFF #2)	MW (g)	c_g (ng/m3)	c_s (ng/µg)	log c_s/c_g	r.s.d.	log $(c_s/c_g)_s$	log p_L° (torr)
n-alkanes							
heptadecane	240	1893.2	5.41e-04	-6.54	0.27	-0.89	-3.27
nonadecane	268	113.9	NA	NA	NA	NA	-4.36
eicosane	282	71.7	2.46e-04	-5.47	0.51	0.19	-4.84
heneicosane	296	29.7	6.97e-04	-4.63	0.81	1.03	-5.18
docosane	310	38.6	2.21e-03	-4.24	0.27	1.42	-5.70
tricosane	324	3.4	6.42e-04	-3.72	0.22	1.93	-6.18
PAHs							
2-methyl phenanthrene	192	624.0	2.56e-04	-6.39	0.80	-0.73	-3.45
fluoranthene	202	226.3	3.86e-04	-5.77	0.44	-0.11	-4.56
pyrene	202	125.4	2.06e-04	-5.79	1.23	-0.13	-4.34
benz(a)anthracene	228	8.7	6.70e-04	-4.11	0.50	1.55	-5.68
2,3 benzofluorene	216	NA	NA	NA	NA	NA	-5.00

Table A.14. Run data from 070892 experiment.

Run Characteristics: **Run 070892** (QFF #1)	T (°C)	RH (%)	tot.vol. (m3)	wt(mg) QFF#1	wt(mg) QFF#2	fore press. (in H2O)	back press. (in H20)
	20 ± 0.2	78	216.7	29.86	29.91	17	13

Compound	MW (g)	c_g (ng/m3)	c_s (ng/µg)	$\log c_s/c_g$	r.s.d.	$\log\ (c_s/c_g)_s$	$\log p_L^\circ$ (torr)
n-alkanes							
heptadecane	240	1802.4	1.00e-03	-6.25	0.39	-0.60	-3.27
nonadecane	268	107.1	2.21e-04	-5.69	0.56	-0.03	-4.36
eicosane	282	109.8	6.22e-04	-5.25	0.11	0.41	-4.84
heneicosane	296	44.0	8.59e-04	-4.71	0.17	0.95	-5.18
docosane	310	46.9	3.06e-03	-4.18	0.19	1.47	-5.70
tricosane	324	4.5	1.05e-03	-3.64	0.36	2.02	-6.18
PAHs							
2-methyl phenanthrene	192	679.4	2.16e-04	-6.50	0.54	-0.84	-3.45
fluoranthene	202	381.5	5.49e-04	-5.84	0.39	-0.18	-4.56
pyrene	202	199.6	3.10e-04	-5.81	0.46	-0.15	-4.34
benz(a)anthracene	228	14.1	5.82e-04	-4.38	0.51	1.27	-5.68
2,3 benzofluorene	216	5.2	0.00	0.00	0.00	NA	-5.00

(QFF #2)	MW (g)	c_g (ng/m3)	c_s (ng/µg)	$\log c_s/c_g$	r.s.d.	$\log\ (c_s/c_g)_s$	$\log p_L^\circ$ (torr)
n-alkanes							
heptadecane	240	2070.8	4.06e-04	-6.71	1.16	-1.05	-3.27
nonadecane	268	109.2	1.51e-04	-5.86	0.15	-0.20	-4.36
eicosane	282	114.4	6.55e-04	-5.24	0.17	0.42	-4.84
heneicosane	296	47.7	9.32e-04	-4.71	0.21	0.95	-5.18
docosane	310	49.0	3.25e-03	-4.18	0.16	1.48	-5.70
tricosane	324	3.7	1.11e-03	-3.52	0.13	2.14	-6.18
PAHs							
2-methyl phenanthrene	192	684.2	2.29e-04	-6.48	0.29	-0.82	-3.45
fluoranthene	202	380.0	5.39e-04	-5.85	0.44	-0.19	-4.56
pyrene	202	198.0	3.25e-04	-5.79	0.09	-0.13	-4.34
benz(a)anthracene	228	12.1	7.01e-04	-4.24	0.22	1.42	-5.68
2,3 benzofluorene	216	5.0	0.00	0.00	0.00	NA	-5.00

BIOGRAPHY

The author was born in Philadelphia, Pennsylvania in 1962. He grew up in Fort Washington, Pennsylvania and attended Germantown Academy through the ninth grade. He went to Groton School in Groton, Massachusetts for high school, graduating in 1979. During his childhood, the first Earth Day in 1970 had a big impact on him, leading him to announce to his parents that he wanted to be a sanitation engineer when he grew up. The author spent an interesting year from 1979-1980 traveling in Papua New Guinea and Australia. After returning to the U.S., he went to college at Harvard University, graduating with a B.A. in Chemistry in 1984. At Harvard, he had a valuable undergraduate research experience with Dr. Stephen Cooper synthesizing macrocyclic ethers.

John went to work for a year doing air pollution source emissions testing for the Environmental Research and Testing group at Standard Oil (Ohio) in Cleveland, Ohio. Deciding that life in school was better than stack-testing, he went on to graduate school in Civil and Environmental Engineering at Duke University. Under the direction of J. Jeffrey Peirce, the author obtained an M.S. in December, 1986 with a thesis on "Influences of Changes in Chemical Concentration on Clay-Particle Interactions". He continued to work at Duke on both academic and consulting engineering research having to do with hazardous and solid waste. While a graduate student at Duke, he coached the men's crew team winning the head of the Tennessee in 1987. He also studied wind patterns on North Carolina's reservoirs and their ability to propel sailboards. He married Susan Coffey in 1987, and moved with her to Portland, Oregon in 1988.

The author went to work for Jim Pankow on surfactant analysis initially, but quickly lost interest in that and went on to the gas/particle partitioning research which is the subject of this dissertation. He spent the next two years developing, with considerable frustration, the experimental apparatus and began to collect worthwhile data in September 1991. On the basis of his theoretical work, he collected a 1991 Graduate Student Research Paper Award in 1991 from the Environmental Chemistry Division of the American Chemical Society. John and Susan had a son, Jedediah Morse, in March, 1991. John completed the requirements for his Ph.D. in October 1992, and has accepted a post-doctoral fellowship with Oak Ridge National Laboratory in Oak Ridge, Tennessee.

PUBLICATIONS

Storey, J.M.E. and Pankow, J.F. " An Overview of Gas/Particle Partitioning." to be published in the *Proceedings of the Fifth International Precipitation and Scavenging and Air-Surface Exchange Processes (IPSASEP)* Meeting held in Richland, WA. 1991.

Storey, J.M.E. and Pankow, J.F. " Gas/Particle Partitioning of Semi-Volatile Organic Compounds to Model Atmospheric Particulate Materials. 1. Sorption to Graphite, Sodium Chloride, Alumina, and Silica Particles under Low Humidity Conditions." *Atmospheric Environment*, **26A**, 435-453, 1992.

Storey, J.M.E. and Peirce, J.J. " Influence of Changes in Methanol Concentration on Clay Particle Interactions". *Canadian Geotechnical Journal*, **26**, 57-63, 1989.

Wolf, R.E.,Jr., Hartman, J.R., Storey, J.M.E., Foxman, B.M., and Stephen R. Cooper."Crown Thioether Chemistry: Structural and Conformational Studies of Tetrathia-12-crown-4, Pentathia-15-crown-5, and Hexathia-18-crown-6. Implications for Ligand Design", *Journal of the American Chemical Society*, **109**, 4328-4335, 1987.